Universität Bremen

The seismic potential of the shallow portions of the northern Cascadia and the North Sumatra subduction zones: Insights from laboratory friction experiments

Dissertation

to obtain the academic degree

– Doctor rerum naturalium –

submitted to the Faculty of Geosciences

University of Bremen

by

Katja Stanislowski

September 2021

marum
Center for Marine Environmental Sciences
University of Bremen

erc
European Research Council
Established by the European Commission

Reviewers/ Gutachter

Dr. Matt J. Ikari

MARUM – Center for Marine Environmental Sciences, and Faculty of Geosciences, University of Bremen

Leobener Str. 8

28359 Bremen

Germany

Dr. Åke Fagereng

School of Earth and Environmental Sciences

Cardiff University

Main Building

Cardiff

CF10 3AT

Wales

Date of defense: 10 December 2021

This doctoral thesis was written at MARUM – Center for Marine Environmental Sciences, and Faculty of Geosciences, University of Bremen

in the junior working group *Experimental Geomechanics* run by Dr. Matt Ikari

and in close collaboration with the working group *Marine Geotechnics* run by Prof. Achim Kopf.

Financial support was given by the European Research Council (ERC) under the European Union's Horizon 2020 research and innovation programme Grant #714430 to M. Ikari.

Summary

Many regions that are prone to experience strong earthquakes and tsunamis are densely populated, such as the coastlines of the Pacific Ocean and some of the Indian Ocean. These regions are subduction zone settings, where one tectonic plate subducts beneath another, which produces a gigantic fault – a megathrust fault. Subduction zone earthquakes largely occur on such megathrust faults. They have cost an incredible number of lives, and future events pose a constant threat to many more. Especially those megathrust earthquakes that nucleate in or propagate to very shallow depths can cause large damage and tsunamis. In general, the seismicity in the shallow portion of subduction zone megathrusts is low, but recent events such as the 2004 Aceh-Andaman earthquake and tsunami offshore North Sumatra have tragically shown the potential of shallow seismicity. Despite extensive investigations of multiple geoscientific disciplines, the shallow extent of earthquake rupture and slip of subduction zones around the world is still poorly constrained. Reasons for this lie in the challenging nature of such investigations, because the shallow extent of subduction zone earthquakes lies at sea and well below the ocean floor. Limited knowledge of this shallow earthquake extent reduces the chance of meaningful earthquake and tsunami hazard assessment and thus damage mitigation.

Because earthquakes are friction phenomena, a large body of work in earthquake research is based on laboratory friction experiments. Early friction experiments have shown that repetitive frictionally unstable stick-slip sliding on artificial faults in the laboratory represents the small-scale equivalent of earthquakes on faults in nature. Friction on a fault evolves with velocity, slip, and time (rate- and state-dependent friction) and thus can lead to unstable sliding. Unstable sliding includes periods of fault locking and accumulation of elastic energy, with intermittent periods of fault rupture and slip, which releases the stored energy. The depth interval on the megathrust fault that is capable of unstable frictional sliding and thus earthquake nucleation is called the seismogenic zone. Crucial to estimating the extent of the seismogenic zone is knowledge of the variation of the velocity-dependent frictional behavior with depth. Especially the velocity-dependent frictional behavior at plate tectonic rate has shown to be crucial. This information can be derived from laboratory friction experiments and application of so-called rate- and state-friction laws. Ideally, such experiments should be conducted on fault-zone material. However, such material is difficult to obtain and its availability is very limited. Subduction zone input materials, which are the marine sedimentary column on the subducting plate, are less difficult to recover and hold important information on where a megathrust forms or what intrinsic frictional behavior the fault-forming material has. Measurements on input material are therefore a valuable alternative to measurements on fault zone material.

Summary

This thesis presents the results of laboratory friction experiments at room temperature, under relatively low pressure, and driven at velocities starting from plate rate. These experiments were designed to investigate the frictional behavior of subduction zone input sediments and its implications on the fault slip behavior and seismic potential of the shallow portions of two subduction zones. The first is the northern Cascadia subduction zone, located along the West coast of North America, where a major earthquake is about to be due. The second is the North Sumatra subduction zone, a region of the Sunda subduction zone and the location of recent destructive earthquakes and tsunamis.

At northern Cascadia, the megathrust has so far not been sampled. Based on measurements of frictional strength contrasts in the input sedimenatry column, we propose that the megathrust fault will likely form in a weak illite-rich hemipelagic clay near the top of the oceanic basement. Because this inference is in good agreement with interpretations of seismic imaging, we focused on the frictional behavior of this specific material. The absence of shallow non-destructive slow slip events at northern Cascadia has recently been interpreted to result from a megathrust that is locked and potentially seismogenic all the way to the trench. In contrast, the results presented in this work indicate that the shallow part of the megathrust is not capable of producing slow slip events nor capable of locking and thus likely not seismogenic. However, our friction data also indicate low resistance to a propagating earthquake nucleating at greater depth. This low resistance is evident from substantially elevated pore pressure, low frictional strength, and low cohesion. Therefore, the northern Cascadia subduction zone holds the potential of shallow earthquake slip and tsunamigenesis.

At North Sumatra, seismic slip during the 2004 Aceh-Andaman subduction zone earthquake was unexpectedly shallow and resulted in a devastating tsunami. Recent work suggested that the cause is a very shallow seismogenic zone that may be created by diagenetic strengthening of fault-forming input sediments prior to subduction. This thesis presents the results of laboratory friction experiments designed to test this hypothesis. We showed that input sediments to the North Sumatra subduction zone exhibit pronounced frictional instability, offering evidence for a frictionally unstable and thus seismogenic shallow megathrust and thus an explanation for shallow earthquake slip in the 2004 event. However, our measurements indicate that the shallow megathrust is not seated in frictionally strong, but in very weak sediments. The combination of weak and unstable sediments is striking because a large number of previous friction studies have established that weak materials under low temperature and pressure conditions are generally associated with stable frictional sliding. This relationship offers an explanation for the observed general lack of seismicity in the shallow portion of subduction zone megathrusts, where unconsolidated, clay-rich, weak materials are typically encountered. We proposed that threshold amounts of dispersed hydrous amorphous

silica in otherwise weak and clay-rich sediments are responsible for an unstable sliding character, which can explain the shallow seismicity at North Sumatra.

To test the hypothesis that small amounts of hydrous amorphous silica induce unstable sliding behavior, we designed friction experiments on artificial mixtures of weak shale and biogenic opal, a type of hydrous amorphous silica. These experiments revealed pronounced potentially unstable behavior in mixtures with ≥ 30 % opal that had low frictional strength. Based on our results, we proposed that potential unstable sliding at low frictional strength can be explained by the viscous behavior of frictional contacts of hydrous amorphous silica. This highlights the necessity to reevaluate the strength-stability relationship. Our findings support the hypothesis on the role of hydrous amorphous silica in unstable sliding behavior, which has important implications for the potential of shallow seismogenesis at other subduction zones where input sediments contain critical amounts of hydrous amorphous silica.

This thesis demonstrates that the northern Cascadia and the North Sumatra subduction zone have very different intrinsic frictional fault slip behavior despite very similar extrinsic properties and attributes, such as temperature or pressure. Thus, intrinsic factors are found to be crucial to the estimation of the slip behavior of shallow megathrust faults, such as a mineral composition of fault material with threshold amounts of hydrous amorphous silica. Hydrous amorphous silica-bearing sediments could form megathrust faults due to intrinsically low strength and potential of overpressure. The shallow portion of megathrust faults formed in such sediments may thus be able to host large and slow earthquakes. This could for instance be the case in the northern Barbados subduction zone, a setting that similar to the North Sumatra subduction zone has been shown to have a porous, overpressured décollement and predécollement consisting of material that contains elevated amounts of hydrous amorphous silica. Thus, this thesis raises the possibility that subduction zones with a shallow seismogenic zone may be more common than predicted by the seismogenic zone model. This inference implies that earthquake and tsunami hazards could be highly underestimated at some subduction zone settings.

Zusammenfassung

Viele Regionen, die für starke Erdbeben und Tsunamis anfällig sind, sind dicht besiedelt, wie die Küsten des Pazifiks und einiger Gebiete des Indischen Ozeans. Bei diesen Regionen handelt es sich um Subduktionszonen, in denen sich eine tektonische Platte unter eine andere absenkt, wodurch eine gigantische Verwerfung - eine Mega-Überschiebung - entsteht. Erdbeben in der Subduktionszone ereignen sich hauptsächlich an solchen Mega-Überschiebungen. Sie haben unglaublich viele Menschenleben gekostet, und zukünftige Ereignisse stellen eine ständige Bedrohung für viele weitere dar. Vor allem Erdbeben entlang Mega-Überschiebungen, die in sehr geringer Tiefe entstehen oder sich dort ausbreiten, können große Schäden und Tsunamis verursachen. Im Allgemeinen ist die Seismizität im untiefen Bereich von Mega-Überschiebungen von Subduktionszonen gering, doch haben jüngste Ereignisse wie das Aceh-Andaman-Erdbeben von 2004 und der Tsunami vor der Küste Nordsumatras auf tragische Weise gezeigt, welches Potenzial in untiefer Seismizität steckt. Trotz umfangreicher Untersuchungen verschiedener geowissenschaftlicher Disziplinen ist das untiefe Ausdehnung von Erdbeben für Subduktionszonen auf der ganzen Welt noch immer nur unzureichend geklärt. Die Gründe dafür liegen in der schwierigen Natur solcher Untersuchungen, da die untiefe Ausdehnung von Subduktionszonen-Erdbeben im Meer und weit unter dem Meeresboden liegt. Die begrenzte Kenntnis dieser untiefen Erdbebenausdehnung verringert die Chance auf eine aussagekräftige Bewertung der Erdbeben- und Tsunamigefahr und damit auf Schadensbegrenzung.

Da es sich bei Erdbeben um Reibungsphänomene handelt, stützt sich ein Großteil der Erdbebenforschung auf Reibungsexperimente im Labor. Frühe Reibungsexperimente haben gezeigt, dass wiederholtes, reibungsinstabiles Stick-Slip-Gleiten auf künstlichen Verwerfungen im Labor das kleinskalige Äquivalent zu Erdbeben auf Verwerfungen in der Natur darstellt. Die Reibung auf einer Verwerfung entwickelt sich mit der Geschwindigkeit, der Versetzung und der Zeit (raten- und zustandsabhängige Reibung) und kann daher zu instabilem Gleiten führen. Instabiles Gleiten umfasst Perioden der Verklemmung der Verwerfung und damit einhergehend der Akkumulation elastischer Energie, und intermittierenden Perioden von Verwerfungsbrüchen und Versetzung, die die gespeicherte Energie freisetzen. Das Tiefenintervall auf der Mega-Überschiebung, das zu instabilem Reibungsgleiten und damit zur Auslösung von Erdbeben führen kann, wird als seismogene Zone bezeichnet. Entscheidend für die Abschätzung der Ausdehnung der seismogenen Zone ist die Kenntnis der Variation des geschwindigkeitsabhängigen Reibungsverhaltens mit der Tiefe. Insbesondere das geschwindigkeitsabhängige Reibungsverhalten bei plattentektonischer Geschwindigkeit hat sich als entscheidend erwiesen. Diese Informationen lassen sich aus Reibungsexperimenten im Labor und der Anwendung sogenannter Raten- und

Zustandsreibungsgesetze ableiten. Idealerweise sollten solche Experimente an Material aus der Störungszone durchgeführt werden. Solches Material ist jedoch schwer zu beschaffen und nur sehr begrenzt verfügbar. Das Eingangsmaterial der Subduktionszone, d. h. die marinen Sedimente auf der subduzierenden Platte, ist weniger schwer zu gewinnen und liefert wichtige Informationen darüber, wo sich eine Mega-Überschiebung bildet oder welches intrinsische Reibungsverhalten das verwerfungsbildende Material hat. Messungen am Eingangsmaterial sind daher eine wertvolle Alternative zu Messungen am Material der Störungszone.

In dieser Arbeit werden die Ergebnisse von Laborexperimenten zur Reibung bei Raumtemperatur und unter relativ geringem Druck vorgestellt, die mit Geschwindigkeiten ab der Plattengeschwindigkeit durchgeführt wurden. Diese Experimente dienten der Untersuchung des Reibungsverhaltens von Sedimenten, die in die Subduktionszone eingespeist werden, und ihrer Auswirkungen auf das Verwerfungsverhalten und das seismische Potenzial der oberflächennahen Bereiche zweier Subduktionszonen. Bei der ersten handelt es sich um die nördliche Cascadia-Subduktionszone, die sich entlang der Westküste Nordamerikas befindet und in der ein großes Erdbeben bevorsteht. Die zweite ist die Nordsumatra-Subduktionszone, eine Region der Sunda-Subduktionszone, in der es in jüngster Zeit zu zerstörerischen Erdbeben und Tsunamis kam.

In der nördlichen Cascadia-Subduktionszone wurde die Mega-Überschiebung bisher noch nicht beprobt. Auf der Grundlage von Messungen der Reibungsfestigkeitskontraste in der Eingangssedimentsäule schlagen wir vor, dass sich die Mega-Überschiebung wahrscheinlich in einem schwachen illitreichen hemipelagischen Ton nahe der Oberseite des ozeanischen Grundgebirges bildet. Da diese Schlussfolgerung in guter Übereinstimmung mit den Interpretationen seismischer Aufnahmen steht, haben wir uns auf das Reibungsverhalten dieses speziellen Materials konzentriert. Das Fehlen untiefer, nicht-destruktiver langsamer Verwerfungsereignisse im nördlichen Cascadia wurde kürzlich als Folge einer Mega-Überschiebung interpretiert, die bis in den Graben hinein verklemmt und potenziell seismogen ist. Im Gegensatz dazu deuten die in dieser Arbeit vorgestellten Ergebnisse darauf hin, dass der untiefe Teil der Mega-Überschiebung weder in der Lage ist, langsame Verwerfungsereignisse zu erzeugen, noch sich zu verklemmen, und daher wahrscheinlich nicht seismogen ist. Unsere Reibungsdaten deuten jedoch auch auf einen geringen Widerstand gegen ein sich ausbreitendes Erdbeben hin, das in größerer Tiefe seinen Ursprung hat. Dieser geringe Widerstand ergibt sich aus dem deutlich erhöhten Porendruck, der geringen Reibungsfestigkeit und der geringen Kohäsion. Daher birgt die nördliche Cascadia-Subduktionszone das Potenzial für sich untief ausbreitende Erdbeben und Tsunamigenese.

In Nordsumatra war die seismische Verwerfung während des Erdbebens in der Aceh-Andaman-Subduktionszone 2004 unerwartet untief und führte zu einem verheerenden

Tsunami. Jüngste Arbeiten deuten darauf hin, dass die Ursache eine sehr untiefe seismogene Zone ist, die durch diagenetische Verfestigung der verwerfungsbildenden Eingangssedimente der Subduktionzone entstanden sein könnte. In dieser Arbeit werden die Ergebnisse von Reibungsexperimenten im Labor vorgestellt, mit denen diese Hypothese überprüft werden soll. Wir konnten zeigen, dass die Eingangssedimente der Nordsumatra-Subduktionszone eine ausgeprägte Reibungsinstabilität aufweisen, was auf eine reibungstechnisch instabile und damit seismogene untiefe Mega-Überschiebung hindeutet und somit eine Erklärung für das untiefe Erdbeben von 2004 liefert. Unsere Messungen deuten jedoch darauf hin, dass die untiefe Mega-Überschiebung nicht in reibungsstarken, sondern in sehr schwachen Sedimenten ruht. Die Kombination aus schwachen und instabilen Sedimenten ist bemerkenswert, da zahlreiche frühere Reibungsstudien ergeben haben, dass schwache Materialien unter niedrigen Temperatur- und Druckbedingungen im Allgemeinen mit stabilem Reibungsgleiten verbunden sind. Diese Beziehung bietet eine Erklärung für das beobachtete generelle Fehlen von Seismizität im flachen Teil von Subduktionszonen-Mega-Überschiebungen, wo typischerweise unverfestigte, tonreiche, schwache Materialien anzutreffen sind. Wir schlugen vor, dass Schwellenwerte von dispergiertem wasserhaltigem amorphem Siliziumdioxid in ansonsten schwachen und tonreichen Sedimenten für einen instabilen Gleitcharakter verantwortlich sind, was die untiefe Seismizität der Nordsumatra-Subduktionszone erklären kann.

Um die Hypothese zu testen, dass geringe Mengen an wasserhaltigem amorphem Siliziumdioxid ein instabiles Gleitverhalten hervorrufen, haben wir Reibungsexperimente mit künstlichen Mischungen aus schwachem Schiefer und biogenem Opal, einer Art wasserhaltiges amorphes Siliziumdioxid, durchgeführt. Diese Experimente zeigten ein ausgeprägtes, potenziell instabiles Verhalten in Mischungen mit ≥ 30 % Opal, die eine geringe Reibungsfestigkeit aufwiesen. Auf der Grundlage unserer Ergebnisse schlugen wir vor, dass potenziell instabiles Gleiten bei niedriger Reibungsfestigkeit durch das viskose Verhalten von Reibungskontakten aus wasserhaltigem amorphem Siliziumdioxid erklärt werden kann. Dies unterstreicht die Notwendigkeit, die Beziehung zwischen Reibungsfestigkeit und Stabilität neu zu bewerten. Unsere Ergebnisse unterstützen die Hypothese über die Rolle von wasserhaltigem amorphem Siliziumdioxid bei instabilem Reibungsverhalten, was wichtige Auswirkungen auf das Potenzial der untiefen Seismogenese in anderen Subduktionszonen hat, in denen die Eingangssedimente kritische Mengen von wasserhaltigem amorphem Siliziumdioxid enthalten.

In dieser Arbeit wird gezeigt, dass die nördliche Cascadia- und die Nordsumatra-Subduktionszone trotz sehr ähnlicher extrinsischer Eigenschaften und Attribute wie Temperatur oder Druck ein sehr unterschiedliches intrinsisches Reibungsverschiebungsverhalten aufweisen. Es hat sich gezeigt, dass intrinsische Faktoren

für die Abschätzung des Reibungsverhaltens flacher Mega-Überschiebungen entscheidend sind, wie z. B. die mineralische Zusammensetzung des Verwerfungsmaterials mit einem Schwellenwert an wasserhaltiger amorpher Kieselsäure. Sedimente, die wasserhaltiges amorphes Siliziumdioxid enthalten, könnten aufgrund ihrer geringen Reibungsfestigkeit und ihres Porenüberdruckpotenzials Mega-Überschiebungen bilden. Der untiefe Teil von Mega-Überschiebungen, die in solchen Sedimenten gebildet werden, kann daher in der Lage sein, große und langsame Erdbeben zu erzeugen. Dies könnte beispielsweise in der nördlichen Barbados-Subduktionszone der Fall sein, die ähnlich wie die Nordsumatra-Subduktionszone nachweislich ein poröses, überdruckbelastetes Décollement und Predécollement aufweist, das aus Material besteht, das große Mengen an wasserhaltigem amorphem Siliziumdioxid enthält. Diese These lässt den Schluss zu, dass Subduktionszonen mit einer untiefen seismogenen Zone häufiger vorkommen, als es das Modell der seismogenen Zone vorhersagt. Diese Schlussfolgerung impliziert, dass die Erdbeben- und Tsunamigefahr an einigen Subduktionszonen-Regionen stark unterschätzt sein könnte.

Contents

1 Introduction

1.1 Subduction zone earthquakes

Subduction zones host the world's largest and most destructive earthquakes, one of the greatest natural hazards to humankind. These earthquakes are typically accompanied by strong ground shaking that can lead to heavy damage or even the collapse of buildings and infrastructure. Another important phenomenon related to subduction zone earthquakes is tsunamis, which additionally cause abrupt and catastrophic flooding not only at the ruptured continental margin itself but also at other coastlines lying within reach of the tsunami waves. Understanding and ultimately predicting the occurrence and characteristics of subduction zone earthquake is vital to meaningful earthquake and tsunami hazard assessment.

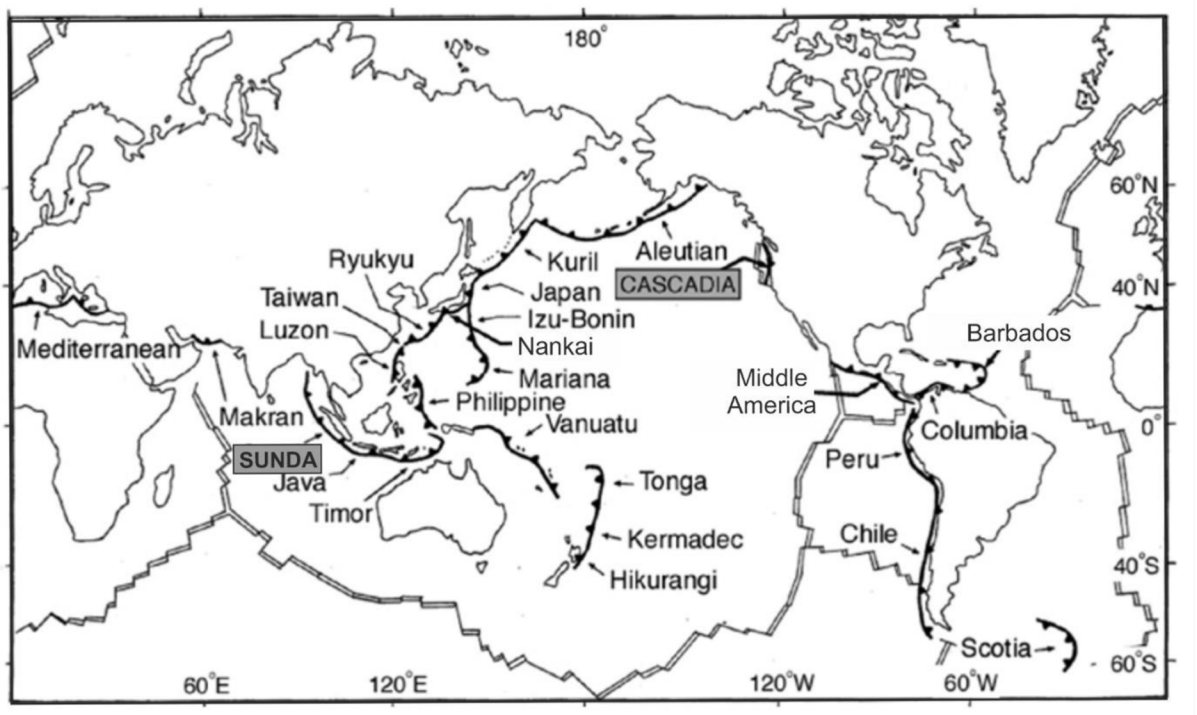

Figure 1.1: Global distribution of active subduction zones (modified after Underwood, 2007). Gray boxes mark the study areas of this work.

At subduction zones, which are a type of convergent tectonic plate margin, the denser plate subducts beneath the less dense plate. Most subduction zones are located around the Pacific Ocean, but are also present in the Indian Ocean, the Lesser Antilles, and the Mediterranean Sea (Fig. 1.1). The majority of subduction earthquakes occur on megathrust faults (or décollement), gigantic interplate faults that mark the interface between overriding and underthrusting plates and accommodate the convergent motion (Fig. 1.2). Such faults initiate

within the sediment of the incoming plate, or are at least bounded by the sediment on one side (e.g. Moore, 1989). For some subduction zones, the plate interface forms at the top of the oceanic crust or within the sedimentary section lying on top of it. In both cases, oceanic sediments above the plate interface are scraped off and accreted onto the continental crust (subduction accretion). At other subduction zones, the entire sedimentary section gets subducted and may even erode the continental crust (subduction erosion).

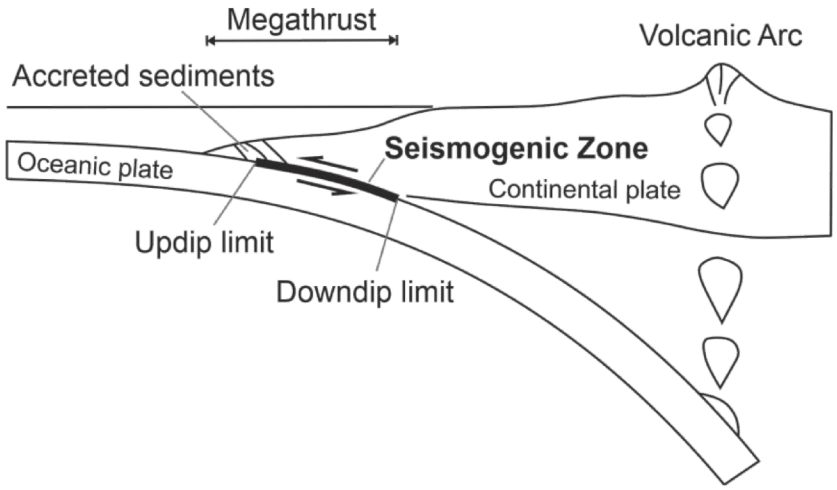

Figure 1.2: Schematic diagram illustrating the megathrust fault in an accretionary subduction zone system, where the denser oceanic plate subducts beneath the less dense continental plate (modified after Lay and Bilek, 2007). The thick black line highlights the seismogenic portion of the megathrust on which large thrust earthquakes occur.

The size of an earthquake is expressed in moment magnitude M_w, which is derived from the seismic moment. Seismic moment in turn, is derived from the product of the rigidity of the deformed crust, the rupture area, and the amount of slip (relative displacement of the two sides of the fault plane) (Wells and Coppersmith, 1994; Kanamori and Brodsky, 2001). Subduction zones account for approximately 90% of the total seismic moment globally released during the last century (Pacheco and Sykes, 1992), including the largest recorded events, the M_w 9.5 Chile earthquake of 1960 and the M_w 9.2 Alaska earthquake of 1964 (Fig. 1.3). The contribution of each subduction zone to the globally released seismic moment is uneven in terms of both magnitude and quantity (Ruff and Kanamori, 1980).

For an assessment of earthquake and tsunami hazard, it is of critical importance to know how close to the crust's surface the earthquake rupture and slip reach (e.g. Hyndman & Wang, 1995). Seismological observations show that subduction zone earthquakes typically nucleate, rupture, and slip in a depth range of approximately 10-40 km below the seafloor

(Zhang and Schwartz, 1992; e.g. Pacheco and Sykes, 1992). These observations led to the model of subduction seismicity, in which this depth interval is seismogenic, termed the

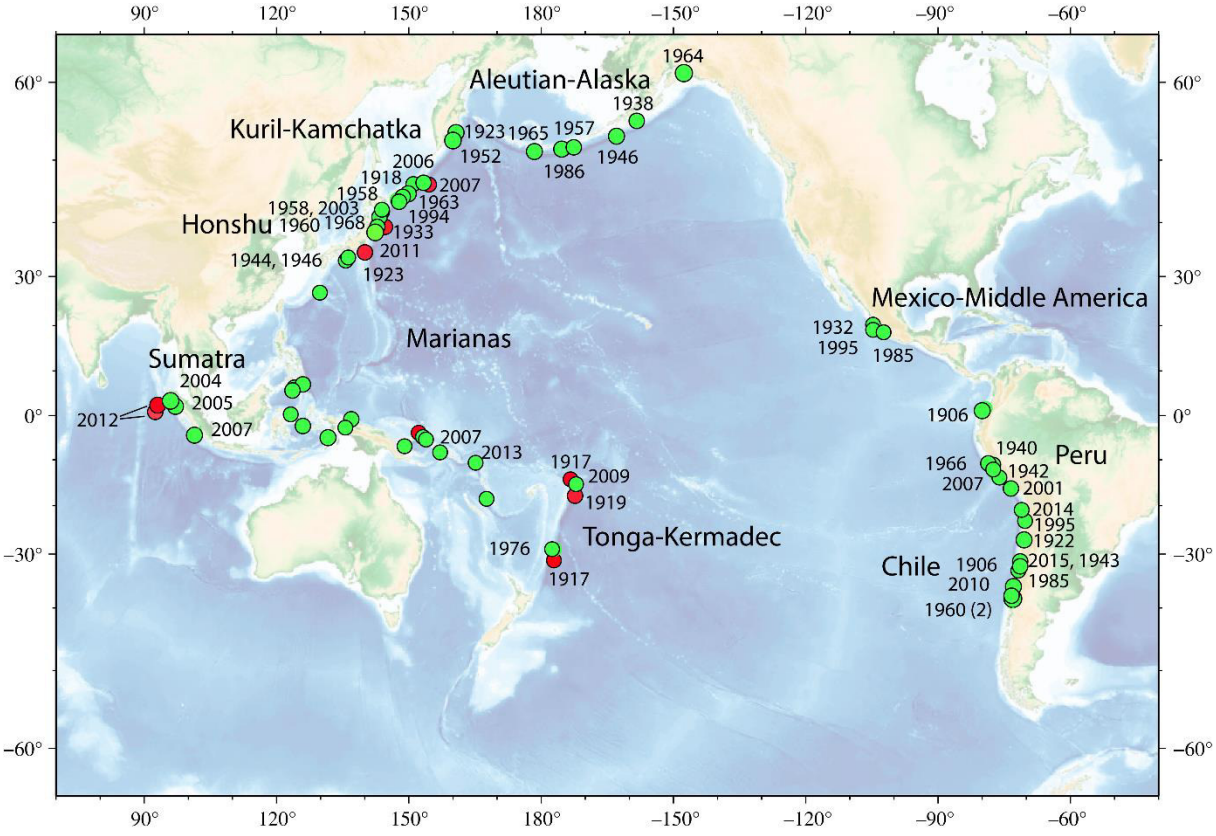

Figure 1.3: Map showing locations of large earthquakes with moment magnitudes $M_W \geq 8$ from 1900 to 2016 by (Bilek and Lay, 2018). Green circles mark events presumed to have occurred directly on the plate interface, red circles represent intraplate ruptures.

seismogenic zone (Fig. 1.3), while the deeper and shallower portions are described as aseismic (Byrne et al., 1988; Marone and Scholz, 1988; Pacheco et al., 1993; Tichelaar and Ruff, 1993; Hyndman et al., 1997; Oleskevich et al., 1999; Moore and Saffer, 2001). However, during recent large subduction zone earthquakes such as the M_w 9.2 Aceh-Andaman earthquake of 2004 offshore Sumatra at the Sunda subduction zone (Fig. 1.1, 1.3) (Ammon et al., 2005; Bletery et al., 2016) or the M_w 9.1 Tohoku-oki earthquake in 2011 at the Japan Trench subduction zone (Fig. 1.1, 1.3) (Fujiwara et al., 2011; Sun et al., 2017) coseismic slip extended much closer to the seafloor than expected from this model and resulted in devastating tsunamis. These examples have tragically shown the seismic potential of shallow portions of subduction zone megathrusts. In particular, the Tohoku-oki event led to the reappraisal of the subduction zone seismicity model.

For most subduction zones, the upper limit of seismicity is still poorly constrained. The depth of the updip limit of the seismogenic zone is highly variable from region to region (e.g. Lay and Bilek, 2007). In addition, the extent of coseismic slip propagation from seismogenic depths into the shallow portion of a subduction zone may be variable (Faulkner et al., 2011; Seyler et al., 2020). To make matters even more complicated, seismic faulting of shallow megathrusts shows strong along-strike heterogeneity (e.g. Lay and Bilek, 2007). Taken together, the high variability of shallow fault slip behavior and associated seismicity demonstrates the great need for the determination and ground-truthing of structures and properties that control the seismic potential of the shallow portion of subduction zones, and this work aims to contribute to that.

1.2 The physics of earthquakes

In order to gather knowledge on the seismic potential at specific locations within a subduction zone, it is important to understand the physical processes behind earthquakes. Equally important is knowledge of the conditions that need to be satisfied for an earthquake to occur. Earthquakes are elastic waves radiating from sudden displacement of the crust along a fault plane following local failure of crust. In most cases, failure and slip occur on pre-existing faults such as subduction megathrust faults, which represent planes of weakness in the crust. Consequently, earthquakes are a friction rather than a fracture phenomenon (e.g. Brace and Byerlee, 1966; Scholz, 1998). The local frictional strength τ of a fault can be described by the Coulomb failure criterion for rocks under compression (Handin, 1969), neglecting the effect of cohesion:

$$\tau = \mu \, \sigma_N' \tag{1.1}$$

where μ is the friction coefficient and σ_N' is the effective normal stress. The effective normal stress represents the load exerted from the crust above minus the stress exerted by the pore-fluid. During frictional sliding on a fault plane driven by the relative motion of the rigid tectonic plates, friction strength changes as a function of slip, velocity, and contact history. When the shear stress on the fault is lower than the local frictional strength the fault is locked. Due to ongoing plate movement and the rigidity of the crust, elastic strain accumulates and the shear stress on the fault increases. Once the shear stress exceeds the frictional strength, the fault fails, the shear stress drops to a new lower level, and the energy stored by strain accumulation is released via seismic wave radiation, fracture growth and shear heating (e.g. Kanamori and Brodsky, 2004).

Short periods of coseismic stress drop are followed by a longer period of interseismic shear stress accumulation, forming the so-called seismic cycle (schematic, Fig. 1.4a). Although the overall long-term process of interseismic stress build-up and seismic release is more or less regular and calculated average recurrence intervals of 100-1000 years for major events fit the observations, there are considerable fluctuations to this process (Fig. 1.4b) (Kanamori and Brodsky, 2001). These fluctuations result from the fact that both stress accumulation rates and fault strength vary over time, and that coseismic stress drops may differ from event to event. This makes prediction of the timing and size of earthquakes extremely difficult.

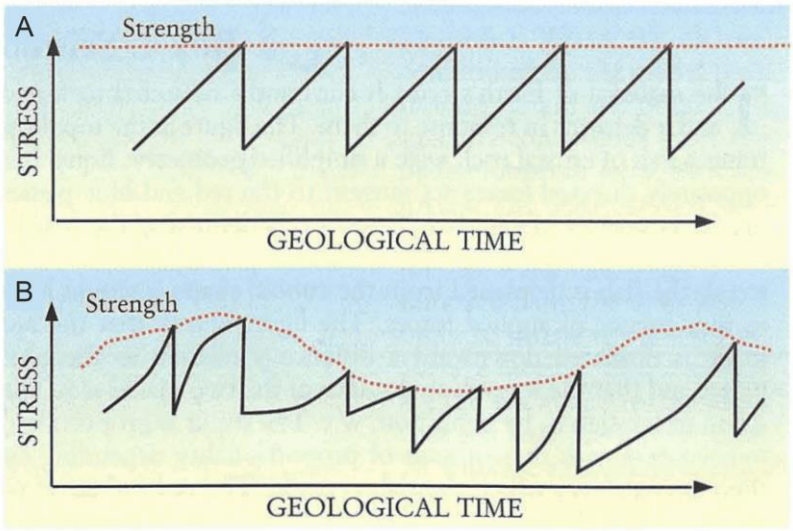

Fig. 1.4: The seismic cycle on a fault illustrated as stress drop over time. a) a simplified regular development of interseismic shear stress accumulation and coseismic stress drop upon reaching the local frictional strength, and b) a more realistic version of the process including fluctuations in fault strength, stress accumulation rate, and stress drop (Kanamori and Brodsky, 2001)

Although the size and recurrence time of earthquakes are variable, they obey a scaling law, which positively correlates the seismic moment of an event to recurrence time (Gutenberg and Richter, 1942). This relation is important, as it provides crude estimates on the recurrence interval of large events. Additionally, other scaling laws are useful, such as the relation of seismic moment and rupture duration (e.g. Vidale et al., 1994), or of stress drop and peak slip velocity (e.g. Ohnaka et al., 1987). However, in the late 1960s and 70s, first evidence of another earthquake category was discovered, so-called slow earthquakes (e.g. Sacks et al., 1978), which do not necessarily follow the same relations as observed for rapid, ordinary earthquakes.

Since the 1990's, advances in the deployment and resolution of geodetic networks as well as ocean bottom or bore hole seismometers and strain meters along subduction zones have brought about an increase in observations of slow earthquake events (Schwartz and

Rokosky, 2007; Beroza and Ide, 2011; Bürgmann, 2018). Slow earthquakes comprise various non-destructive slip phenomena, such as episodic tremor and slip (ETS) (Obara, 2002; Rogers and Dragert, 2003), low frequency earthquakes (LFE) (Katsumata and Kamaya, 2003), very low frequency earthquakes (VLF) (Ito and Obara, 2006), slow slip events (SSE) (Hirose and Obara, 2005), and silent earthquakes (EQ) (e.g. Hirose et al., 1999). While LFEs and VLFs radiate seismic waves, SSEs do not and thus can only be detected by geodetic or strain measurements (Saffer and Wallace, 2015). Although the seismic moment of slow earthquakes scales with event duration, as observed for ordinary earthquakes, the relation can be different (Ide et al., 2007; Gao et al., 2012). Slow earthquakes in various forms are characterized by much less radiated energy and less rapid stress release, but by moment magnitudes as large as 7 (Hirose and Obara, 2005). Additionally, slow earthquakes encompass a large range of durations, from minutes to years to even decades. Thus, it has been suggested that they represent a continuum between aseismic fault slip and ordinary, rapidly slipping earthquakes (e.g. Peng and Gomberg, 2010; Leeman et al., 2016).

An often suggested factor important to the occurrence of shallow slow earthquakes is an elevated pore-fluid pressure and thus a reduction in effective normal stress (Kodaira et al., 2004; Kitajima and Saffer, 2012; Saffer and Wallace, 2015). However, intrinsic frictional properties have also been proposed to control slow slip (Ikari and Kopf, 2017; Ikari, 2019). Because slow earthquakes occur either around the downdip or updip transition or within the seismogenic zone itself (e.g. Ruiz et al., 2014; Saffer and Wallace, 2015), the question about their influence on the occurrence of ordinary earthquakes quickly arose: However, the answer is still debated. On the one hand, slow earthquakes are suggested to relieve stress from seismogenic fault regions (Radiguet et al., 2012; Husker et al., 2018), thus reducing earthquake hazard. On the other hand, they are thought to trigger earthquakes on adjacent fault regions by transferring stress (e.g. Wech and Creager, 2011; Koulali et al., 2017). Additionally, observations of a change in recurrence time of slow earthquakes prior to the occurrence of large earthquakes have led to the hypothesis that slow events may function as precursors for larger events (Obara and Kato, 2016; Voss et al., 2018). Therefore, slow earthquakes may play an important role in the seismic cycle of subduction megathrusts.

The combined efforts of many different geoscientific disciplines constantly improve the understanding of the origin and occurrence of slow and large earthquakes. Typical methods to study earthquakes are geological observations of exhumed faults, geodetic measurements of crustal motion, heat-flow measurements, earthquake cataloging, numeric modeling, and laboratory experiments. In the context of this thesis, I will focus on laboratory friction experiments. Such experiments are a powerful way to investigate the effects of individual intrinsic and extrinsic factors on the frictional properties of synthetic and natural geological

materials under controlled conditions. As such, they can deliver valuable information on the controls of the frictional fault slip behavior and thus seismicity of fault zones in nature.

1.3 Laboratory friction experiments

In 1966, Brace & Byerlee observed periodic “stick-slip” motion during laboratory friction tests along a predefined surface and interpreted it to be analogs for the seismic cycle. “Stick” corresponds to the period of fault locking and interseismic stress accumulation, and “slip” accompanied by a stress drop represents an earthquake. Considering earthquakes to result from repetitive frictional instability entirely changed the understanding of earthquake mechanics from a fracture to a friction phenomenon and set the cornerstone for modern laboratory earthquake research. Thus, the body of work studying the influences on the frictional behavior of rocks started to grow, often based on information on the concept of friction developed on materials relevant to material sciences.

One of the major findings was that frictional stability is a system response, dependent on the stiffness of the material in frictional contact and that of the elastic surrounding (e.g. Cook, 1981). This led to the introduction of constitutive laws, which described friction as a function of constitutive parameters applicable to different mechanical settings in the laboratory but also in nature (e.g. Dieterich, 1981; Ruina, 1983).

Another major finding was the time dependence of friction, first observed by Rabinowicz (1951) on metals and later on artificial rock powder (gouge) as an equivalent to the gouge produced by frictional wear in a fault system (Dieterich, 1972). The observation was that static friction (friction at zero displacement) increases with logarithm of time of stationary contact (Fig. 1.5a). The explanation for this dependence is based on the adhesion theory (Bowden and Tabor, 1964), which forms the base for the modern concept of friction. In this theory, two contacting frictional surfaces of any material are envisioned to have topography, and only the positions of real contact (asperities) are responsible for friction. These asperities deform plastically and grow until they are able to support the normal load, resulting in the welding of surfaces in contact. The total shear strength of the sum of welded contacts is the frictional force. Thus, it was proposed that the time-dependence of friction results from either growth of individual asperities or from an increase in the number of asperities with time and applied normal stress, a process often referred to as frictional healing (Scholz and Engelder, 1976; Beeler et al., 1994; Dieterich and Kilgore, 1994; Wang and Scholz, 1994).

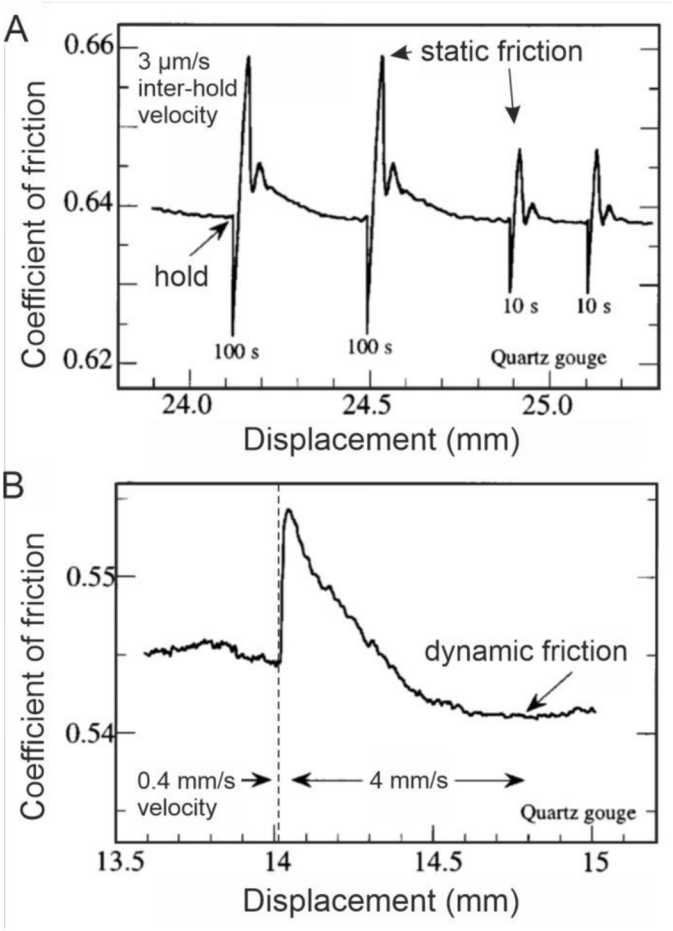

Figure 1.5: Laboratory friction data on quartz gouge shown as coefficient of friction versus displacement, demonstrating the time- and velocity dependence of friction (Marone, 1998). a) Varying static friction after different hold times, b) change in dynamic friction upon a sudden change in velocity.

Equally important as the time dependence was the discovery of the velocity dependence of friction (Scholz, 1972; Scholz and Engelder, 1976; Dieterich, 1978). Early laboratory studies on bare rock surfaces as well as gouge documented that upon a sudden change in shear velocity, the dynamic friction (friction during displacement) evolves to a new level (Fig. 1.5b) (Scholz and Engelder, 1976; Dieterich, 1978; Kilgore et al., 1993). In particular, the dynamic friction may either increase with velocity (velocity strengthening) or decrease (velocity weakening), with specific velocity domains favor either behavior (Shimamoto, 1986; Blanpied et al., 1987; Kilgore et al., 1993; Tsutsumi and Shimamoto, 1997; Beeler, 2009). In both cases, dynamic friction changes over a finite slip distance, assumed to represent the distance necessary to renew the population of asperity contacts characteristic for the old velocity (Dieterich, 1978, 1979; Ruina, 1983). Since higher velocities reduce the time for growth of asperity contact area induced by plastic deformation, it follows that the velocity is inversely proportional to the lifetime of asperity contacts.

The recognition of the importance of asperity contact lifetime for both velocity and time dependence of friction by Dieterich (1979) and thus the connection of both behaviors set the foundation for friction constitutive laws (Dieterich, 1979, 1981; Ruina, 1983). These laws are able to describe the frictional behavior of rocks and other materials, and form the base of modern investigations on the mechanical processes of faulting and earthquakes. They are known as rate- and state friction (RSF) laws.

1.4 Rate- and state friction laws

Based on the initial formulation by Dieterich (1979) and on additional considerations by Ruina (1983), the first part of the constitutive laws provides the relation of time and velocity dependence of friction, expressed in its modern form (Marone, 1998):

$$\mu = \mu_0 + a \ln\left(\frac{V}{V_0}\right) + b_{1,2} \ln\left(\frac{V_0 \theta_{1,2}}{D_{C1,2}}\right) \tag{1.2}$$

where μ is the coefficient of friction, V_0 and V are the initial and final velocities, μ_0 is the steady-state friction coefficient at V_0, D_C is interpreted as the critical slip distance necessary to change asperity contacts according to the new velocity V, and θ is a state variable that represents any changes occurring with contact lifetime (Ruina, 1983). The parameters *a* and *b* are empirical unitless constants, where *a* scales the direct response of friction to a velocity perturbation (direct effect) and *b* scales the evolution of friction to a new steady state (evolution effect) (Fig. 1.6). To model the evolution of friction in response to changes in slip velocity or contact lifetime and thus obtain a full constitutive law, Equation 1.2 needs to be coupled with a description of state evolution. The two most commonly used state evolution laws are the aging law (Dieterich, 1981) and the slip law (Ruina, 1983):

Aging law
$$\frac{d\theta}{dt} = 1 - \frac{V\theta}{D_C} \tag{1.3}$$

Slip law
$$\frac{d\theta}{dt} = -\frac{V\theta}{D_C} ln\left(\frac{V\theta}{D_C}\right) \tag{1.4}$$

with *t* being time. The two constitutive laws differ most in their description of state und thus friction evolution under stationary conditions when V=0. While the aging law allows for state evolution without any movement, the slip law predicts a change in state only during slip. Additionally, the aging law describes an asymmetry between velocity upsteps and downsteps, whereas the slip law predicts symmetry (e.g. Marone, 1998). Despite their difference, both laws have been shown to approximate observations of frictional behavior well (Beeler et al., 1994; Nakatani, 2001; Rathbun and Marone, 2010; Bhattacharya et al., 2015).

However, at steady state, that is when the state variable does not change with time ($d\theta/dt$=0), the two constitutive laws yield the same description for θ, and thus the same expression for the change of steady-state friction μ_{SS} with a change in slip velocity (e.g. Tullis and Weeks, 1986):

$$a - b = \frac{\Delta\mu_{SS}}{\Delta\ln(V)} \tag{1.5}$$

Positive values of the rate-dependent parameter *a-b* indicate that friction increases with increasing velocity (velocity strengthening), whereas negative values indicate a decrease of friction with decreasing velocity (velocity weakening) (Fig. 1.6).

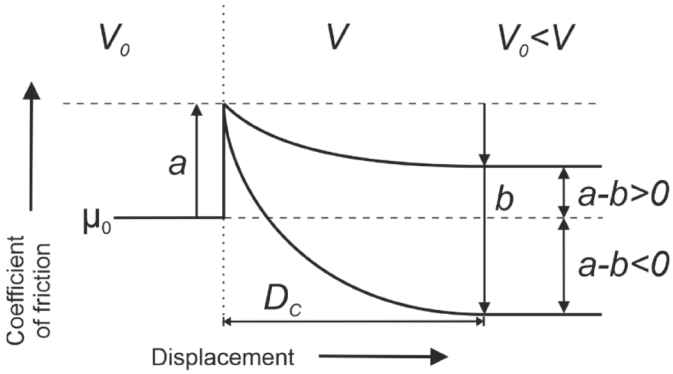

Figure 1.6: Schematic diagram explaining the friction parameters and the concept of velocity weakening and strengthening (modified after Scholz, 1998).

To derive the friction parameters *a*, *b*, and D_C from experimental friction data, Equations 1.2 and 1.3 or 1.4 need to be solved along with a description of the elastic interaction between the frictional surfaces and their surroundings. Neglecting the effect of inertia and assuming the frictional surface to be rigid, a description of a single-degree-of-freedom elastic coupling is sufficient for laboratory experiments (Cook, 1981; Gu et al., 1984; Tullis, 1988; Marone, 1998):

$$\frac{d\mu}{dt} = \frac{k}{\sigma_N}(V_{lp} - V) \tag{1.6}$$

Solving the set of equations is done by inverse modeling (Reinen and Weeks, 1993; Skarbek and Savage, 2019). To extract the purely velocity-dependent frictional behavior, any long-term slip-dependent trends are removed from the data prior to modeling (Blanpied et al., 1998).

According to the critical stiffness theory (Cook, 1981; Gu et al., 1984; Scholz, 1998):

$$k < k_C = \frac{(b-a)\sigma_N'}{D_C} \tag{1.7}$$

frictional slip instability occurs when the fault can release stress faster than the fault surroundings. This condition is satisfied when the stiffness of the fault surroundings *k*, represented by the testing device in the laboratory or wall rock in nature, is smaller than the stiffness of the fault material k_c. The fault material stiffness k_C is defined by the friction parameters *a*, *b*, and D_C under effective normal stress σ_N'. It follows that the condition for slip instability cannot be satisfied by positive values of *a-b* and that negative *a-b* values are a necessary but not sufficient condition for any type of frictional slip instability to occur (Rice and Ruina, 1983; Tullis and Weeks, 1986; Kilgore et al., 1993). Consequently, velocity-strengthening behavior leads to stable, aseismic sliding, whereas velocity-weakening behavior is required for earthquake slip (Marone, 1998; Scholz, 1998). Slow earthquakes envisioned as

a continuum between stable and unstable fault slip are suggested require transitional frictional stability conditions (Dieterich, 1986; Scholz, 1998; Liu and Rice, 2005; Lowry, 2006; Ampuero and Rubin, 2008).

Whether an instability on a fault develops into an earthquake depends on the initial slip patch length *L* of an event (Ohnaka et al., 1986; Dieterich, 1992). If a critical initial slip patch length L_C is reached, the instability dynamically propagates and evolves into an earthquake. If *L* is smaller than L_C, slow slip events may occur. The value of L_C is derived from Equation 1.7 combined with a description of the wall rock stiffness k as the ratio of the wall rock's shear modulus *G* and *L* (Dieterich, 1992):

$$L_C = \frac{G\,L}{(b-a)\sigma_N'} \tag{1.8}$$

To apply the concept of frictional behavior and stability to nature, laboratory friction experiments are utilized to validate the constitutive laws and investigate the frictional behavior under a wide range of conditions relevant to faulting. Up to now, it has been shown that frictional behavior depends on numerous variables, including temperature, normal stress, the presence and thickness of a gouge layer, mineral composition, grain size and shape, humidity, pore-fluid pressure, shear velocity and strain, stiffness contrast, and roughness of the frictional surfaces. In spite of their empirical nature and the problem of scaling them from the laboratory to nature (e.g. Marone, 1998), RSF laws are capable of describing the full range of observed fault behaviors, such as earthquake nucleation, coseismic rupture, earthquake afterslip, slow earthquakes, and stable sliding (Dieterich, 1986; Tse and Rice, 1986; Marone et al., 1990; Liu and Rice, 2005). In addition, the laws have been used to model systematic variations in seismic behavior. The variation most relevant to this work is the depth of seismic faulting, where shallow, unconsolidated material is velocity strengthening and stably sliding and deeper consolidated and/or cemented material is velocity-weakening and prone to unstable sliding (e.g. Tse and Rice, 1986; Marone and Scholz, 1988).

1.5 Motivation and research questions

To assess the seismic and tsunamigenic hazard of a subduction zone, knowledge of the seaward shallow limit of the seismogenic zone is essential because this limit largely controls the extent of coseismic rupture and slip during an earthquake. However, despite extensive work within and between different geophysical disciplines, this updip limit is still poorly constrained for most subduction zones. This is in part due to the challenging nature of such investigations: It is difficult to learn from past events because of the generally long intervals between large events on a fault. In addition, the resolution of geodetic data to

sufficiently monitor crustal deformation at the shallow portion of the subduction zone is still too small due to generally low coverage by offshore GPS stations. Furthermore, samples from fault zones for friction testing are scarce.

Based on laboratory experiments, it has long been recognized that the velocity-dependent friction behavior, the parameter crucial for the estimation of fault slip behavior and thus seismic potential, changes over the different domains of the slip velocity range found during the earthquake cycle (from plate rate of 10^{-9} m/s to coseismic slip of 10^{1} m/s) (Shimamoto, 1986; Blanpied et al., 1987; Kilgore et al., 1993; Tsutsumi and Shimamoto, 1997; Beeler, 2009). Testing at plate rate is of particular relevance because it represents the natural driving condition for major faults. The velocity-dependent frictional behavior at these velocities can give valuable information on the nucleation of fault slip instabilities. However, most laboratory experiments only cover velocities higher than 10^{-7} m/s. Recently, laboratory friction experiments on rare shallow fault zone samples performed at driving velocities approximating plate rates revealed the seismic potential of various shallow faults as well as the potential of shallow slow slip events (Ikari et al., 2015a; Ikari and Kopf, 2017). These results have raised the question of whether other shallow faults also reveal a similar potential when sheared at velocities approximating plate rates.

To contribute to the knowledge and understanding of the seismic potential of shallow subduction zone faults, the aim of this thesis was to investigate the intrinsic velocity-dependent frictional behavior of material relevant to subduction zones. Since testing at driving velocities starting from plate rates has been shown to be crucial for these investigations, I used laboratory shear devices at MARUM, which are capable of shearing at such low velocities. I studied two subduction zone settings, for which the updip limit of their seismogenic zone has not yet been constrained, but which are of specific interest since the coastal population is dense (Fig. 1.1). One of these is the Cascadia subduction zone, located along the west coast of North America, which has been shown to bear high tsunamigenic potential (Satake et al., 1996) and where a major earthquake event is about to be due (e.g. Wang and Tréhu, 2016). Another setting is the North Sumatra subduction zone, a part of the Sunda subduction zone and the location of recent large earthquakes and tsunamis, including the devastating 2004 Aceh-Andaman event with unexpectedly shallow coseismic slip (Ammon et al., 2005; Bletery et al., 2016). Since samples directly from the fault zones of these settings are limited to non-existing, I made use of samples recovered from the sedimentary columns that are input to these subduction zones (details in Chapter 2) – specifically to the northern Cascadia and to the North Sumatra subduction zone regions. In particular, this thesis aimed to answer the following research questions:

1) Are the northern Cascadia and the North Sumatra subduction zones seismogenic all the way to the trench?

2) If not, are other shallow fault slip phenomena such as slow slip events or coseismic rupture propagation to be expected?

Investigations on the North Sumatra subduction zone showed that hydrous amorphous silica may play an important, yet little investigated role in the shallow fault slip behavior of this particular setting. Thus, I performed another set of experiments on synthetic mixtures of hydrous amorphous silica and shale in order to answer the following questions:

3) What is the influence of hydrous amorphous silica on the shallow seismic fault slip behavior of the North Sumatra and also other subduction zones?

1.6 Outline and author contributions

Based on the directions of topics, I divided my thesis into four chapters:

This chapter (**Chapter 1**) introduces the reader to the phenomenon and characteristics of subduction zone earthquakes, as well as to the discrepancy between the seismogenic zone model and the occurrence of shallow large earthquakes, and why this is relevant. In addition, the physics behind different types of earthquakes are explained in short. Furthermore, this chapter highlights the essential role of laboratory friction experiments and empirical laws in earthquake research. Finally, the specific motivation behind this thesis and the research questions can be found here.

Chapter 2 focusses on the importance of subduction zone input sediments for investigations on their seismic potential, especially in the absence of fault zone material. It includes two subsections, which represent two manuscripts on the results of laboratory friction experiments at velocities including plate rate, performed on input material to the northern Cascadia and the North Sumatra subduction zone. In the subsection on the northern Cascadia subduction zone (Manuscript 1), we show that the shallow megathrust fault at this subduction setting is likely not seismogenic but coseismic rupture propagating from a deeper earthquake may be possible. The second subsection on the North Sumatra subduction zone (Manuscript 2) reports on pronounced unstable slip in input lithologies linked to the predécollement. These results show that a shallow seismogenic zone at North Sumatra is possible, which could be the cause of the shallow seismic slip during the 2004 Aceh-Andaman earthquake. A major finding is that hydrous amorphous silica may be responsible for the unstable sliding character of the tested lithologies and that a systematic study of this effect is needed to test this hypothesis.

Manuscript 1 is published in revised form in the Journal *Earth and Planetary Science Letters* (doi: 10.1016/j.epsl.2021.117297). Matt Ikari had the idea for this project and together with me designed the project and the experimental program. Matt Ikari provided the sediment samples

and I prepared them for laboratory testing. I performed the laboratory shear experiments on all samples, including cohesion tests, velocity step tests, and plate rate tests. I processed and modeled the raw data in collaboration with Alexander Roesner to obtain values for coefficients of sliding friction, coefficients of peak friction, cohesion coefficients, and the rate-dependent parameter *a-b*. I visualized the data and created the figures. Alexander Roesner provided the map of the study area. The data were analyzed by me and Matt Ikari. I wrote the manuscript. Matt Ikari strongly revised and Alexander Roesner commented on the manuscript.

Manuscript 2 is based on my idea. I designed the project and the experimental program with supervision by Matt Ikari. Andre Hüpers provided the sediment samples as well as the opal samples, and I prepared them for laboratory testing. I conducted the laboratory shear experiments on all samples, including cohesion tests and velocity step tests. I processed and modeled the experimental raw data to obtain values for coefficients of sliding friction, coefficients of peak friction, cohesion coefficients, and the rate-dependent parameter *a-b*. Furthermore, I carried out porosity measurements on both intact and consolidated powdered samples. I visualized and analyzed the data. I created the figures and wrote the manuscript. Matt Ikari revised and Andre Hüpers commented on the manuscript.

Chapter 3 represents Manuscript 3 and demonstrates the potential of small amounts of opal, hydrous amorphous silica, to induce potentially unstable frictional behavior in clay-rich material. The implications of this finding is that for subduction zones with fault-forming input materials, that contain critical amounts of hydrous amorphous silica shallow seismogenesis, slow slip, and rupture propagation are possible. We show that the viscous behavior of frictional contacts of hydrous amorphous silica is responsible for the potentially unstable frictional sliding behavior.

Manuscript 3 is based on my idea and experimental design. I prepared the samples for laboratory testing. I performed the velocity step tests, and processed and modeled the experimental raw data to obtain coefficients of sliding friction, coefficients of peak friction, and the rate-dependent parameter *a-b.* Additionally, I conducted porosity measurements on all samples. I visualized and analyzed the data. Matt Ikari provided guidance and support throughout the project, especially for mathematical relations of variables influencing the friction parameter *a*. I created the figures and wrote the manuscript. Matt Ikari revised the manuscript.

Chapter 4 provides the answers to the research questions of this thesis. It combines the main findings of the different studies and discusses the broader implications for future earthquake research.

2 The role of input sediments in investigating megathrust fault slip behavior

Since subduction zone earthquakes result from frictional instability of megathrust faults, it is crucial to study the frictional properties of the fault material. To that end, sampling and testing of the fault material would be ideal. However, megathrust faults are often located at great depths, which makes it challenging to obtain samples, as also I experienced myself during IODP cruise 358. This was the last of many expeditions during the ~10 years long Nankai Trough Seismogenic Zone Experiment (NanTroSEIZE) project, dedicated to drill the megathrust of the Nankai Trough subduction zone at seismogenic depths, which ultimately proved unsuccessful. The complex internal architecture of an accretionary wedge and its chaotic small-scale stress fields pose extreme challenges to the drilling process. Consequently, such deep and difficult drilling targets not only demand immense financial, time-consuming, and organizational efforts, but also often remain unreached. Therefore, laboratory investigations of frictional properties largely rely on samples from drilling targets that can be reached with less difficulties but still hold crucial information on the fault slip behavior of a subduction zone setting. These drill targets are exhumed, ancient subduction zone faults, megasplay faults which are long thrust faults connecting the megathrust fault with the sea floor, and the sedimentary column on the subducting plate. Samples from such sites have been extensively used in laboratory friction experiments, for example the Shimanto Belt, Japan (e.g. Schumann et al., 2014; Trütner et al., 2015), the Nankai Trough megasplay fault, Japan (Ikari et al., 2009a; Ujiie and Tsutsumi, 2010; Ikari and Saffer, 2011; Tsutsumi et al., 2011; Roesner et al., 2020), and sedimentary column seaward of the Hikurangi Trench, New Zealand, the Nankai Trough, Barbados subduction zone, Cascadia subduction zone, Costa Rica subduction zone, or the Japan Trench (Ikari and Saffer, 2011; Ikari et al., 2013, 2018; Kopf, 2013; Rabinowitz et al., 2018; Seyler et al., 2020).

The undeformed marine sedimentary column represents the input to a subduction zone and thus delivers valuable information on the incipient physical, mechanical, and hydrogeological properties of the material forming the megathrust/décollement. Although these incipient properties can be affected by temperature-, pressure-, and time-dependent processes that act towards the deformation front and further towards seismogenic zone, they can deliver valuable information on the intrinsic frictional behavior of the material and thus provide important boundary conditions (e.g. Underwood, 2007; Ikari et al., 2018). Furthermore, knowledge of the incipient properties of input sediments is important to determine the stratigraphic locus of the décollement (megathrust fault) and thus frictional behavior and subduction zone geometry. In settings where the décollement has not been drilled, studying input material can also be used to determine the stratigraphic position of the décollement and

ground-truth the interpretation of seismic reflection images that connect the input sample site with the subduction zone.

The stratigraphic architecture and mineralogical compositions of the individual lithologies exert first-order controls over contrasts in strength, permeability, and fluid flow both prior to and during subduction (Underwood, 2007). Megathrust faults likely form within weak stratigraphic intervals (e.g. Moore, 1989), as a result of low cohesion and intrinsic frictional strength (Ikari et al., 2013, 2018; Kopf, 2013) and/or by elevated pore-fluid pressure that reduces the normal stress (Hubbert and Rubey, 1959; Byerlee, 1990; Faulkner and Rutter, 2001; Tobin and Saffer, 2009; Rowe et al., 2012). The subduction-zone stratigraphy is divers among different subduction zones (Underwood and Moore, 1995), but also individual subduction zones reveal marked along-strike heterogeneity (Underwood, 2002, 2007). Therefore, it is vital to study each subduction zone region individually. However, with each new region studied, finding more systematics in the factors controlling megathrust fault formation and fault slip behavior becomes more likely.

2.1 Laboratory friction studies on subduction zone input sediments

2.1.1 The northern Cascadia subduction zone

Implications for megathrust slip behavior and pore pressure at the shallow northern Cascadia subduction zone from laboratory friction experiments (Manuscript 1)

Katja Stanislowski, Alexander Roesner, Matt J. Ikari

MARUM – Center for Marine Environmental Sciences, and Faculty of Geosciences, University of Bremen, Leobener Str. 8, 28359 Bremen, Germany

Abstract

Geological records of past megathrust earthquakes on the Cascadia subduction zone give a valid reason to assume that another event will occur in the future. Both the magnitude and tsunamigenic potential of such an earthquake depend on the extent of seismic rupture and slip on the shallow megathrust, which are still under debate for Cascadia. The absence of shallow slow slip events at northern Cascadia has recently been interpreted to result from a megathrust that is locked and potentially seismogenic all the way to the trench. A crucial factor

controlling both the nucleation and propagation of an earthquake is the frictional slip behavior of the material in the fault system, of which little is currently known for this setting. Here, we report on laboratory friction experiments on all major lithologies of Juan de Fuca plate sediments being input to the northern Cascadia subduction zone. The material was obtained from cores recovered during Integrated Ocean Drilling Program Expedition 301 at Site U1301 in the depth range of 65 to 260 meters below the seafloor. From tests on both intact and powdered samples under in-situ effective normal stress and room temperature, we observe a significant decrease in friction coefficient from 0.76 to 0.19 with increasing depth. A frictionally weak hemipelagic illite-rich unit located directly above the basement is expected to host the décollement upon subduction. This unit reveals predominantly velocity-strengthening frictional behavior at slip velocites of ~10^{-9} to 10^{-4} m/s, and exhibits no slow slip events in the laboratory, indicating a frictionally stable material. Coulomb wedge modeling based on our friction measurements and interpretation of décollement stratigraphic location suggests significant overpressure on the décollement near the trench. Our data offer a possible explanation for the lack of shallow slow slip activity on the northern Cascadia plate-boundary fault, and raise the possibility that the megathrust is not locked near the trench.

Introduction

The densely populated west coast of North America faces the hazard of a future large-magnitude earthquake and associated tsunami along the extent of the Cascadia subduction zone (Fig. 2.1.1a). Although there has never been an instrumentally-recorded earthquake with a moment magnitude M_w > 7.5 at Cascadia, geological studies of earthquake-related deposits (e.g. Goldfinger et al., 2012) demonstrate the history and size of past megathrust earthquakes and tsunamis. The last major event (M_w ~9) was dated to 26 January 1700 by a historically-documented tsunami hitting the east coast of Japan (Satake et al., 1996). Recurrence intervals of paleoseismic events that ruptured the entire length of the subduction zone are estimated to range on average from 300-600 years (e.g. Goldfinger et al., 2012). Based on these estimates as well as geodetic measurements, the Cascadia subduction zone is currently assumed to be in a late stage of its interseismic period, with a megathrust event possibly reaching the trench being imminent (e.g. Wang and Tréhu, 2016).

To assess earthquake hazard it is crucial to know the seaward limit of coseismic rupture and slip propagation on the subduction zone plate boundary (e.g. Hyndman & Wang, 1995). Generally, earthquakes nucleate in a depth range of ~10-40 km on the plate boundary, known as the seismogenic zone (e.g. Hyndman et al., 1997). In this work, we refer to the seismogenic zone as the depth interval of the plate-boundary or megathrust fault where large-magnitude earthquakes nucleate. This portion of the megathrust is capable of frictional locking resulting in interseismic strain accumulation via crustal deformation, which is released coseismically by

rupture of and slip along the fault during earthquakes (Kanamori and Brodsky, 2001). However, coseismic rupture and slip may propagate outside of the seismogenic zone, beyond the updip limit of frictional locking as seen during the 2011 Tohoku-Oki earthquake (Loveless and Meade, 2011; Sun et al., 2017).

Although the Cascadia subduction zone is well studied, at the northern region offshore Washington and British Columbia the updip extent of the seismogenic zone cannot unambiguously be constrained (e.g. Wang and Tréhu, 2016). Because the plate interface is seismically nearly quiet (Obana et al., 2015), estimates so far are based on elastic models using geodetic data (e.g. Hyndman and Wang, 1995; Schmalzle et al., 2014). However, the resolution of offshore crustal deformation in existing elastic models suffers from a lack of offshore geodetic measurements (e.g. Pollitz and Evans, 2017). Potential evidence for a frictionally fully locked and potentially seismogenic shallow megathrust offshore Vancouver Island was recently interpreted from the observed lack of shallow slow slip activity (McGuire et al., 2018).

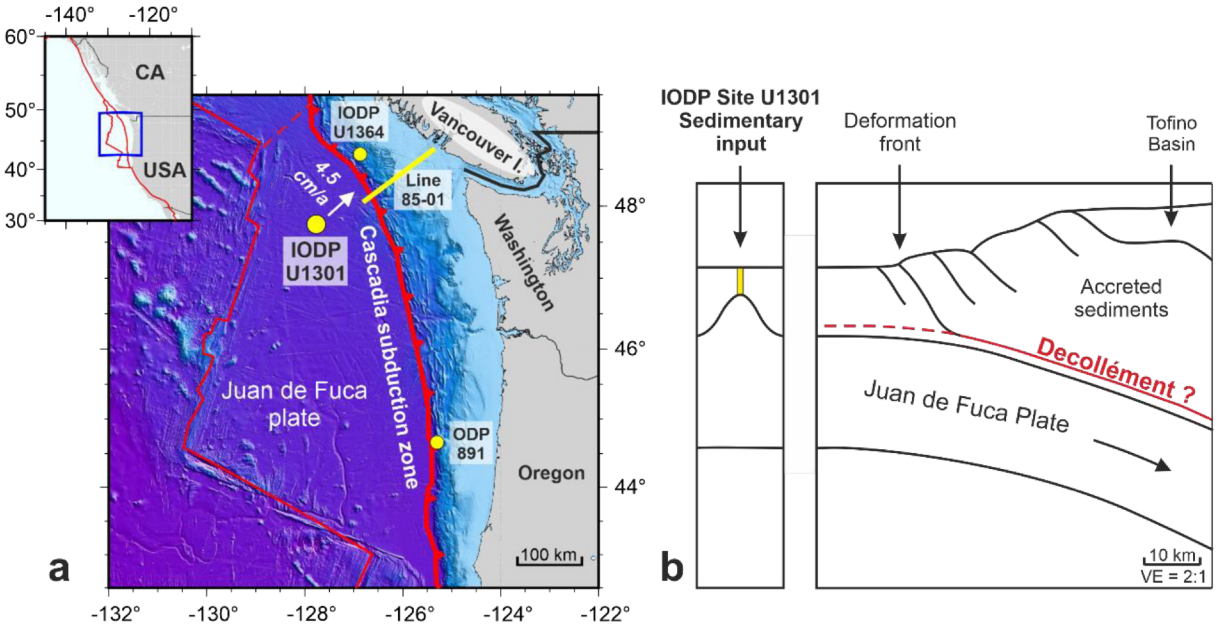

Figure 2.1.1: a) Bathymetric map of the Cascadia Basin and locations of IODP Site U1301, IODP Site U1364, ODP Site 891, and multichannel seismic line 85-01; red lines mark plate boundaries. b) Schematic drawing of interpreted features across the northern Cascadia subduction zone as well as IODP Site U1301 located above a local basement high in the Cascadia basin (modified after Hyndman et al., 1990).

An important factor controlling the depth interval of frictional plate locking is the frictional slip behavior of the material in the fault system, where unstable slip occurs in regions of fault locking (Scholz, 1998). Laboratory shearing experiments investigating frictional strength and

its evolution with slip velocity, are a powerful tool to determine the frictional stability of fault zone sediment under controlled boundary conditions. Both the depth ranges of frictional stability regimes and the strength of the fault are strongly influenced by pore-fluid pressure levels on the fault (Scholz, 1998). Since the updip limit of the seismogenic zone is unconstrained for the northern Cascadia subduction zone, identifying the fault's frictional slip behavior and strength may deliver valuable information for the improvement of elastic models and pore pressure estimation, as well as for comparisons along-strike and with other subduction zones. However, these aspects of the northern Cascadia megathrust are so far not well constrained, due to a lack of experimental friction data. Because the plate-boundary décollement has not yet been drilled or cored, fault zone material is not available to investigate its frictional properties. Furthermore, the stratigraphic position of the décollement estimated from seismic reflection data (Davis and Hyndman, 1989; Hyndman et al., 1990) and therefore its lithological composition has not yet be verified through structural observations on sediment cores.

In this study, we investigate the slip behavior of the shallow plate-boundary fault between the Juan de Fuca plate and North American plate offshore Vancouver Island by performing laboratory shearing experiments on major lithologies recovered from Site U1301 (Fig 2.1.1a), drilled during Integrated Ocean Drilling Program (IODP) Expedition 301. The sediments at this site represent the input material to the subduction zone (Fig. 2.1.1b) and, given the unavailability of fault zone material, provide crucial information to predict how geomechanical properties and behavior develop during subduction (Underwood, 2007; Ikari et al., 2013). The goals of this work are to: (1) identify the lithological unit of Cascadia Basin sediments expected to host the plate-boundary décollement offshore Vancouver Island, (2) constrain the pore-fluid pressure on the décollement, (3) determine how the shallow plate boundary is expected to slip, and (4) gain insight into the current locking state of the shallow plate boundary.

Geological setting

Cascadia subduction zone

The Cascadia subduction zone is located off the west coast of North America, spanning 1100 km from northern California to southern British Columbia (Fig. 2.1.1a). The Juan de Fuca plate has been underthrusting the North American plate since the Eocene (Hyndman et al., 1990), forming a large accretionary prism between northern Oregon and southern Vancouver Island (Fig. 2.1.1b). At the northern portion of the Cascadia subduction zone, the Juan de Fuca plate moves toward southern Vancouver Island at a rate of 4.5 cm/yr (Riddihough, 1984). The overlying sediments, the Cascadia Basin fill, can be divided into two main lithological units: a

rapidly-deposited Pleistocene turbidite section originating from highly active submarine canyons, overlying a pre-Pleistocene seismically-transparent unit of primarily fine-grained hemipelagic sediments (Kulm and von Huene, 1973; Davis and Hyndman, 1989). Just seaward of the deformation front, the pre-Pleistocene sediment section is 1.5 km thick, and the Pleistocene section is approximately 1.7 km thick. Seismic imaging indicates that the plate boundary forms within the pre-Pleistocene sediments along landward-dipping thrust faults that end in a main décollement near the basement of the subducting Juan de Fuca plate (Davis and Hyndman, 1989; Hyndman et al., 1990) (Fig.2.1.1b). The accretionary prism exhibits a low taper angle near the deformation front, which Davis & Hyndman (1989) suggested may result from high pore-fluid pressures imposed by rapid Pleistocene sedimentation. The Cascadia subduction zone is relatively warm, likely a consequence of the very young age of the oceanic plate (7 Ma) and the insulating effect of a very thick sediment section (Davis and Hyndman, 1989; Hyndman and Wang, 1993, 1995). Heat flow modeling estimated temperatures of ~250°C at the base of the sedimentary sequence near the deformation front offshore Vancouver Island (Hyndman and Wang, 1993).

IODP Site U1301

Site U1301 is located on the western edge of a major Pleistocene distributary channel for turbidites and above a buried basement high (Expedition 301 Scientists, 2005), approximately 100 km seaward from the deformation front (Fig. 2.1.1a, b). The sediment column was discontinuously cored to the basement at 265 meters below seafloor (mbsf). Two major lithostratigraphic sedimentary units were identified (Expedition 301 Scientists, 2005), confirming the seismically-identified units of Davis & Hyndman (1989) (Fig. 2.1.3a). The upper unit is divided into two subunits. Unit IA (0-13 mbsf) is composed of clay with interbedded silty clay turbidites and sandy layers. Unit IB (13-236 mbsf) consists of interbeds of silt to sand turbidites, hemipelagic clay, and gravel beds. Unit II (236-265 mbsf) is predominantly hemipelagic clay (Fig. 2.1.3a). The basement age was determined to be 3.5 Ma and the temperature at the top of the basement was estimated to be 62°C (Expedition 301 Scientists, 2005).

Sample description

For our laboratory shearing experiments, we selected a total of six mineralogically-distinct samples from depths of 64 to 260 mbsf, which were obtained from cores recovered from Holes C and D (Tab. 2.1.1, Fig. 2.1.3a). The samples cover the mineralogical variability of the two major lithostratigraphic units of hemipelagic clay and (silty) sand turbidites found at the drill site. The mineralogical composition of the six samples was measured using X-Ray

Diffraction (XRD) following Vogt et al. (2002) (Table 2.1.1). The two uppermost samples, sand turbidites from Unit IB at 64 and 93 mbsf, consist of > 50 wt% plagioclase and quartz, and < 35 wt% phyllosilicates. The other four samples, hemipelagic clays from Units IB and II at 120-260 mbsf, contain < 40 wt% plagioclase and quartz with a total phyllosilicate content ranging from 29-52 wt%. Hemipelagic samples with lower phyllosilicate content tend to have larger amounts of calcite, up to 36 wt%. Illite is the most abundant phyllosilicate mineral, constituting 27 wt% of the hemipelagic sample from 260 mbsf.

Table 2.1.1: Sample details and composition in weight percent from X-Ray diffraction measurements (abundances ≥5 wt%)

Hole	Sample	Depth (mbsf)	Lithostr. Unit	Lithology	quartz	plagioclase	orthoclase	calcite	amorphous SiO_2	mixed layer clays	illite	muscovite	glauconite	chlorite	Sum phyllosilicates
C	8H-2	64.3	I B	Sand turbidite	27	40	11	-	-	-	-	-	-	5	12
C	11H-2	92.8	I B	Sand turbidite	20	33	-	-	-	-	6	6	6	12	35
D	1H-1	120	I B	Hemipelagic clay	11	18	-	-	-	17	14	-	6	7	52
D	15H-4	185	I B	Hemipelagic clay	8	14	-	36	-	-	9	-	8	-	29
C	17H-2	238	II	Hemipelagic clay	17	21	-	7	-	-	10	-	-	12	35
C	19H-3	259.5	II	Hemipelagic clay	10	16	-	11	5	-	27	-	-	6	44

Experiments and modeling

We conducted laboratory shearing experiments on both intact and powdered samples under in-situ effective normal stresses, room temperature (22°C), and drained conditions in the presence of simulated seawater (3.5% NaCl). For intact samples, we selected parts of whole round core segments free from defects and desiccation, and carefully trimmed them to fit the cylindrical sample cell (~2 cm height, 2.5 cm diameter). In our apparatus, the trimmed sample cylinder axis is aligned with the cylinder axis of the drill cores, which is assumed to represent the in-situ direction of vertical overburden. Material that was not suitable for intact sampling was tested only as powdered samples. For their preparation, we air-dried the sediment, disaggregated it with a mortar and pestle, and sieved the material to a grain size < 180 µm. This powder was mixed with simulated seawater to form a stiff paste that was pressed into the sample cell. In-situ effective normal stresses of 0.5-2.2 MPa (Tab. 2.1.2) were calculated by integrating shipboard density measurements over depth. Hydrostatic pore-fluid pressure is assumed for the recovery depth of each sample, as there were no elevated pore-fluid pressures observed within the sediment section (Fisher et al., 2014). Since pore-fluid pressure cannot be measured in our experimental setup, the sample was consolidated for ~24

hours until steady-state sample height was attained, after which we assume that the sample is fully drained so that the applied normal stress equals the effective normal stress. The characteristic diffusion time was calculated to be 11-342 minutes following Ikari et al. (2009b) for the intact clay-rich (44 wt%) sample 19H-3 under in-situ effective normal stress, supporting this assumption (Supplementary Material Eq. S2.1.1).

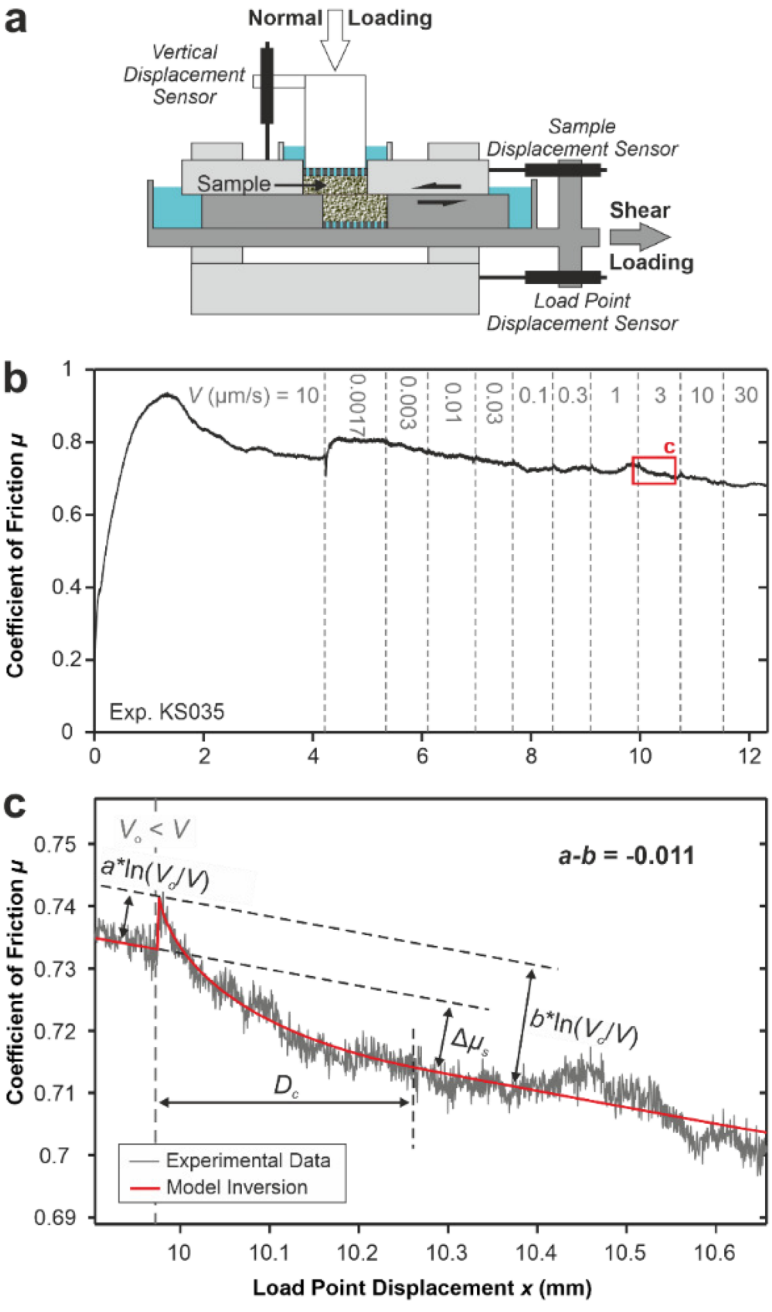

Figure 2.1.2: a) Schematic drawing of the direct shear device used in this study. Dark gray parts of the shearing device move to the right under shear, the light gray parts are stationary. b) Example of experimental data. Red box shows c) the frictional response to the velocity step, with the model inversion (red) superimposed on experimental data (gray).

The shearing experiments were performed using a Giesa RS5 direct-shear device (Fig. 2.1.2a) (see Ikari and Kopf, 2011 for details). In this device, normal stress is applied parallel to the sample cylindrical axis by a vertical piston. A stepper motor drives the bottom part of the shear cell in the horizontal direction at constant rates past the upper half of the cell and perpendicular to the sample cylinder axis, thus forcing the sample to shear along a planar surface. Load point and sample displacement as well as shear stress and normal stress are measured continuously during the experiment. The shear stress τ depends on the coefficient of friction μ of the material, the effective normal stress σ_N', and the cohesion c, as described by the Coulomb-Mohr criterion (Handin, 1969):

$$\tau = \mu\sigma_N' + c \qquad (2.1.1)$$

To be consistent with the majority of previous friction studies, however, we report friction as the apparent coefficient of sliding friction $\mu = \tau / \sigma_N'$ at steady state, and measure cohesion separately.

We began each experiment with the direct measurement of the cohesion (Eq. 2.1.1). The samples were sheared with zero normal stress at 1 µm/s until failure, following the approach of Ikari & Kopf (2011) and Roesner et al. (2020). We report cohesion as the cohesion coefficient χ, calculated from the peak shear stress measured during the cohesion test, divided by the effective normal stress which the sample has seen in-situ (Ikari et al., 2013) (Tab. 2.1.2, Supplementary Material Fig. S2.1.1). The cohesion of intact samples can be measured immediately, whereas powdered samples were consolidated at in-situ effective normal stress prior to the test. After completion of the cohesion test, the shear cell was reset to zero sample displacement, and the in-situ effective normal stress was reapplied. The samples were then initially sheared at a constant rate of 10 µm/s (Fig. 2.1.2b). This so called "run-in" generates a mature shear surface (Dieterich, 1972), mostly within ~5 mm of horizontal displacement. We measure the peak friction μ_P at ~1 mm displacement, and the coefficient of sliding friction μ_S at the end of the run-in (Tab 2.1.2). Following the run-in we performed a velocity step test (VST), during which the shear rate was increased by a factor of three in up to nine near-instantaneous steps from 1.7×10^{-9} m/s (0.0017 µm/s or 5.3 cm/yr) to 3×10^{-5} m/s (30 µm/s) over 0.7-1 mm displacement (Fig. 2.1.2b). Some tests were repeated to check reproducibility (Tab. 2.1.2).

Sliding friction is both velocity and time dependent and can be empirically described by:

$$\mu = \mu_o + a \ln\left(\frac{V}{V_o}\right) + b_1 \, ln\left(\frac{V_o \theta_1}{D_{c1}}\right) + b_2 \, ln\left(\frac{V_o \theta_2}{D_{c2}}\right) \qquad (2.1.2)$$

where a, b_1, and b_2 are unitless constants, μ_o is the initial steady-state friction coefficient, V_o and V are the sample shear velocities before and after the velocity step, θ_1 and θ_2 are state variables having units of time, and D_{c1} and D_{c2} are the critical slip distances over which friction evolves to a new steady state (Dieterich, 1981; Marone, 1998). Obtaining individual parameters describing the frictional behavior requires a description of state evolution (Dieterich, 1981):

$$\frac{d\theta_i}{dt} = 1 - \frac{V\theta_i}{D_{ci}} \;, \; i = 1, 2. \qquad (2.1.3)$$

Given steady state before and after the velocity change, Equations 2.1.2 and 2.1.3 can be simplified to:

$$a - b = \frac{\Delta\mu_{ss}}{\Delta lnV} \quad (2.1.4)$$

where $\Delta\mu_{ss}$ is the change in steady-state friction coefficient upon an instantaneous change in sliding velocity, and $b = b_1 + b_2$ if two state variables are used (Marone, 1998).

Table 2.1.2: Experiment details and results.

Exp.	Sample	Sample depth (mbsf)	Sample condition	Eff. normal stress (MPa)	shearing velocity (μm/s)	Test type	Cohesion coeff. χ	Coeff. of peak friction μ_p at 10 μm/s	Coeff. of sliding friction μ_S at 10 μm/s	Coeff. of sliding friction μ_S at 5.3 cm/yr
KS020	8H-2	64.3	powdered	0.5	0.06	Cohesion	0.06			
KS034	8H-2	64.3	intact	0.5	0.06	Cohesion	0.18			
KS014	8H-2	64.3	powdered	0.5	0.1-30	VST		0.64	0.65	
KS021	8H-2	64.3	powdered	0.5	0.0017-30	VST		0.68	0.65	0.72
KS035	8H-2	64.3	intact	0.5	0.0017-30	VST		0.93	0.76	0.80
KS019	8H-2	64.3	Powdered	0.5	0.0017	Plate rate		0.68	0.69	0.68
KS006	11H-2	92.8	powdered	0.8	0.06	Cohesion	0.08			
KS007	11H-2	92.8	powdered	0.8	0.06	Cohesion	0.08			
KS008	11H-2	92.8	powdered	0.8	0.1-30	VST		0.49	0.46	
KS013	11H-2	92.8	Powdered	0.8	0.0017	Plate rate		0.59	0.55	0.52
KS030	1H-1	120	intact	1.1	0.06	Cohesion	0.12			
KS040	1H-1	120	powdered	1.1	0.06	Cohesion	0.19			
KS032	1H-1	120	intact	1.1	0.0017-30	VST		0.33	0.26	0.32
KS041	1H-1	120	powdered	1.1	0.0017-30	VST		0.33	0.30	0.36
KS037	15H-4	185	powdered	1.6	0.06	Cohesion	0.09			
KS038	15H-4	185	powdered	1.6	0.0017-30	VST		0.38	0.25	0.26
KS004a	17H-2	238	powdered	2.0	0.06	Cohesion	0.07			
KS004b	17H-2	238	powdered	2.0	0.1-30	VST		0.35	0.34	
KS005	17H-2	238	Powdered	2.0	0.0017	Plate rate		0.33	0.33	0.36
KS017	19H-3	259.5	intact	2.2	0.06	Cohesion	0.04			
KS022	19H-3	259.5	powdered	2.2	0.06	Cohesion	0.01			
KS003	19H-3	259.5	powdered	2.2	0.1-30	VST		0.31	0.21	
KS018	19H-3	259.5	intact	2.2	0.0017-30	VST		0.30	0.25	0.27
KS024	19H-3	259.5	powdered	2.2	0.0017-30	VST		0.28	0.19	0.23
KS095	19H-3	259.5	powdered	2.2	0.0017-30	VST		0.31	0.21	0.28
KS046	19H-3	259.5	powdered	2.2	0.0017	Plate rate		0.31	0.20	0.22
KS049	19H-3	259.5	powdered	19.0	0.0017	Plate rate		0.27	0.21	0.27

The rate-dependent friction parameter *a-b* in Equation 2.1.4 describes the response of the steady-state friction coefficient of a material to a velocity perturbation. Positive values indicate that the material strengthens with increasing velocity, meaning that stable slip is expected. If *a-b* is negative, the material weakens with increasing velocity, which, along with specific stiffness conditions of the fault surroundings, is necessary for any type of frictional slip instability to occur (Marone, 1998; Scholz, 1998). To obtain *a-b* and other rate-dependent parameters, we use inverse modeling of the frictional response to a velocity step (e.g. Skarbek and Savage, 2019) (Fig. 2.1.2c). In order to model each velocity step, we remove background trends in friction from our data (Blanpied et al., 1998) to isolate the velocity-dependent frictional response from changes in friction-slip dependence.

For the hemipelagic sample 19H-3 from 260 mbsf, we performed two additional experiments on powdered material, one at 2.2 MPa (in-situ) and one at 19 MPa effective normal stress (Tab. 2.1.2), which is near the upper vertical stress limit of our apparatus. Following the run-in, the sample was sheared at the plate-rate velocity of ~5 cm/yr over a horizontal displacement of 2 mm to simulate plate convergence and evaluate the ability of the sediment to produce unstable slip events under laboratory conditions. In previous experiments using the same device, natural fault zone sediments capable of producing laboratory slow slip events (SSEs) exhibited such events well before 2 mm (Ikari, 2019). Additionally, plate rate tests at effective normal stresses were performed for several other lithologies for comparison (Tab. 2).

Results

We observe a consistent and marked decrease in the coefficient of sliding friction from 0.76 to 0.19 throughout the tested depth range of 64-260 mbsf (Fig. 2.1.3b, Tab. 2.1.2). Intact samples of the sand turbidite from 64 mbsf (8H-2) and the hemipelagic clay from 260 mbsf (19H-3) exhibit values of μ_S of 0.76 and 0.25, which are 0.11 and 0.04-0.06 higher than their powdered equivalents, whereas the intact sample of the hemipelagic clay from 120 mbsf (1H-1) shows a μ_S value of 0.26, which is 0.04 lower than the powdered version. Thus, the effect of powdering the samples is a strength reduction of 14% for the sand turbidite and of 16-24% for hemipelagic clay from 260 mbsf, and a strength increase of 15% for the hemipelagic clay from 120 mbsf. Measured coefficients of peak friction μ_p range from 0.93 to 0.28, and exhibit a decrease with depth very similar to that of the sliding friction (Tab. 2.1.2). For the hemipelagic clays from 120 and 260 mbsf, intact and powdered samples show little to no difference (≤0.02) in peak friction. However, the sand turbite from 64 mbsf reveals a difference of 0.25-0.29, where the higher peak friction of the intact sample reaches a value of 0.93.

In our experiments, cohesion coefficients χ range from 0.01 to 0.19 (Fig. 2.1.3c, Tab. 2.1.2). We observe the lowest values in the hemipelagic clay from 260 mbsf, with χ = 0.04 for the intact sediment and 0.01 for the powdered equivalent. The two high cohesion coefficients are obtained for powdered hemipelagic clay from 120 mbsf with χ = 0.19 and the intact sand turbidite from 64 mbsf with χ = 0.18.

The two turbidite samples, both powdered and intact, show predominantly velocity-weakening behavior, with *a-b* ranging from -0.031 to 0, whereas the other sediments, powdered and intact, exhibit predominantly velocity-strengthening behavior (Fig. 2.1.3d, Supplementary Material Tab. S2.1.1). The frictionally weakest sediment, the lowermost hemipelagic clay, shows only velocity-strengthening frictional behavior, with *a-b* values ranging from 0 to 0.006 and little difference between intact and powdered samples (Fig. 2.1.4a). For this lithology, we notice a general trend of increasing *a-b* as a function of increasing shearing velocity. However, all experiments on this hemipelagic clay exhibit a minimum in *a-b* value at 0.1 µm/s. In more detail, the parameter *a* ranges from 0.001 to 0.009 and shows a dependence on slip velocity that is similar to that of *a-b* (Supplementary Material Fig. S2.1.2a). Values of the parameter *b* range from -0.003 to 0.008 and exhibit a slightly decreasing trend with velocity (Supplementary Material Fig. S2.1.2b).

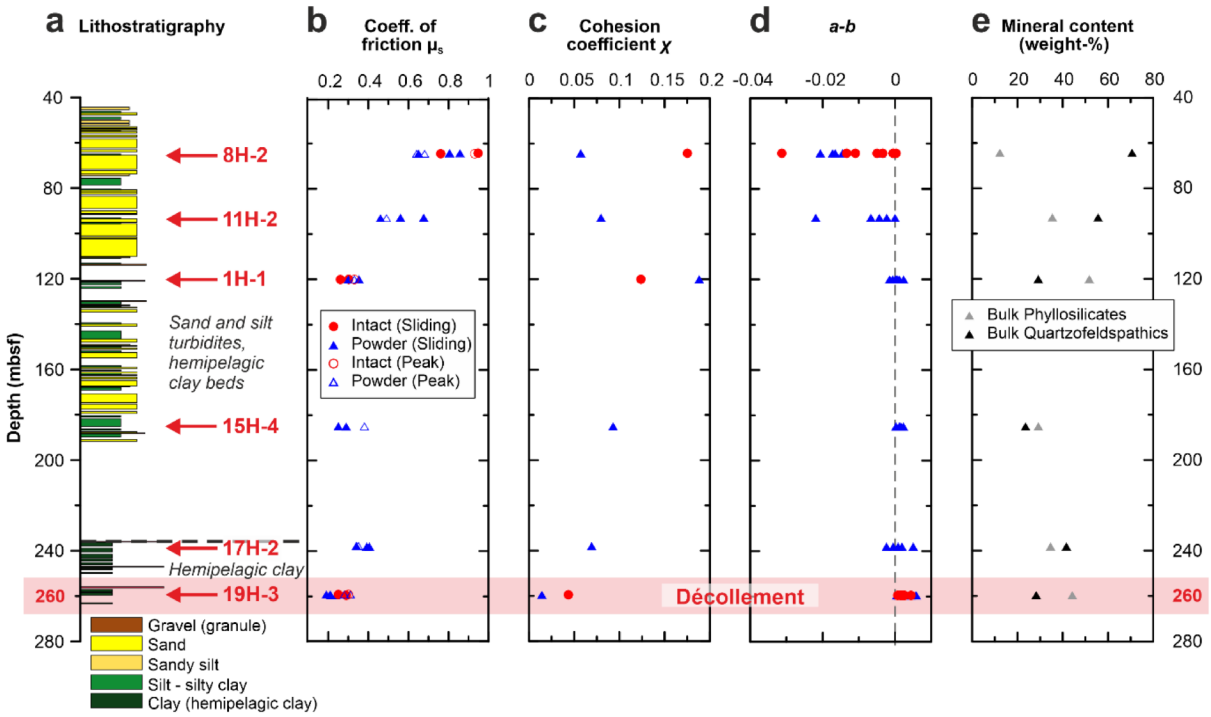

Figure 2.1.3: a) The lithostratigraphic column of IODP Site U1301 (Expedition 301 Scientists, 2005), b) the coefficients of peak and sliding friction, c) the cohesion coefficient, d) the velocity-dependent friction parameter a-b, and e) the weight percentage of total phyllosilicates and total quartzofeldspatic minerals from XRD measurements.

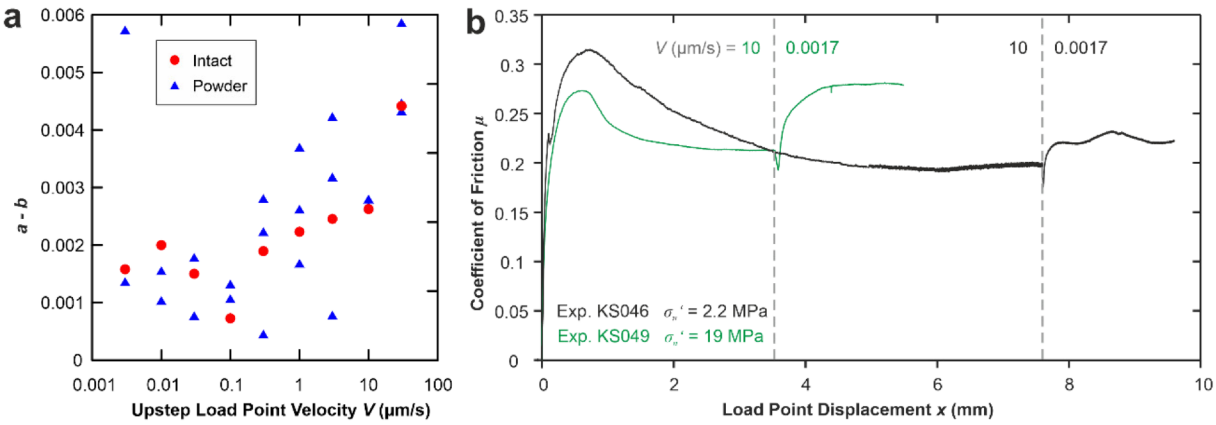

Figure 2.1.4: Results of tests on material from 260 mbsf (19H-3). a) The velocity-dependent friction parameter a-b at 2.2 MPa effective normal stress, and b) tests sheared at plate rate (5.3 cm/yr) for 2 mm displacement under 2.2 (in-situ) and 19 MPa effective normal stress.

When driven at ~5 cm/yr under 2.2 MPa (in-situ) effective normal stress, the μ_S value obtained from a powdered sample of hemipelagic clay from 260 mbsf is comparable to that measured at 10 µm/s (Fig. 2.1.4b, Tab. 2.1.2). The same test at the elevated effective normal stress of 19 MPa shows sliding friction of 0.21 at 10 µm/s, and 0.27 at ~5 cm/yr (Fig. 2.1.4b, Tab. 2.1.2). No perturbations in shear stress resembling slow slip events were observed in any test conducted at the near plate-rate velocity.

Discussion

Lithostratigraphic position of the décollement

Plate-boundary faults are expected to develop in zones of weakness, either due to strata containing weak minerals (e.g. Underwood, 2007) or elevated pore-fluid pressures lowering the effective normal stress (Hubbert and Rubey, 1959; Saffer and Tobin, 2011). The frictionally weakest materials we tested are encountered in the hemipelagic clay packages at around 120 mbsf (1H-1), and at around 260 mbsf (19H-3) near the top of the basaltic basement of the Juan de Fuca plate. These samples have low coefficients of sliding friction ($\mu_S \leq 0.3$) both intact and as powders (Fig. 2.1.3b, Tab. 2.1.2). Higher cohesion and coefficients of sliding friction are observed in intact compared to powdered samples from 260 mbsf, possibly due to diagenesis.

The two frictionally weak lithologies also have relatively high total phyllosilicate contents of 52% (sample from 120 mbsf) and 44 wt% (sample from 260 mbsf) (Fig. 2.1.3e, Tab. 2.1.1), which is consistent with the well-known observation from laboratory experiments that clay minerals are associated with low friction coefficients (Lupini et al., 1981; Morrow et al., 1992;

Tembe et al., 2010). For binary mixtures of clay and quartz, previous experimental work has determined friction coefficients of 0.35-0.55 for 40-50 % kaolinite under 50 MPa effective stress and water saturation (Crawford et al., 2008) and of 0.44-0.50 for 50 % illite measured at 40 MPa effective normal stress (Tembe et al., 2010). Friction coefficients of the samples from 120 and 260 mbsf are markedly lower than the values for mixtures from those studies. This discrepancy may either result from a difference in tested normal stress, or from other clay minerals in our samples, such as the significant amount of mixed-layer clays (17 wt%) for the sample from 120 mbsf, compared to 2 wt% for the sample from 260 mbsf. Laboratory friction experiments on mixtures of 50-75 % quartz with 25-50 % of equal parts of illite and montmorillonite, a first approximation of mixed-layer clays (Morrow et al., 1992), reveal friction coefficients of 0.2-0.35 at 40 MPa effective normal stress (Tembe et al., 2010), matching the value for our sample measured at ~1 MPa. Friction coefficients of both samples, from 120 and 260 mbsf, also compare well with those measured on samples from the Nankai Trough décollement. This material has a total clay content of 40-60 % and shows friction coefficients of 0.20-0.24 at 25 MPa effective normal stress (Ikari and Saffer, 2011).

The apparent coefficients of sliding friction of samples from 120 and 260 mbsf are very similar, with only a difference of 0.01. However, besides using the apparent coefficient of sliding friction to determine the stratigraphic position of the décollement as done in other input studies, the coefficient of peak friction may also be relevant, because fault formation depends on the initial breakage of the material. Since the coefficient of peak friction for the intact sample from 260 mbsf is 0.03 lower than that of sample from 120 mbsf (Tab. 2.1.2), the lithology at 260 mbsf is more prone to initial failure. Furthermore, based on seismic imaging across the accretionary prism offshore Vancouver Island, the position of the décollement is interpreted to be located directly above the oceanic crust (Davis and Hyndman, 1989; Hyndman et al., 1990), which implicates the lowermost lithology represented by sample from 260 mbsf. Taken together, we propose that the weak, lower part of the hemipelagic strata found between 235 and 265 mbsf at IODP Site U1301 is the most likely candidate to host the plate-boundary fault upon subduction (Fig. 2.1.5a, b).

Pore-fluid pressure estimates from Coulomb wedge analysis

The strength of the décollement together with the pore-fluid pressure and strength of the wedge control the shape of accretionary wedges (Dahlen, 1990). This relation can be described by a critically-tapered, non-cohesive Coulomb wedge model, which is simplified by the assumption that the pore-fluid pressure in the wedge is equal to that on the décollement. According to Dahlen (1990), the model is expressed as:

$$\alpha + \beta = \frac{1}{2} arcsin\left(\frac{\sin(\varphi_b')}{\sin(\varphi_w)}\right) - \frac{1}{2}\varphi_b' - \frac{1}{2} arcsin\left(\frac{\sin(\alpha')}{\sin(\varphi_w)}\right) - \frac{1}{2}\alpha' \quad (2.1.5)$$

with

$$\alpha' = arctan\left(\frac{1 - \frac{\rho_f}{\rho}}{1 - \lambda}\tan(\alpha)\right) \quad (2.1.6)$$

$$\varphi_b' = \arctan(\mu_b) \quad (2.1.7)$$

where α is the surface slope angle, β the décollement dip angle, φ_w, and φ_b are the friction angles of the wedge and the décollement, ρ_f is the pore-fluid density, and ρ the bulk density of the accretionary wedge. The pore-fluid pressure ratio λ usually ranges from ~0.4 for hydrostatic to 1 for lithostatic pressure conditions, and is defined as (Hubbert and Rubey, 1959; Saffer and Tobin, 2011):

$$\lambda = \frac{p_f}{\sigma_v} \quad (2.1.8)$$

where σ_v is the total overburden and p_f the absolute pore-fluid pressure.

For northern Cascadia, values for α and β were obtained from interpretations of multichannel seismic line 85-01 offshore Vancouver Island, migrated and interpreted by Davis & Hyndman (1989) (Fig. 2.1.1a, 2.1.5b). They found that the morphology of the continental slope is variable, where α is 3.5° on average, and 1-2° for the trench-most lower slope. The décollement dip angle β continuously increases from 3° in Cascadia Basin, to 6° behind the deformation front, to 11° below the continental shelf. Given our experimental conditions, we focus on the lower slope and therefore choose α = 1-2° and β = 4-6° to be consistent with Davis & Hyndman (1989). We set the fluid density ρ_f to be 1 g/cm³ and the bulk density ρ of the accretionary wedge offshore Vancouver Island to be 2.36 g/cm³ for the portion that lies directly underneath the surface of the lower slope. This value is based on the assumption of an average porosity of 20% for the first 6 km below seafloor (Yuan et al., 1994), which is the maximum depth of the décollement below the lower continental slope (Fig. 2.1.5b).

Davis & Hyndman (1989) used the critical Coulomb wedge model (Eq. 2.1.5) and estimated near-lithostatic pore-fluid pressures with λ > 0.9 for the trenchmost wedge portion at northern Cascadia. However, they assumed a basal friction coefficient μ_b of 0.85, and an average friction coefficient of the wedge material μ_w of 1.03. Based on our measurements on natural input sediments to the northern Cascadia subduction zone, the actual friction coefficients are much lower. Because the material within the accretionary wedge has undergone deformation, we use coefficients of sliding friction instead of peak friction for our calculations. The friction coefficient of the shallow décollement, as represented by the value

measured on the sample from 260 mbsf (19H-3) at ~5 cm/yr shearing velocity and 19 MPa effective normal stress, is μ_b = 0.27 (Tab. 2.1.2). The value at plate rate is chosen, since it approximates long-term in-situ conditions best.

The strength of the accretionary wedge is more difficult to estimate because of the wide range of measured friction coefficients at plate rate (μ_S = 0.26-0.80) for the tested sediments being input to the wedge (Fig. 2.1.3b, Tab. 2.1.2). Initially, we perform Coulomb wedge modeling using Equation 2.1.5 with endmember friction values μ_w = 0.27 and 0.80, where the lower value is slightly higher than the measured minimum to satisfy the model with a μ_b of 0.27. However, the model with the lower value of μ_w is not able to match the wedge geometry, and the model with the higher value yields subhydrostatic pore pressures (λ < 0.4), which is unrealistic (Supplementary Material Fig. S2.1.3). Therefore, we need to inform the Coulomb wedge model with more realistic values of μ_w that better represent the wedge lithologic composition.

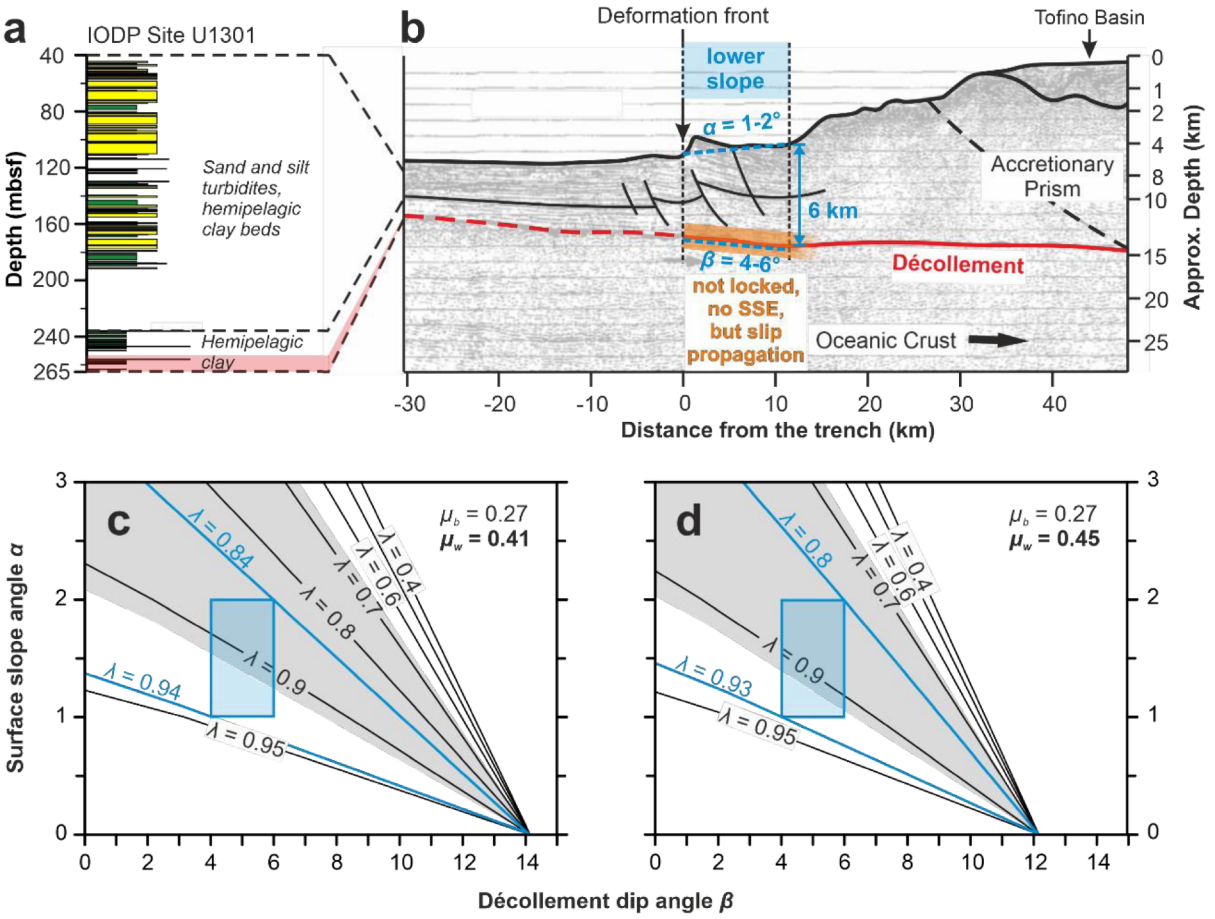

Figure 2.1.5: a) The lithology hosting the décollement upon subduction (red), and b) the migrated and tectonically interpreted time section of multichannel seismic line 85-01 (Fig. 2.1.1a) off southern Vancouver Island (Davis and Hyndman, 1989), with interpretations based on our laboratory measurements. Plots at the bottom: Surface slope angle α versus décollement dip angle β for various

uniform pore pressure conditions for a critically tapered accretionary wedge as predicted by the model of Dahlen (1990) with a décollement friction μ_b of 0.27 and with wedge material having a coefficient of friction μ_w of c) 0.41 and d) 0.45. Light blue boxes indicate the northern Cascadia accretionary prism geometry with angles of décollement dip and surface slope adopted from Davis & Hyndman (1989). Shaded gray areas indicate the pore pressure range calculated from effective friction coefficients of previous studies (Wang and He, 1999; Gao and Wang, 2014).

The sedimentary column just seaward of the deformation front is known to consist of the two main lithostratigraphic units in nearly equal proportion (Kulm and von Huene, 1973; Davis and Hyndman, 1989). Therefore, we perform another Coulomb wedge analysis using a value for μ_w that is the average of the friction coefficients of both units above the assumed décollement. We employ the following approach: for the portion of the hemipelagic unit, we have one measurement on a powdered sample from 238 mbsf (17H-2). For the turbiditic unit consisting of both turbidite deposits and clay, we calculate the mean of friction coefficients using values measured on powdered samples from 64, 93, 120 and 185 mbsf. Next, from the mean value for the turbiditic unit and the single value for the hemipelagic unit we calculate a mean value for the entire wedge sequence, which is 0.41. To account for the difference in friction coefficient between powdered and intact samples, where our intact samples exhibit on average 0.04 higher friction coefficients than our powdered samples, we use μ_w = 0.41 and 0.45 for modeling. We apply these values to calculate the pore-fluid pressure ratio λ for a critically-tapered Coulomb wedge using Equation 2.1.5.

The Coulomb wedge model based on a more realistic wedge composition using our averaged wedge friction coefficients yields λ ranging from 0.84-0.94 for μ_w = 0.41, and λ ranging from 0.80-0.93 for μ_w = 0.45 (Fig. 2.1.5c, d). These results show that, given the friction values and assumed stratigraphic décollement position from this study, significant and possibly near-lithostatic pore pressure is likely. This is consistent with the interpretation of high pore-fluid pressure near the basal décollement from the observation of low fault dip angles (Davis and Hyndman, 1989). However, the choice of the wedge friction coefficient can have a large effect on the estimated pore pressure ratios. For example, models with $\mu_w \geq 0.55$ cover almost the entire range of possible λ values, therefore it should be noted that our results should be treated with caution.

We now compare our pore pressure values with those obtained from estimates of effective basal friction for the northern Cascadia subduction zone from previous studies. The comparison can be done via the effective friction coefficient μ', which describes the effect of pore-fluid pressure on the coefficient of friction μ, and is defined as (Wang and He, 1999):

$$\mu' = \mu(1 - \lambda) \qquad (2.1.9)$$

Modeled values of μ' = 0.03-0.09 for the décollement offshore Washington (Wang and He, 1999) correspond to λ = 0.67-0.89. Heat flow modeling at northern Cascadia yielded an effective coefficient of basal friction of 0.024 (Gao and Wang, 2014), representing λ = 0.91. These pore pressure estimates are in good agreement with our calculations (Fig. 2.1.5c, d), indicating that the input parameters for our Coulomb Wedge analysis are realistic. Our calculated overpressure ratios λ = 0.80-0.94 result in remarkably low values of μ' = 0.02-0.05 for the interpreted décollement sediment. If the model input parameters are accurate, our measurements suggest that the shallow northern Cascadia décollement offshore Vancouver Island is not only hosted in intrinsically weak sediment, but may also be substantially overpressured. Like all models, the model we used to predict pore pressure is a simplification. In particular, the assumptions of a non-cohesive, homogenous accretionary wedge and of constant pore-fluid pressure are not necessarily supported by our observations. Nevertheless, the model may help further constrain the hydrogeological setting of the northern Cascadia subduction zone.

Slip behavior of the shallow plate boundary

Northern Cascadia

In the tested sedimentary section, friction velocity dependence (as quantified by the parameter *a-b*) increases with depth, while the coefficient of sliding friction (as measured during the run-in phase at constant sliding velocity) generally decreases (Fig. 2.1.3d, b). This can be explained by the general decrease in the amount of strong, quartzofeldspathic minerals with depth (Fig. 2.1.3e), which have a tendency to exhibit velocity-weakening friction (Logan and Rauenzahn, 1987; Tembe et al., 2010; Ikari et al., 2011a). Given that we interpret the hemipelagic clay package from 260 mbsf (19H-3) to host the décollement upon subduction, we focus on its friction velocity dependence to evaluate the slip behavior on the shallow megathrust. Our tests reveal that this sediment consistently exhibits velocity-strengthening friction both as intact and powdered material. Velocity-strengthening behavior favors aseismic stable sliding and inhibits earthquake nucleation because of a negative stress drop suppressing the generation of accelerating slip (Scholz, 1998). Consequently, slip instabilities are not expected to nucleate at the shallow depths of Cascadia plate boundary targeted in this study.

However, an important factor for frictional stability is temperature. Thermal modeling suggests temperatures of 250-300°C on the shallow Cascadia megathrust at ~3-6 km depth (Hyndman and Wang, 1993). Such high temperatures could lead to a different frictional behavior compared to our observations at room temperature. The most abundant mineral in our potential décollement sample is illite (27 wt%; Tab. 2.1.1). Laboratory friction experiments

on illite-rich gouge (59 and 70 wt%) indicate that temperatures comparable to those on the shallow Cascadia megathrust can induce a change from velocity-strengthening to velocity-weakening friction (Moore et al., 1989; den Hartog et al., 2012). These studies, however, employed effective normal stress conditions of 170 MPa (den Hartog et al., 2012) and 50-250 MPa (for tests at 200°C) (Moore et al., 1989). This range of effective normal stresses is unlikely to be expected in the geological setting targeted in this study, if we consider high pore-fluid pressure near the basal décollement as interpreted from the observation of low fault dip angles (Davis and Hyndman, 1989) as well as our Coulomb wedge analysis. Aseismic slip behavior of the shallow northern Cascadia megathrust can therefore not be ruled out.

On the contrary, McGuire et al. (2018) suggested that the shallow northern Cascadia megathrust might be currently locked. Their suggestion is based on the lack of slow slip events (SSEs) in recently obtained data from a borehole observatory at IODP Site U1364 located above the shallow megathrust (Fig. 2.1.1a). This observation contrasts with those at the downdip end of the seismogenic zone (e.g. Rogers and Dragert, 2003) as well as at the shallow portions of other subduction zones, such as the Nankai Trough (Araki et al., 2017). However, the occurrence of SSEs requires the frictional behavior of the fault interface to be unstable, or near the transition from stable to unstable (Liu and Rice, 2005; Leeman et al., 2016), provided sufficient shear stress for failure of the fault. Our results show that the interpreted plate-boundary fault material exhibits consistently velocity-strengthening behavior, suggesting that the shallow megathrust cannot generate slip instabilities, and may not be capable of frictional locking. In some cases, however, laboratory SSEs have been reported from plate-rate tests on both velocity-weakening and velocity-strengthening samples of other shallow subduction zones, which resemble natural SSEs of these geological settings in concise characteristics (Ikari, 2019). Numerical modeling studies also show that SSEs are possible in velocity-strengthening material in under certain conditions (Perfettini and Ampuero, 2008; Kanu and Johnson, 2011). Therefore, we additionally performed plate rate tests of longer slip displacement (2 mm) at both in-situ and 19 MPa effective normal stress (Fig. 2.1.4b, Tab. 2.1.2). Based on our estimated pore pressure ratios of λ = ~0.80-0.94, our 19 MPa experiment would approximate in-situ stress conditions at ~4-14 km depth (Eq. 2.1.8), which includes the 4.5 km depth of the plate boundary beneath the U1364 borehole observatory (Yuan et al., 1994; McGuire et al., 2018). However, we did not observe SSEs in any of our experiments. Based mainly on our observations of velocity-strengthening behavior and partially because SSEs are neither observed in the borehole observatory at the near-trench region of northern Cascadia, nor in our laboratory experiments conducted at plate-rate driving velocities, we suggest that the shallow megathrust is unlikely to be able to produce SSEs. Our findings raise the possibility that the lack of slow slip activity is a consequence of a frictionally stable fault, rather than frictional locking (Fig. 2.1.5b).

We do however acknowledge that the shallow megathrust could lie within the updip stress shadow of the locked fault patch and therefore may be kept from slipping (e.g. Hetland and Simons, 2010). This possibility is consistent with several elastic models based on onshore geodetic data allowing interseismic creep close to the deformation front (e.g. Schmalzle et al., 2014). In this case, the frictional behavior of the shallow plate interface may not necessarily explain the geodetic observations and models. Nevertheless, because the elastic models rely on land-based geodetic measurements, it is not conclusive as to whether the shallow megathrust fault at the northern Cascadia subduction zone lies in a stress shadow.

Although our data suggest that the shallow northern Cascadia megathrust is unlikely to generate ordinary or slow earthquakes, it is not clear how far coseismic slip nucleating on the deeper seismogenic portion of the plate boundary can propagate updip. Provided sufficient shear stress on the shallow megathrust (Lu et al., 2010), several of our observations support the hypothesis that coseismic slip propagation may be relatively easily facilitated (Fig. 2.1.5b). These include: (1) the low intrinsic frictional strength at low (this study) and also high slip velocities (Faulkner et al., 2011; Seyler et al., 2020), (2) the material's relatively low cohesion (Ikari et al., 2015b), and (3) the estimated high pore-fluid pressure (Hubbert and Rubey, 1959; Saffer and Tobin, 2011).

Comparison with southern Cascadia and Nankai Trough

The results of our work contrast with observations from the southern Cascadia subduction zone offshore central Oregon. There, some shallow tremor activity has been reported (Wech and Creager, 2011). In the laboratory, SSEs were observed for fault zone material from the frontal thrust in the prism toe (ODP Site 891, Fig. 2.1.1a) at 10 MPa effective normal stress and 5.3 cm/yr driving velocity using the same shear device (Ikari, 2019). These laboratory SSEs support the hypothesis of Wech & Creager (2011) that the observed tremor accompanies yet-undetected natural SSEs in this region. The differences between our experimental results for the northern subduction zone compared with the southern part of the margin are consistent with other previously reported along-strike differences at the Cascadia subduction zone (Underwood, 2002; Brudzinski and Allen, 2007; Han et al., 2017). The southern Cascadia subduction zone material differs markedly from the northern potential décollement sediment in its mineralogical composition. For example, the frontal thrust sample from southern Cascadia tested by Ikari (2019) has a quartz+feldspar content of 55 wt%, which is much higher than that of the hemipelagic clay sample tested here (28 wt%, Tab. 2.1.1, Fig. 2.1.3e). Since these minerals have been shown to have a negative friction-velocity dependence (Logan and Rauenzahn, 1987; Scruggs and Tullis, 1998; Ikari et al., 2011a), we interpret that their abundance could explain the unstable, velocity-weakening behavior for the

southern Cascadia material, as opposed to the stable, velocity-strengthening behavior for the northern Cascadia material.

McGuire et al. (2018) also point out that the response of the updip end of the Cascadia subduction zone offshore Vancouver Island to stress perturbations appears to be very different compared to, for example, the Nankai Trough. There, fluid pressure changes recorded by borehole observatories indicated the occurrence of triggered SSEs in the shallow accretionary prism (Araki et al., 2017). Correspondingly, laboratory friction experiments driven at 6.3 cm/yr under 10 MPa effective normal stress showed laboratory SSEs in a sample from the megasplay fault zone (Ikari, 2019), which is a candidate host for the shallow Nankai SSEs (Araki et al., 2017). The contrast between northern Cascadia and the Nankai Trough can therefore broadly be attributed to the differences in frictional behavior. Whereas our experiments document consistent velocity strengthening in input sediment likely hosting the décollement of the northern Cascadia subduction zone, recent experiments on samples recovered from shallow fault zones in the Nankai Trough reported mainly velocity-weakening behavior under in-situ conditions (Roesner et al., 2020). Like the southern Cascadia sample, the tested Nankai Trough fault materials also generally consist of more quartzofeldspathic minerals (31-54 wt%) compared to our potential décollement material at northern Cascadia (28 wt%, Tab. 2.1.1, Fig. 2.1.3e) (Shipboard Scientific Party, 2001; Expedition 316 Scientists, 2009a, 2009b), which have a tendency for velocity weakening (Logan and Rauenzahn, 1987; Scruggs and Tullis, 1998; Ikari et al., 2011a). Consequently, based on mineral content, the Nankai Trough fault zone materials may be more prone to unstable sliding than the northern Cascadia hemipelagic sample we tested, and may therefore explain the observed differences in frictional behavior.

Conclusions

We measured the frictional strength and rate-dependent frictional behavior of input sediments to the northern Cascadia subduction zone using laboratory shearing tests primarily under in-situ effective normal stress of up to 2.2 MPa on intact and powdered samples. Our results support the inference that the décollement forms in the frictionally weak illite-rich hemipelagic sediments located just above the top of the oceanic basement at IODP Site U1301. This lithology displays solely velocity-strengthening behavior at tested driving velocities within ~10^{-9} (plate rate) to 10^{-4} m/s. No laboratory SSEs were observed at effective normal stresses up to 19 MPa. Together, these observations suggest that, in the absence of a stress shadow, the shallow northern Cascadia megathrust is frictionally stable and may not necessarily be locked. Coulomb wedge modeling based on our friction measurements indicates significant overpressures in excess of ~80% of the lithostatic load on the shallow

décollement. Despite its velocity-strengthening behavior, a combination of low sliding friction, low cohesion, and high pore-fluid pressures implies that coseismic slip from a deep-seated earthquake may easily propagate updip through the shallow portion of the décollement.

Acknowledgements

We thank Jeff McGuire and Andre Hüpers for helpful discussions. We appreciate the thorough reviews of André Niemeijer and Marion Thomas, which helped improve the manuscript. We thank Achim Kopf for providing laboratory support. This work is based on samples and data provided by the Integrated Ocean Drilling Program (IODP). RSF modeling was performed using the program “xlook”, courtesy of Chris Marone. Financial support was given by the European Research Council (ERC) under the European Union’s Horizon 2020 research and innovation programme Grant #714430 to M. Ikari.

Supplementary

Following Ikari et al. (2009b), the characteristic diffusion time t, which represents the time necessary for fluid pressure to dissipate after a perturbation, is given by:

$$t = \frac{h^2 S}{2k} \quad with \quad S = \gamma_w(\beta_p + \varphi\beta_w) \tag{S2.1.1}$$

where h is sample height (here: 0.015 m), k is the hydraulic conductivity, γ_w is the specific weight of water (9810 N/m³), φ the fractional porosity, β_p is the compressibility of the solid, and β_w is the compressibility of water (here: 4.5895^{-10} m²/N (20°C, 0 MPa) and 4.4725^{-10} m²/N (20°C, 10 MPa) (Fine and Millero, 1973)). We assume a minimum intrinsic permeability of 10^{-17} m² based on samples from the Nankai Trough with similar clay content (Ikari and Saffer, 2012), a porosity of average 55% (Expedition 301 Scientists, 2005), and a compressibility range of 6.9×10^{-8} to 2.1×10^{-6} m²/N for medium hard to plastic clay (Domenico and Mifflin, 1965).

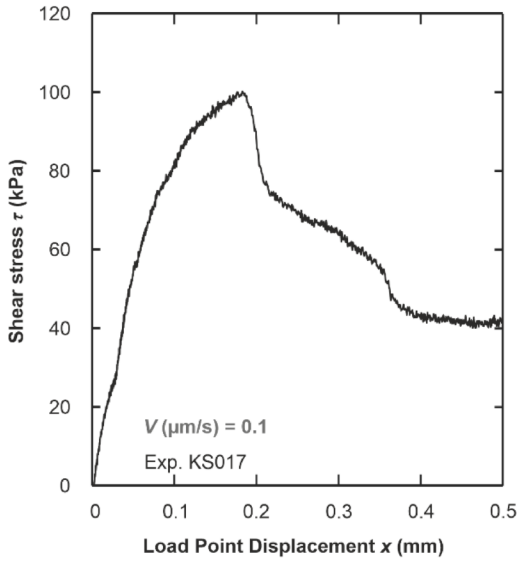

Figure S2.1.1: Data example of a cohesion test.

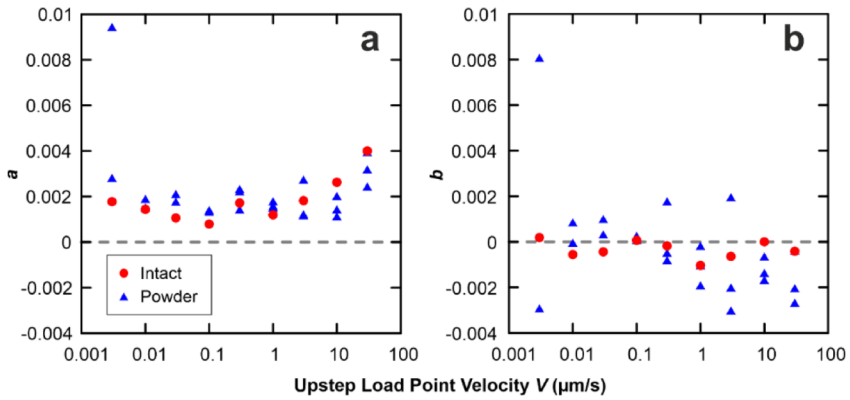

Figure S2.1.2: Rate- and state dependent friction parameter a) a and b) b for experiments on material from 260 mbsf (19H-3) under 2.2 MPa (in-situ) effective normal stress.

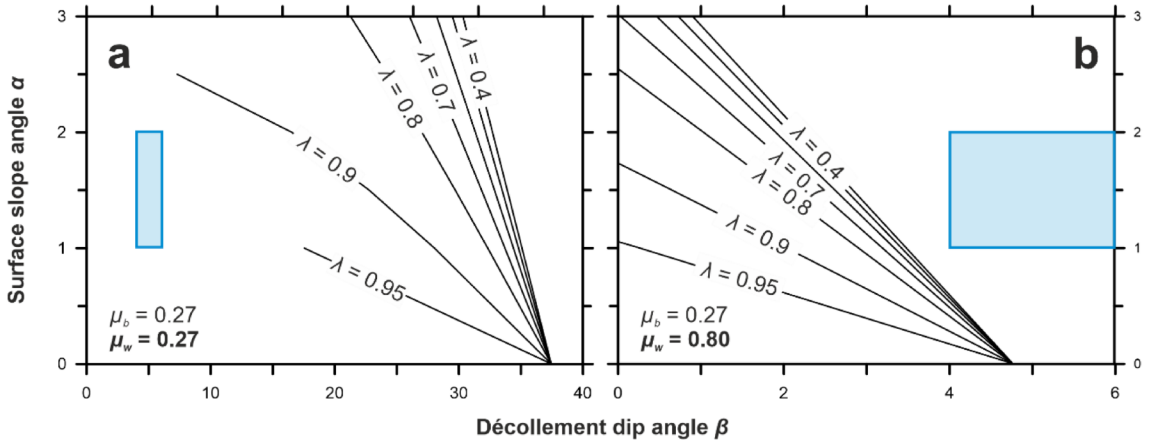

Figure S2.1.3: Angles of surface slope α versus décollement dip β for various uniform pore pressure conditions for a critically tapered accretionary wedge as predicted by the model of Dahlen (1990) with a décollement friction μ_b of 0.27 and with wedge material having a coefficient of friction μ_w of a) 0.27 and b) 0.80. Light blue boxes indicate the northern Cascadia accretionary prism geometry with décollement dip and surface slope angle adopted from Davis & Hyndman (1989).

Table S2.1.1: Rate-dependent friction parameter a-b modeled from velocity step tests for all samples.

			Upstep load point velocity (μm/s)								
Exp.	Sample depth (mbsf)	Sample condition	0.003	0.01	0.03	0.1	0.3	1	3	10	30
KS014	64.3	powdered	-	-		-0.021	-0.016	-0.004	-0.015	-0.017	
KS035	64.3	intact	0.000	0.000	-0.001	-0.005	-0.013	-0.031	-0.011	-0.003	
KS008	92.8	powdered	-	-	-	-	-0.022	-0.007	-0.002	-0.004	0.000
KS041	120	powdered	-0.001	-0.002	0.000		0.001	0.001	0.000	0.002	
KS038	185	powdered		0.002	0.001	0.000		0.000	0.002	0.001	
KS004	238	powdered	-	-	-	-	-0.002	0.000	0.001	0.002	0.005
KS018	259.5	intact	0.002	0.002	0.002	0.001	0.002	0.002	0.002	0.003	0.004
KS003	259.5	powdered	-	-	-	-	0.003	0.003	0.001	0.003	0.004
KS024	259.5	powdered	0.006	0.002	0.001	0.001	0.002	0.002	0.003	0.003	0.004
KS095	259.5	powdered	0.001	0.001	0.002	0.001	0.000	0.004	0.004	0.003	0.006

2.2.2 The North Sumatra subduction zone

Weak but frictionally unstable input sediments as a cause of shallow seismogenesis at the North Sumatra subduction zone (Manuscript 2)

Katja Stanislowski, Andre Hüpers, Matt J. Ikari

MARUM – Center for Marine Environmental Sciences, and Faculty of Geosciences, University of Bremen, Leobener Str. 8, 28359 Bremen, Germany

Abstract

The cause of the unexpectedly shallow seismic slip during the 2004 Aceh-Andaman subduction zone earthquake offshore North Sumatra that resulted in a devastating tsunami is still under debate. It was recently suggested that diagenetic strengthening of décollement-forming input sediments prior to subduction could create a shallow seismogenic zone. However, this hypothesis remains untested because knowledge of the frictional behavior of the shallow décollement is lacking. Using laboratory friction experiments, we show that input sediments to the North Sumatra subduction zone display pronounced frictional instability. Our findings provide evidence for the hypothesis of a frictionally unstable and thus seismogenic shallow décollement, that is however seated in frictionally weak sediments. The combination of weak and unstable sediments is striking due to its deviation from the established frictional strength-stability relation. We propose that threshold amounts of dispersed hydrous amorphous silica in otherwise weak and clay-rich sediments are responsible for an unstable sliding character. Thus, our results hold important implications for the seismicity of shallow subduction zones, where incoming sediment horizons contain critical amounts of hydrous amorphous silica.

Introduction

During the M_w 9.2 Aceh-Andaman subduction zone earthquake in 2004 offshore North Sumatra, seismic rupture and slip extended to the shallow, seaward end of the subduction zone, possibly to the trench (Fig. 2.2.1a) (Ammon et al., 2005; Ishii et al., 2005; Henstock et al., 2006; Banerjee et al., 2007; Bletery et al., 2016). The result was a wide rupture zone and thus a large earthquake with a devastating tsunami (Lay et al., 2005; e.g. Ammon et al., 2005). The extent of seismic slip is largely controlled by the frictional sliding behavior of the plate boundary fault (décollement), which in turn depends on the lithological, mechanical, and hydrogeological properties of the décollement material (Scholz, 1998; Underwood, 2007;

Saffer and Tobin, 2011). For the North Sumatra subduction zone, it was recently suggested that the predécollement sediments experience advanced diagenetic processes (Hüpers et al., 2017), which may change the sediment properties towards facilitating strengthened and unstably sliding sediments (Lockner and Byerlee, 1986; Trütner et al., 2015; Ikari and Hüpers, 2021). Thus, décollement-forming sediments might already be frictionally unstable when they enter the subdcution zone and that can cause shallow seismogenesis (Hüpers et al., 2017).

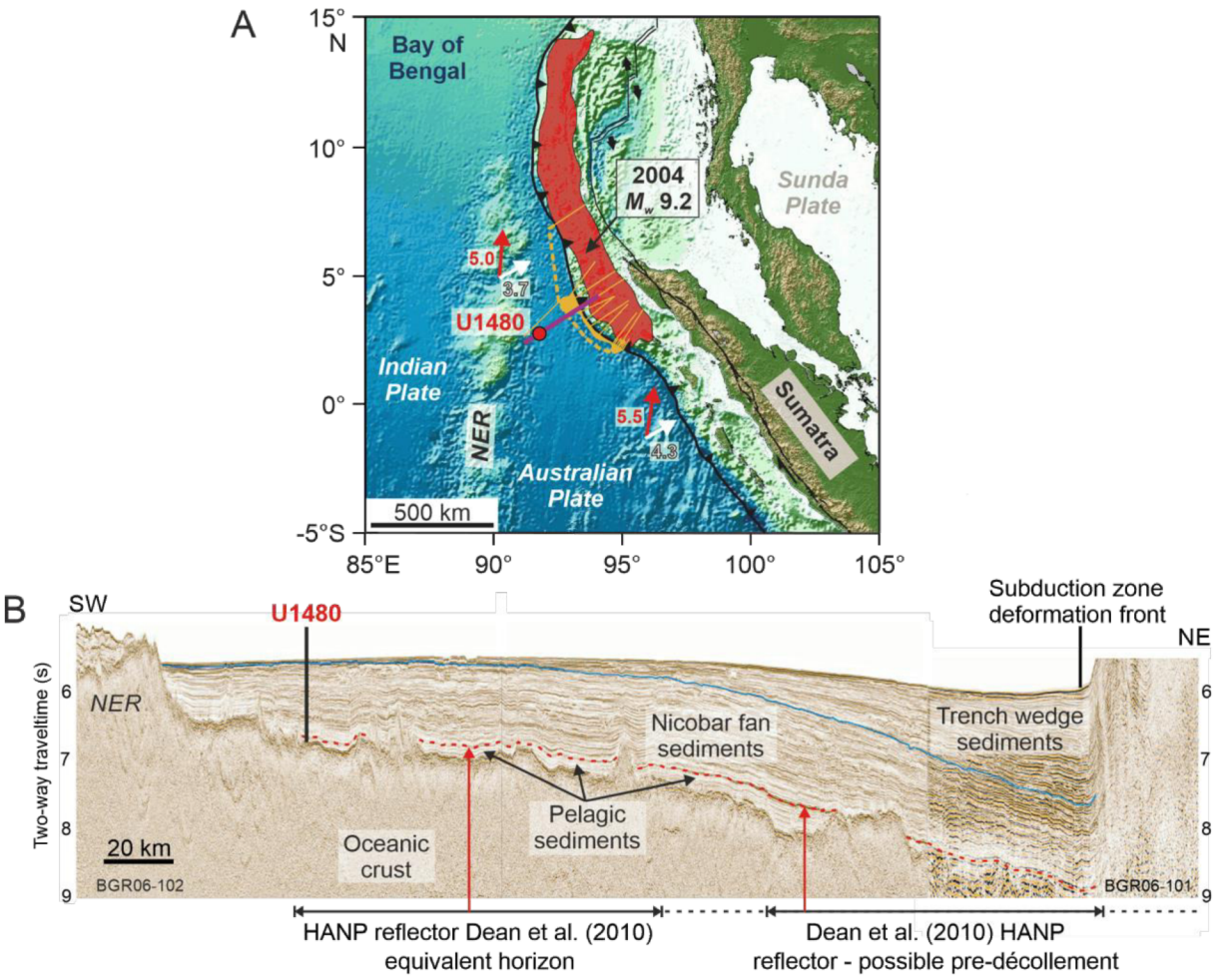

Figure 2.2.1: a) Map showing the study area including the rupture zone of the 2004 earthquake in red (Subarya et al., 2006; Chlieh et al., 2007), and the sampling location IODP Site U1480 (modified after Hüpers et al., 2017). Red and white arrows and numbers (cm/yr) indicate convergence vectors and subduction vectors accounting for forearc motion (McNeill and Henstock, 2014). Yellow lines delineate locations of seismic lines imaging or reporting a HANP reflector (yellow area) (Dean et al., 2010; Singh et al., 2011; Geersen et al., 2013). Dashed yellow line marks the estimated extent of the HANP reflector (Hüpers et al., 2017). The orange line shows the location of b) seismic lines BGR06-102 and -101 (modified after Hüpers et al., 2017). HANP = High Amplitude Negative Polarity, NER = Nintyeast Ridge.

The proposed diagenetic processes include quartz precipitation, smectite-illite transformation, and pore-fluid pressure dissipation. Although the suggestion by Hüpers et al. (2017) contrasts with established models where completion of these processes is expected to occur only within

the subduction zone and shallow décollement is consequently thought be stable (e.g. Moore and Saffer, 2001; Saffer and Tobin, 2011), it is consistent with burial-related dewatering, lithification, and thus strengthening of the incoming sediments inferred in previous work (Gulick et al., 2011; Geersen et al., 2013; Stevens et al., 2021). However, friction data necessary for verification of the hypothesis are lacking.

In the absence of available fault zone material, this work seeks to evaluate the initial mechanical characteristcs of subduction zone input sediments, and their implications for the possibility of a shallow seismogenic zone. For that, we performed laboratory friction experiments and porosity measurements on sediments recovered at IODP Site U1480, which is located 225 km away from the North Sumatran subduction zone. We chose sediment samples between 1250-1360 meters below seafloor (mbsf) covering lithostratigraphic Unit III, which has been correlated with the seaward extension of a high-amplitude negative-polarity (HANP) seismic reflector assumed to represent the protodécollement horizon (Fig. 2.2.1b) (Dean et al., 2010).

Experimental methods

Laboratory friction experiments were conducted in a GIESA *RS5* direct shear device at room temperature and under saturation with simulated sea water (Suppl. Material Fig. S2.2.1). Eight different lithologies across the targeted depth interval were tested as powdered (grain size < 125 µm) and where possible as intact samples (Fig. 2.2.2). X-ray diffraction shows that the non-calcareous samples consist of 28-64 weight (wt) % phyllosilicate minerals, 13-36 wt% quartz + feldspar, and 0-20 wt% nearly amorphous silica (Fig. 2.2.2). Applied normal stresses correspond to vertical hydrostatic effective stresses equivalent to the depth range of sample recovery of 1250-1360 mbsf (~13.00-14.25 MPa). Powdered samples were water saturated and consolidated at respective normal stress, until no further measurable change in thickness, assuming full pore-fluid overpressure dissipation.

In each experiment, the samples were sheared in three successive phases: (1) at a constant velocity V of 10 µm/s for ~5 mm sample displacement x to establish steady state sliding described with the coefficient of sliding friction μ_S, (2) at plate convergence rate (5.3 cm/yr = 1.7×10^{-3} µm/s) for x = 2 mm, and (3) in a sequence of threefold increasing velocity in the range of 0.003-30 µm/s for x = 0.7 mm per velocity (Suppl. Material Fig. S2.2.1). The apparent coefficient of friction μ was calculated from the ratio of the continuously measured shear stress to the applied effective normal stress (Handin, 1969). Where possible, the frictional response to a velocity step was modeled inversely to obtain the velocity-dependent friction parameter $a\text{-}b = \Delta\mu_{SS}/\Delta \ln V$ (Reinen and Weeks, 1993; Skarbek and Savage, 2019) (Suppl. Material Fig. S2.2.1, Fig. 2.2.2). Positive values of $a\text{-}b$ indicate velocity-strengthening

behavior associated with stable slip. Negative values indicate velocity-weakening behavior required for slip instability and thus earthquake nucleation (Dieterich, 1981; Marone, 1998; Scholz, 1998).

In addition, porosity measurements as well as microstructural analyses were carried out on most samples. The latter is not discussed in this work but the most outstanding details are summarized in the Supplementary Material.

Most of our samples had an aspect ratio favoring a side friction effect (or Poisson effect), exerted from the walls of sample cell. This aspect ratio allowed the removal of both sample halves from the cell after shearing, in order to create and analyze thin sections. Although the side friction effect may lead to underestimation of friction strength by more than 5% (Fagereng and Ikari, 2020) for frictionally stronger, powdered samples, the effect on weaker, powdered samples as well as on intact samples is estimated to be minor.

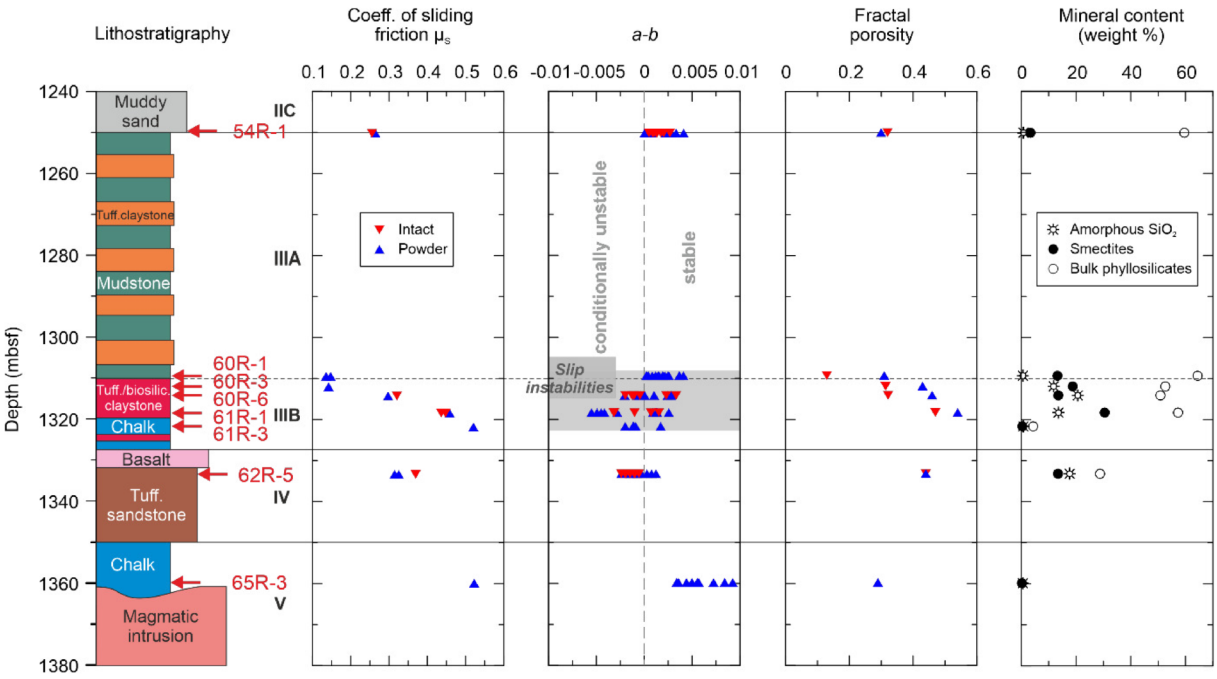

Figure 2.2.2: Lithostratigraphic column (modified after McNeill et al., 2017), coefficient of sliding friction μ_S obtained from experiment phase 1, rate-dependent friction parameter *a-b*, fractal porosity, and specific mineral contents for the tested set of samples. Sample names and depths are indicated by red text and arrows at the lithostratigraphic column.

Mechanical and physical properties

Steady-state coefficients of sliding friction measured at the end of the first shearing phase range from μ_S = 0.14 to 0.52 (Fig. 2.2.2). The highest value is found for the two powdered calcareous samples, the lowest for powdered mudstone from 1309 mbsf (60R-1)

and red silty clay with ash from 1312 mbsf (60R-3). Friction coefficients for intact and powdered samples deviate by maximum 0.05. This small difference could be due to minor lithification as indicated by the measured low cohesion in both sample types (Suppl. Material Fig. S2.2.4) or to discrepancies between applied and in-situ experienced effective normal stress for intact samples.

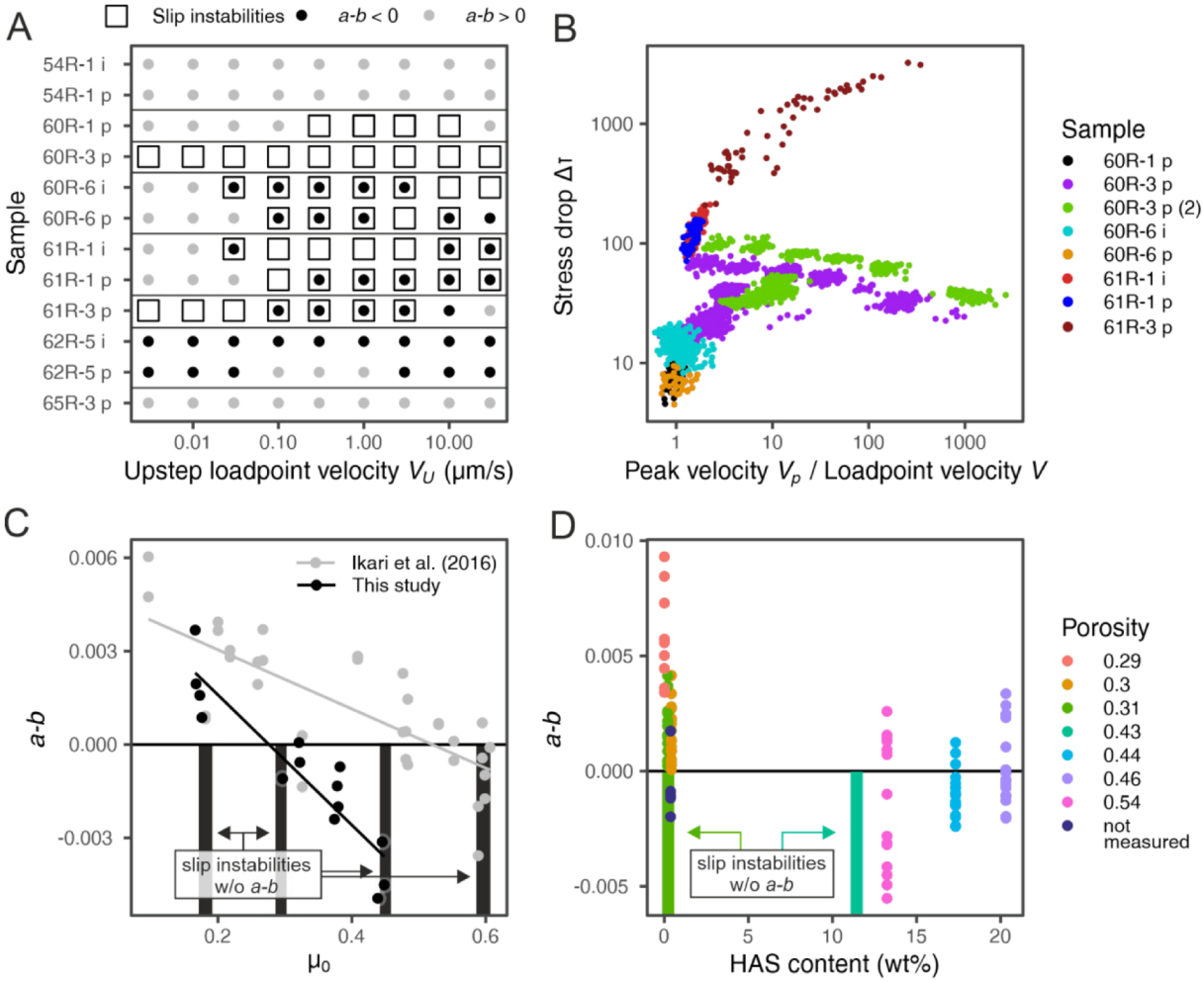

Figure 2.2.3: a) Algebraic sign of friction velocity dependence (*a-b*) and occurrences of slip instabilities versus upstep loadpoint velocity, b) stress drop versus peak slip velocity normalized to loadpoint velocity of slip instabilities, c) *a-b* versus the coefficient of friction (μ_0) obtained at steady state prior to a velocity step for all non-calcareous samples at upstep loadpoint velocities of 3-10 µm/s, d) *a-b* versus weight percentage of hydrous amorphous silica (HAS). i = intact, p = powder.

Both velocity-weakening and -strengthening behavior are observed with values of *a-b* ranging from -0.006 to 0.009 (Fig. 2.2.2). While the mud from 1250 mbsf (54R-1) and the chalk from 1360 mbsf (65R-3) are strictly velocity strengthening and stably sliding, samples that fall into the depth interval of 1309 to 1333 mbsf show (partial) velocity weakening and/or slip instabilities (Fig. 2.2.2, Fig. 2.2.3a). The stress drops of recorded slip instabilities vary markedly between the lithologies, but they all follow a trend of increasing values with increasing peak velocity V_P normalized to loadpoint velocity V (Fig. 2.2.3b) (e.g. Ohnaka et al., 1987). However,

the slope of this trend is variable, especially due to instabilities of chalk from 1322 mbsf (61R-3) with relatively large stress drops and those of red silty clay with ash from 1312 mbsf (60R-3).

Porosities of the undeformed intact samples deviate from those of the undeformed powdered samples by 0 to 18 % (Fig. 2.2.2). We attribute this difference to the desiccation of several intact samples. Therefore, we focus on porosities of the powdered samples. Most samples from the interval that displays (potential) unstable sliding, have high (43-54%) porosities. While the porosities of the other samples (29-32%) fall onto the normal compaction trend (Hüpers et al., 2017), the high porosities of this distinct depth interval far exceed the trend.

Frictional instability of potential décollement sediments

Instances of velocity weakening and/or slip instabilities are recorded for all tested samples from lithostratigraphic Units III and IV (Fig. 2.2.2, 2.2.3a). Unit III has been correlated by previous work with the seaward extension of the HANP seismic reflector assumed to represent the predécollement (Fig. 2.2.1b) (Dean et al., 2010; Hüpers et al., 2017). Therefore, our data show an unstable sliding character of the predécollement material, and possibly of the shallow décollement. The lithology of red silty clay with ash from 1312 mbsf encountered at sample 60R-3 is frictionally unstable even at plate rate and up to the maximum velocity tested in this study (Fig. 2.2.3a). Given its very low friction coefficient (μ_S = 0.14, Fig. 2.2.2), this lithology could likely be the locus of décollement formation upon subduction and be capable of earthquake nucleation even at shallow depths. Two less probable alternatives are the tuffaceous sandstone (62R-5) from 1333 msbf (Unit IV) with a μ_S value of 0.37 (Fig. 2.2.2), which when tested intact exhibits velocity-weakening behavior over the entire velocity range (Fig. 2.2.3a), and the chalk (61-3) from 1322 mbsf (Unit III) with a μ_S value of 0.52 (Fig. 2.2.2), which fails in slip instabilities with relatively large stress drops already at plate rate (Fig. 2.2.3a, b). Samples 60R-6 and 61R-1 (Unit III) exhibit (potentially) unstable sliding behavior at slip velocities above plate rate (Fig. 2.2.3a). Consequently, they would need to be triggered by slip propagation of a deeper-seated earthquake or by a slow slip event to behave unstably. Collectively, our findings provide the first evidence of an unstable shallow décollement, offering an explanation for seismogenic slip to the deformation front during the Aceh-Andaman subduction zone earthquake.

Cause of frictional instability

Hüpers et al. (2017) also suggested that shallow seismogenic slip was facilitated by frictional instability of the shallow décollement. However, they proposed that a potential unstable behavior could require diagenetic processes of quartz precipitation, smectite-illite

transformation, and pore-fluid pressure dissipation in the predécollement, all of which act toward strengthening the fault and thus making it favorable for unstable sliding (Lockner and Byerlee, 1986; Trütner et al., 2015; Ikari and Hüpers, 2021). Our findings imply that diagenetic strengthening is not necessarily required for unstable behavior of the shallow décollement material. This result is in contrast to the prevailing understanding of the relation of frictional strength and stability.

Unstable sliding behavior is generally expected for stronger materials and faults (e.g. Scholz and Engelder, 1976; Kanamori, 1978). Based on laboratory friction experiments, the tendency of frictionally strong materials (with $\mu_S > 0.5$) for unstable velocity-dependent frictional behavior has been well established (Logan and Rauenzahn, 1987; Ikari et al., 2011a, 2016). However, most of the non-calcareous sediments tested in this study are weak (μ_S = 0.14 – 0.46) and velocity weakening or even unstable (Fig. 2.2.2, 2.2.3c). Compared to the empirical relationship of velocity-dependent frictional behavior, as expressed by the paramter *a-b*, and frictional strength, as described by the friction coefficient μ, which was derived from measurements on various natural and synthetic materials measured at 20 MPa and ambient relative humidity (100%) (Ikari et al., 2016), the non-calcareous sediments tested in this study show negative *a-b* values and/or slip instability at markedly lower μ values (Fig. 2.2.3c).

The low fricitonal strength can be explained by the high amounts of phyllosilicates (up to 64 wt%, Fig. 2.2.2) (Lupini et al., 1981; Morrow et al., 1992; Tembe et al., 2010). However, phyllosilicate-rich materials are also known to have a tendency toward stable slip behavior over a large range of conditions (Shimamoto and Logan, 1981; Saffer and Marone, 2003; Ikari et al., 2009b). An exception to this is smectite under room humidity which is shown to be weak and velocity-weakening at low normal stress (Saffer et al., 2001; Ikari et al., 2011a). Smectite contents of the non-calcareous samples that exhibit velocity weakening and/or slip instability range from 13 to 30 wt% (Fig. 2.2.2). However, we exclude smectite to be the cause of the observed (potential) instability of these samples, since the presence of water in our experiments likely facilitates an increase of *a-b* values to the velocity-strengthening regime for smectite (Ikari et al., 2007, 2016). In addition to smectite, these samples (aside from a mudstone from 1309 mbsf, sample 60R-1) comprise noteworthy amounts of nearly amorphous silica (11-20 wt%) (Fig. 2.2.2, Fig. 2.2.3d), which is typical of Unit III sediments (Lyle and Lyle, 2002; Dugan et al., 2017; Hüpers et al., 2017). Smear slide analysis on a tuffaceous mud from 61R-6 showed that this silica mostly comprise palagonite and minor parts of biogenic opal (Hüpers et al., 2017). Palagonite is a poorly crystalline alteration product of basaltic volcanic glass, which is, like opal, a hydrous mineral and thus contain significant amounts of water.

Biogenic silica has been shown to have a relatively high friction coefficient of μ_S = 0.62 (Kopf and Brown, 2003). To our knowledge the velocity-dependent frictional behavior of

biogenic silica has not yet been tested. Velocity-weakening behavior reported for Japan Trench fault wall rock consisting of average 60% of amorphous silica may be the closest approximation (Ikari et al., 2015b; Kameda et al., 2015). Therefore, we performed another velocity step test on a powdered sample of pure biogenic opal from Humboldt County, Nevada, at an effective normal stress of 13.75 MPa. This test revealed a friction coefficient μ_S of 0.57 and slip instabilities throughout the experiment. These findings support the assumption of hydrous amorphous silica being a key factor for the observed velocity-dependent frictional behavior of the tested input samples (Fig. 2.2.3c). The question that arises is how relatively small amounts of amorphous silica dispersed in frictionally weak sediments may cause unstable sliding.

Threshold contents of amorphous silica dictate unstable frictional behavior

A noteworthy property of the amorphous silica-bearing sediments tested in this study is their high porosity, exceeding the normal compaction trend both as intacts (Hüpers et al., 2017) and powdered equivalents (Fig. 2.2.2, Fig 2.2.3d). Elevated porosities in the targeted depth interval have been previously suggested to represent an artifact from mineral-bound water of smectite (Dutilleul et al., 2020), which is relatively abundant in Unit III sediments at Site U1480 (Dutilleul et al., 2020; Rosenberger et al., 2020). An alternative explanation may be found in investigations on the high porisity zone (HPZ) at the Nankai Trough. This HPZ was proposed to result from the presence of mineral aggregates or mineral coatings, suspected to prevent the collapse of intergranular pore space during loading (Spinelli et al., 2007; White et al., 2011; Hüpers et al., 2015). Hüpers et al. (2015) proposed that threshold concentrations of 20-30 % of volcanic ash in a sediment are needed for the observed patchy precipitation of amorphous silica cement along grain-to-grain contacts that forms aggregates. Spinelli et al. (2007) suggested that ~1 wt% of amorphous silica cement, which is assumed to be sourced from disseminated volcanic glass (White et al., 2011), could inhibit normal sediment compaction und result in elevated porosities.

SEM imaging reveals the presence of roundish aggregates of 10^0-10^1 µm diameter in both intact and powdered samples tested in this study (Fig. 2.2.4a). These aggregates seem to contain both grain-to-grain bridges and mineral coatings (Fig. 2.2.4b, c). Because of the similarity to the observations for the HPZ at the Nanaki Trough, we infer that the amounts of hydrous amorphous silica in samples 60R-3, 60R-6, 61R-1, and 62R-5 were sufficient to form mineral aggregates under relatively low temperatures and pressures. Based on our mechanical data, we speculate that aggregates and/or the angular-shaped grains of hydrous amorphous silica (Fig. 2.2.4d) create a grain packing that produces a stress-supporting framework, which is usually expected for granular materials with 85-100% strong minerals (e.g. Tembe, Lockner and Wong, 2010). This grain packing would allow frictional sliding to be

accomodated on hydrous amorphous silica, which likely results in velocity-weakening behavior.

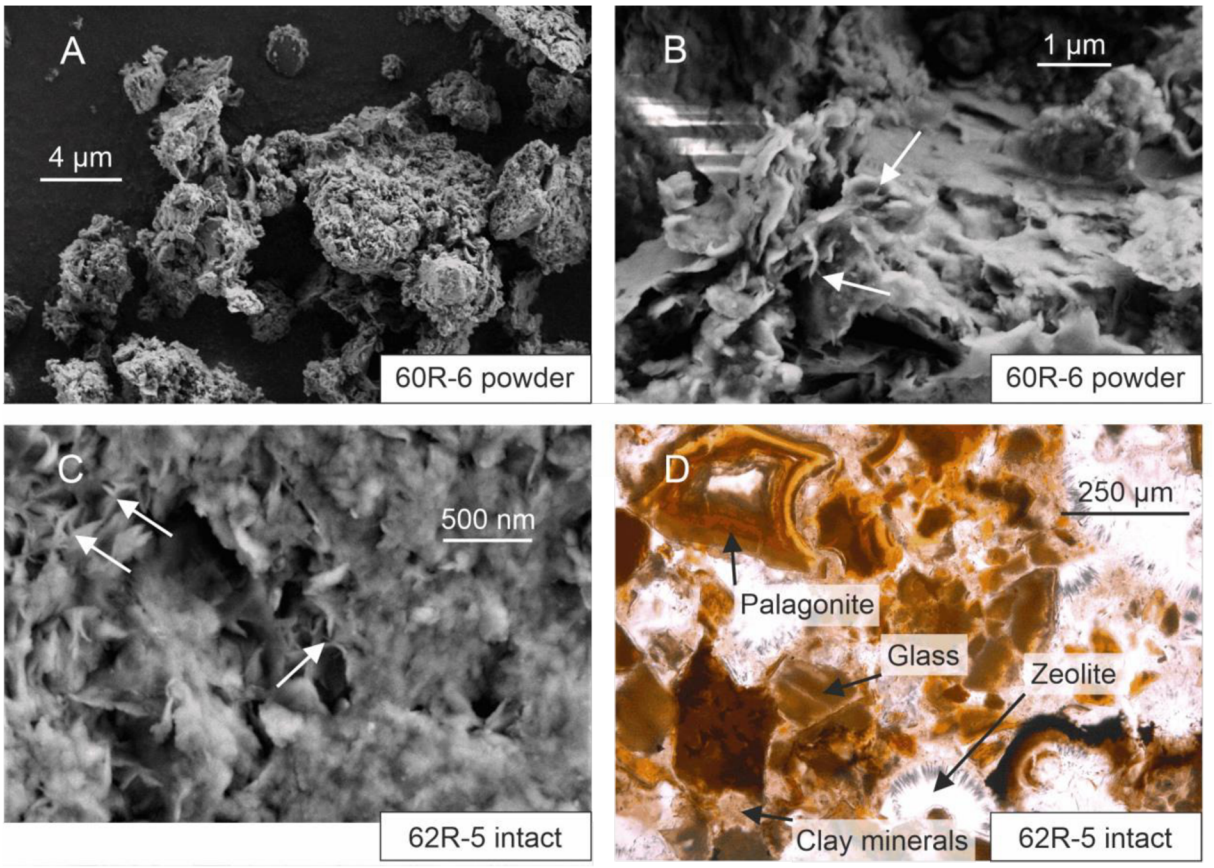

Figure 2.2.4: SEM images of a) aggregates of the powdered undeformed sample 60R-6. Potential grain-to-grain bridges marked by white arrows in b) powdered undeformed sample 60R-6 and c) intact undeformed sample 62R-5. Note the blurred areas especially in c), which may indicate mineral coating. d) Micrograph showing texture and minerals of the intact undeformed sample 62R-5.

From input to décollement material

Although our experiments revealed frictional instability under relatively low effective normal stresses and at room temperature, our findings are transferable to the predécollement or even the shallow décollement. Elevated temperatures at the deformation front estimated to range from 125 to 160°C (Stevens et al., 2021) probably lead to the complete diagenetic transformation of opal to quartz (Keller and Isaacs, 1985) and may enhance the tranformation of palagonite into smectite (Berger et al., 1987; Hodder et al., 1993) and of smectite into illite (Pytte and Reynolds, 1989), associated with a change in sliding behavior (Moore et al., 1989). However, palagonite kinetics are still under debate (Stroncik and Schmincke, 2002; Walton and Schiffman, 2003) and without available data for palagonite kinetics, the possibility of palagonite in the predécollement sediments at the deformation front cannot be ruled out.

The effective normal stress at the deformation front may be much higher than tested in our experiments, since pore-fluid dissipation has been estimated to complete seaward of the deformation front (Hüpers et al., 2017; Stevens et al., 2021). However, the interpretation of seismic images as well as pore pressure modelling indicate significant overpressure in the predécollement and shallow décollement sediments (Dean et al., 2010; Zhang et al., in prep.), which allows the assumption of low effective normal stresses at shallow décollement positions.

If the presence of mineral aggregates is responsible for elevated porosities, these aggregates may inhibit pore space collapse up to effective stresses of at least 8 MPa (Hüpers et al., 2015), indicating the presence of aggregates in the fault-forming sediments up to equivalent depths. Despite the possibility of cementation processes (Moore and Saffer, 2001), the possibility of porosity and thus grain packing preservation to the deformation front may be supported by the interpreted porous, fluid overpressured character of the HANP horizon traceable all the way to the outer prism (Osborne and Swarbrick, 1997; Dean et al., 2010).

Therefore, we propose that concentrations above 11 wt% of dispersed strong amorphous silica in weak sediments entering the North Sumatra subduction zone may be the cause of an unstable shallow décollement, which is responsible for unexpectedly shallow seismogenic slip during the 2004 Aceh-Andaman earthquake. Since sources of hydrous amorphous silica such as volcanic ash and opaline fossils are abundant in the sedimentary inputs to most subduction zones (Vrolijk, 1990; Rea and Ruff, 1996; Underwood, 2007), our findings may also be valuable for the seismic and tsunami hazard assessment of other subduction margins.

Acknowledgment

We highly appreciate the work of Philipp Haberkorn, who modified the laboratory devices and software to our needs. We value the helpful discussions on microstructural analysis with Åke Fagereng and Aagje Eijsink. Christoph Vogt is thanked for XRD analysis. We thank Petra Witte for operating the SEM in times where access to buildings and laboratories was restricted. Laboratory support by Achim Kopf is greatly appreciated. This work used samples from the International Ocean Discovery Program. Rate- and state friction modeling was performed using the program “RSFit3000”, courtesy of Rob Skarbek and Heather Savage. This work was funded by the European Research Council (ERC) under the European Union’s Horizon 2020 research and innovation programme Grant #714430 to M. Ikari.

Supplementary Material

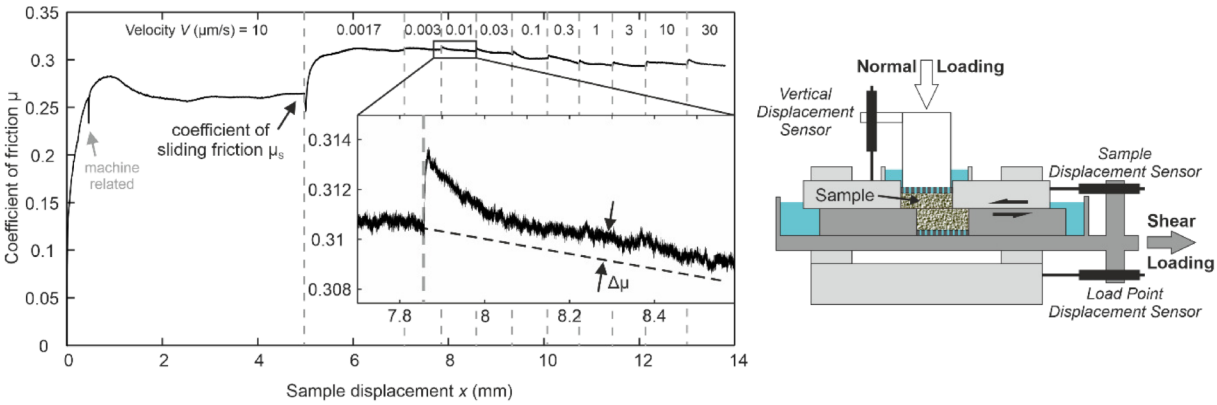

Figure S2.2.1: Exemplary experimental data and schematic of the used direct shear apparatus.

Microstructural analysis

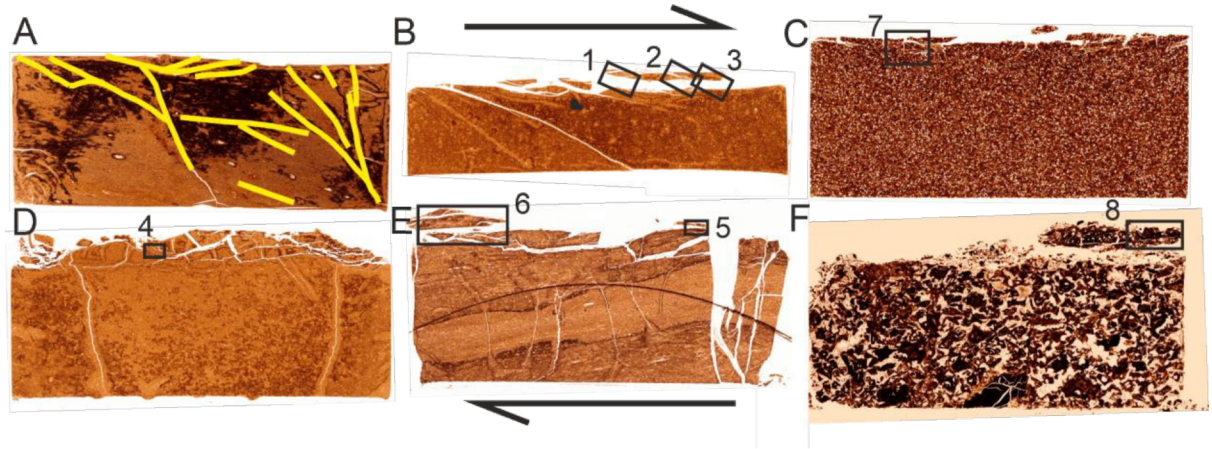

Figure S2.2.2: Micrographs of halves of sheared samples a) 54R-1 intact, b) 61R-1 powdered, c) 62R-5 powdered, d) 60R-6 powdered, e) 61R-1 intact, and f) 62R-5 intact. Note that the upper edge of the sample halves represents the shear surface. Black boxes indicate areas of close-ups depicted in Figure S2.2.3. Black arrows at the top and bottom of this figure indicate the shear sense.

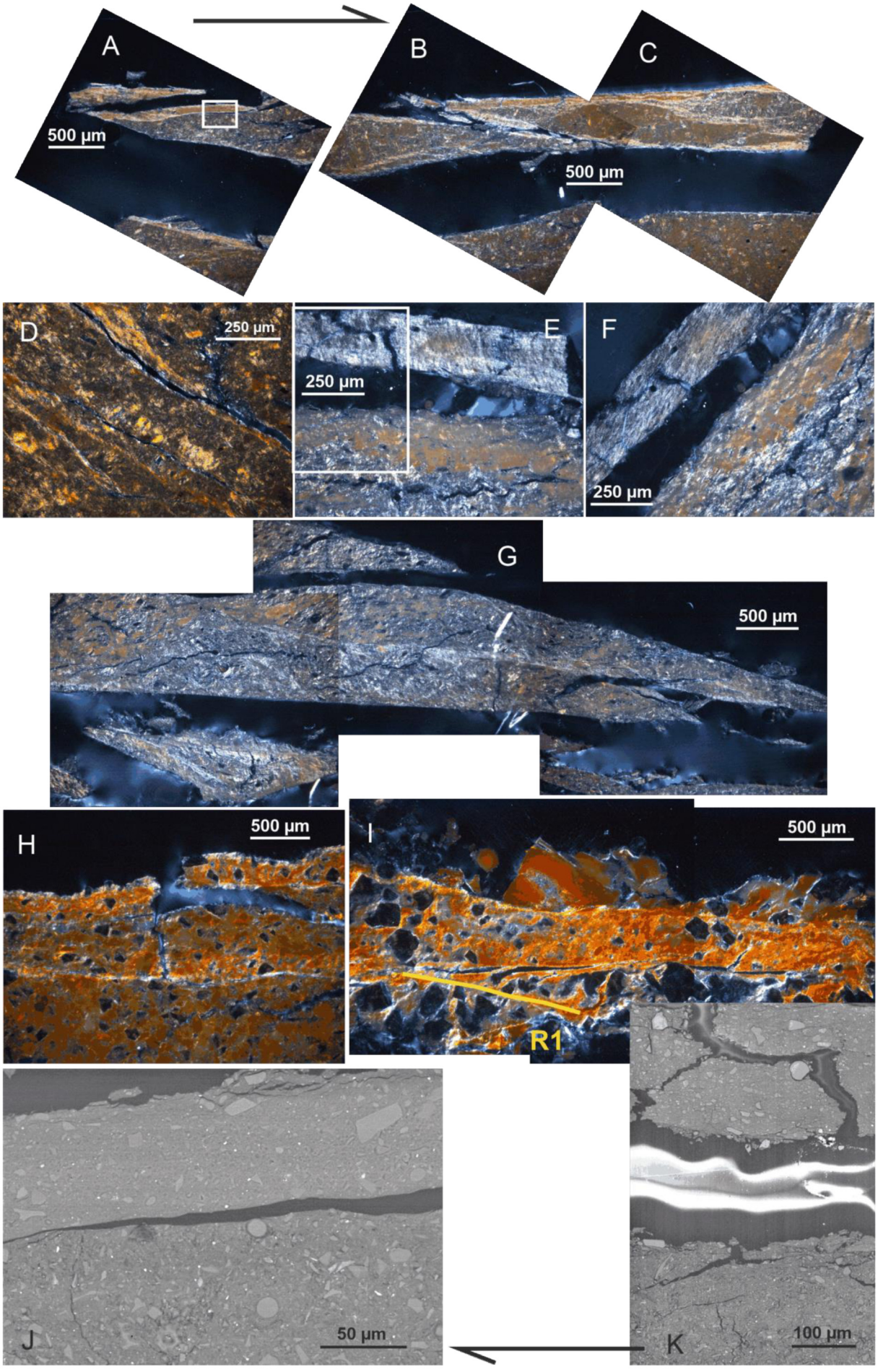
A
500 µm
B
C
500 µm
D
250 µm
E
250 µm
F
250 µm
G
500 µm
H
500 µm
I
500 µm
R1
J
50 µm
K
100 µm

Figure S2.2.3: a)-i) Micrographs under crossed polarized lights, representing close-ups of locations indicated by black boxes in Fig. S2.2.2. J) and k) are back-scattered images representing close-ups of locations indicated by white boxes in the micrographs. Black arrows at the top and bottom of this figure indicate the shear sense.

A striking observation of this study is, that while strictly velocity-strengthening and stably sliding samples (54R-1, powdered and intact) show a deformation fabric matching their velocity-dependent frictional behavior (Fig. S2.2.2a), most velocity-weakening and unstably sliding samples (except for 60R-1) show a more complex deformation fabric than expected (Fig. S2.2.2b-f, Fig. S2.2.3). These include the samples 60R-6 powder, 61R-1 (powdered and intact), 62R-5 (powdered and intact), which are most of those comprising nearly amorphous silica. For other samples with amorphous silica, 60R-3 powdered and 60R-6 intact, there is no microstructural analysis.

The velocity-strengthening samples exhibit pervasive shear fractures in the Riedel R1-orientation with angles of 20-26° and even smaller angles up to 9° as well as some in the X-orientation (58-72°), most of which are found at initial positions along the shear path, reaching from the forced shear plane to deep within the sample half (Fig. 2.2.2a). Additionally, at positions of final sample-sample contact, Riedel R2-oriented cracks of 37-77° are present as well as P-oriented foliation with maximum angles of 33° and P-oriented cracks, which merge with low angle R1-shears to form shear-parallel to -subparallel, shallow fractures. Grain size does not seem to be significantly reduced along any of the fractures. These features are consistent with a shear deformation fabric that is kinematically favorable for distributed slip in a forced-localization experimental setup. With increasing shear strain that accumulates as the sample halves get displaced against each other, R1-fractures reorient from higher to lower angles to the interface, in the extreme becoming parallel to the Y-orientation as a function of rotating maximum principal stress (e.g. Logan et al., 1992).

Sample 60R-1 shows deformation features matching the observed unstable slip. Through-going shear-parallel to -subparallel, sigmoidal fractures, Y-fractures, extend over the range of the final sample-sample contact and a little further, some of which seem to have emerged from R1-shears of 15-24° at the distant side. Additionally, some R1-shears of 22-24° bend into and partly connect the Y-fractures. Y-fractures have undergone grain size reduction. All of these features are consistent with a kinematically favorable fabric for velocity-weakening behavior. Additionally, the fabric of sample 60R-1 looks very similar to that of an intact, velocity-weakening sample of Roesner et al. (2020) sheared in the same type of device under similar boundary conditions.

In the analyzed samples that comprise nearly amorphous silica, Riedel shears are generally scarce and short. We observe a highly fractured zone of multiple, anastomosing, interconnected Y-shears with material of reduced grain size (Fig. S2.2.3a-i), sometimes traceable over the entire length of the sample. Foliation seemingly originating from the rotation and alignment of clay minerals (Logan and Rauenzahn, 1987) is found in the Y- and R1-orientation and often coincide with positions of fractures. While the observed formation of through-going Y-fractures and grain size reduction along them is associated with unstable sliding (Logan and Rauenzahn, 1987; Beeler et al., 1996; Scruggs and Tullis, 1998), the observed formation of a complex fracture zone, as well as foliation are not necessarily (e.g. Collettini et al., 2009). Nevertheless, previous laboratory friction experiments show that complicated, anastomosing features at low angles are common for phyllosilicate-rich samples (Ikari et al., 2011b).

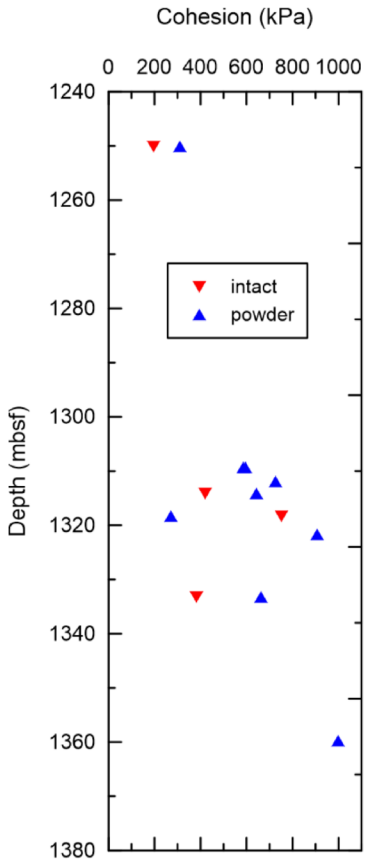

Figure S2.2.4: Area-corrected internal cohesion for all tested samples.

3 The role of hydrous amorphous silica in megathrust fault slip behavior

Threshold amounts of dispersed amorphous silica in weak gouge induce velocity-weakening frictional behavior (Manuscript 3)

Katja Stanislowski, Alexander Roesner, Matt J. Ikari

MARUM – Center for Marine Environmental Sciences, and Faculty of Geosciences, University of Bremen, Leobener Str. 8, 28359 Bremen, Germany

Abstract

Frictionally weak materials are generally associated with inherently stable frictional sliding behavior under low temperature and pressure conditions. This relationship offers an explanation for the observed general lack of seismicity in the shallow portion of subduction zone megathrusts, where unconsolidated, clay-rich, weak materials are typically encountered. In contrast, unexpectedly shallow seismic slip during the 2004 Aceh-Andaman earthquake offshore North Sumatra has been proposed to result from a shallow upper limit of the seismogenic zone, potentially resulting from weak but unstable fault input material that contains critical amounts of hydrous amorphous silica. In this work, we investigate the hypothesis of threshold amounts of hydrous amorphous silica to induce velocity weakening behavior in weak gouges, a property crucial for slip instability. Friction experiments under low temperature, pressure, and sliding velocity conditions on mixtures of weak shale and biogenic opal, a type of hydrous amorphous silica, reveal pronounced velocity weakening at opal contents of ≥ 30 % with a minimum friction coefficient of 0.38. Our observations support the hypothesis for North Sumatra input sediments, but deviate from the prevailing understanding of the strength-stability relationship. We propose that velocity weakening at low frictional strength can be explained by the viscous behavior of hydrous amorphous silica contacts. Our findings hold important implications for the reevaluation of the strength-stability relationship as well as for shallow seismogenesis at North Sumatra and other subduction zones where input sediments contain critical amounts of hydrous amorphous silica.

Introduction

Subduction zone megathrust faults can generate large earthquakes and tsunamis. The frictional properties of the material in the fault zone are crucial to the nucleation of such slip events. Fault zone materials are often composed of clay-rich lithologies (Chester and Logan, 1987; Solum et al., 2006; Underwood, 2007; Schleicher et al., 2010), which are well known to be weak (Lupini et al., 1981; Shimamoto and Logan, 1981; Ikari et al., 2007). However, weak materials are generally associated with inherently stable frictional sliding behavior under moderate temperatures and pressures (Shimamoto and Logan, 1981; Brown et al., 2003; Tembe et al., 2010; Ikari et al., 2016). Unstable sliding of weak materials may be induced by elevated temperatures and pressures (Moore et al., 1989; den Hartog et al., 2012). Specifically, compaction, lithification due to cementation, and dehydration have been proposed to be important processes for weak sediments to strengthen and thus to develop an unstable sliding character during ongoing subduction (Bernabé et al., 1992; Moore and Saffer, 2001; Trütner et al., 2015; Ikari and Hüpers, 2021). These suggestions support the model which describes faults as seismogenic only in a certain depth range, with the shallow portion sliding stably and aseismic (Hyndman et al., 1997; Moore and Saffer, 2001; Wang and Hu, 2006). Although this model generally fits with seismological observations (e.g. Zhang and Schwartz, 1992), it seems to be in conflict with the shallow seismic slip during the M_w 9.2 Aceh-Andaman subduction zone earthquake of 2004 offshore North Sumatra (e.g. Henstock et al., 2006; Bletery et al., 2016).

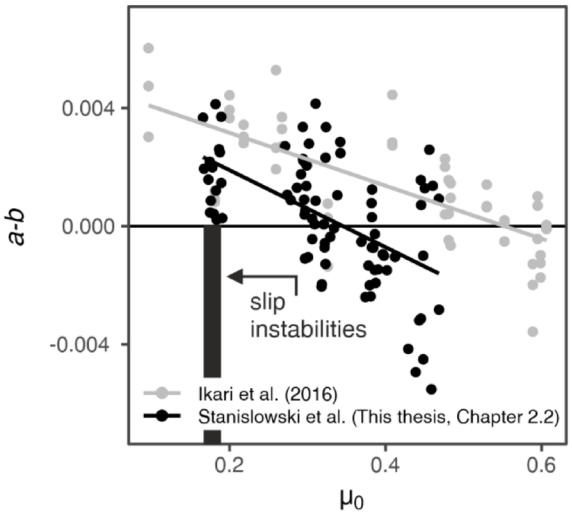

Figure 3.1: The relationship of friction coefficient μ_0 and friction rate dependence, as expressed by the rate-dependent friction parameter *a-b*, from data of Ikari et al. (Ikari et al., 2016) over a variety of synthetic and natural gouge materials and of Stanislowski et al. (This thesis, Chapter 2.2) over inputs sediments to the North Sumatra subduction zone. Vertical bars that mark occurrences of slip instability were reduced to those samples where negative *a-b* values could not be modelled. Note that the stability transition of North Sumatra subduction zone inputs is clearly shifted towards lower frictional strengths.

Hüpers et al. (2017) have shown that the presumed fault-forming lithologies of the North Sumatra subduction zone may be completely dehydrated prior to subduction. The consequence would be a strengthened and seismogenic shallow megathrust fault, consistent with other work (Dean et al., 2010; Gulick et al., 2011; Geersen et al., 2013; Stevens et al., 2021). Stanislowski et al. (This thesis, Chapter 2.2) corroborate the hypothesis of a shallow

seismogenic zone, however with the explanation of clay-rich and weak but unstably sliding input sediments, even at low normal stresses and temperatures. Their observations clearly deviate from the established relation between frictional strength and friction rate dependence (Fig. 3. 1), a parameter crucial to frictional stability (Scholz, 1998), which they attribute to threshold amounts of dispersed hydrous amorphous silica (in this case: palagonite and biogenic opal). Given the volcanism as well as upwelling along subduction zone margins, volcanic ash and opaline fossils, which are sources of hydrous amorphous silica, are abundant in the sedimentary inputs to most subduction zones (Vrolijk, 1990; Rea and Ruff, 1996; Underwood, 2007). Consequently, the potential of hydrous amorphous silica to favor unstable sliding in weak, potentially fault-forming sediments at shallow depths may not only be applicable to North Sumatra but be of global relevance for shallow seismogenesis. However, the hypothesis of Stanislowski et al. (This thesis, Chapter 2.2) needs investigations under controlled conditions.

Therefore, in this work, we used laboratory friction experiments to systematically explore the effect of varying amounts of hydrous amorphous silica on frictional strength and sliding behavior of clay-rich gouges under low temperature and pressure conditions. Since the evolution of these frictional properties with clay content has been related to grain packing of gouge mixtures (Lupini et al., 1981; Kohli and Zoback, 2013) and the deformation of frictional contact junctions (Engelder and Scholz, 1976; Logan and Teufel, 1986; Wang and Scholz, 1994), we measured porosity of the individual mixtures under applied normal load and compare them to the ideal packing model, which can be used to infer the grain packing of a binary gouge material (Clarke, 1979; Marion et al., 1992).

Methods

Sample preparation

We used biogenic opal (hydrous amorphous silica) from Humboldt County, Nevada, and Rochester Shale (RS), an illite shale which consists of 68 % clay minerals (59 % illite and 9 % kaolinite/dickite), 23 % quartz, and 4 % plagioclase (Saffer and Marone, 2003). Both starting materials were dried at room temperature, and then ground and sieved to grain sizes < 125 µm. In addition to the two endmembers, five mixtures of illite shale and opal were produced, which were mixed with deionized water to form a stiff paste that was gently pressed into the sample cell. The ratios of material mixtures were based on weight. The weight of the bulk mixture was adjusted to achieve a gouge thickness after consolidation/prior to shearing that was comparable among the different mixtures. Figure 3.2c shows the fabric and grain shapes of the pure opal sample consolidated at 10 MPa effective normal stress.

Experimental procedure and data modeling

We performed laboratory friction experiments in a GIESA *RS5* direct shear device at room temperature, 10 MPa effective normal stress, and under drained conditions. Experiments on each sample followed the same sequence (Fig. 3.2a): an initial run-in for 5 mm horizontal sample displacement at 10 µm/s, and a subsequent velocity step test with a stepwise three-fold increase of sliding velocities ranging from 0.01 to 30 µm/s and with 0.7 mm displacement per velocity step. The continuously measured shear stress was used to calculate the coefficient of friction μ, neglecting cohesion (Handin, 1969).

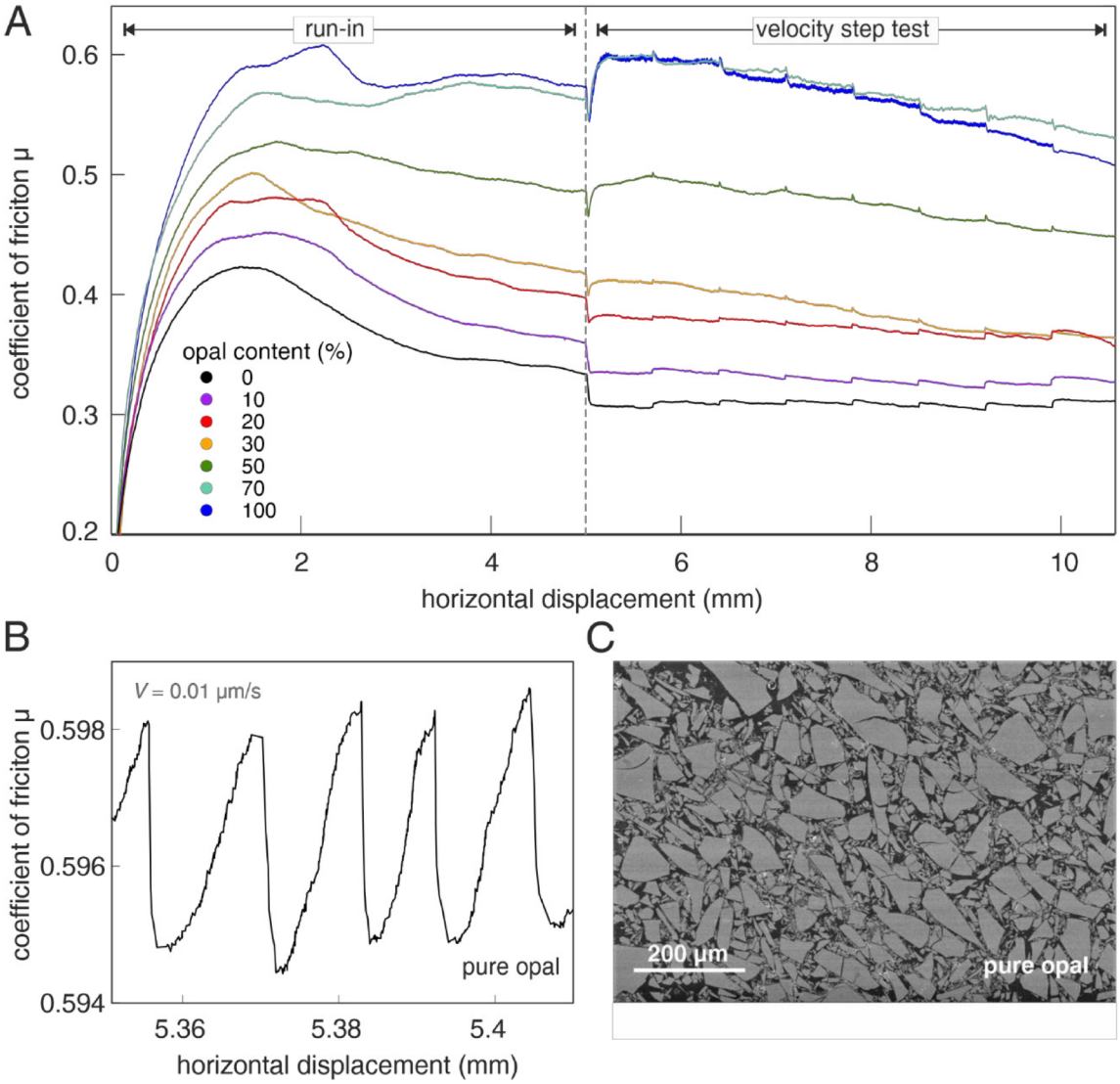

Figure 3.2: a) Experimental data showing run-in phase and velocity step tests of individual gouge mixtures, b) slip instabilities recorded during the test on pure opal at 0.01 µm/s driving velocity, c) back-scatter image of pure opal.

From the run-in, we determined the coefficient of peak friction μ_P as well as the coefficient of steady state sliding friction μ_S, and the velocity steps were inversely modeled to

obtain the rate-dependent friction parameter $a\text{-}b = \Delta\mu_{SS}/\Delta\ln(V)$ (e.g. Skarbek and Savage, 2019). Velocity-strengthening behavior and associated stable sliding are shown by values of $a\text{-}b > 0$, while values of $a\text{-}b < 0$ indicate velocity weakening, a requirement for unstable sliding (Dieterich, 1981; Scholz, 1998).

Porosity

For all water-saturated samples, porosity was determined by means of a geometrical approach. Under full drainage, each sample was consolidated at 10 MPa effective normal stress for 24 hours and then unloaded to approximately ambient effective normal stress (0.1 MPa) for another 24 hours, while the change in sample height was tracked continuously. Afterwards, we removed the water from the basin, took the sample out of the cell and measured the sample height as well as wet weight. Dry weight was measured after 24 hours at 105°C. From controlled sample unloading, we determined the change in sample thickness due to elastic deformation. Subtracting this change in sample height due to elastic deformation from the height under ambient conditions allowed us to obtain the sample height at 10 MPa effective normal stress. Since the sample container only allows volumetric change of the sample in vertical direction, we could calculate the bulk volume of the sample at 10 MPa effective normal stress. From the difference in wet and dry weights of a sample we determined pore water volume allowing the calculation of porosity at applied effective normal stress. We carried out repeated consolidation tests and porosity measurements to capture the variation in porosity for mixtures with opal contents of 10-30%. Precision of these measurements was deemed crucial because the opal contents correspond to those of hydrous amorphous silica in the unstable marine sediments of Sumatra subduction zone inputs (Stanislowski et al., This thesis, Chapter 2.2).

Ideal packing model

To evaluate the grain packing of the gouge mixtures, we compared our porosity measurements with those derived from an ideal packing model. For binary granular mixtures of fine and coarse particles under uniaxial loading, porosity can be determined under the assumption of an ideal grain packing model (McGeary, 1961; Marion et al., 1992; Revil et al., 2002). This model describes two load-bearing geometrical configurations: (1) a framework of connected, coarse grains with the intergranular pore space, filled to varying degrees with particles of the fine endmember material; and (2) a matrix of finer particles with entirely embedded coarse grains. In accordance with this model, two simple bimodal mixing laws can be used to derive the dependence of gouge porosity on the volume fraction of the fine particles, where the mixture's porosity φ is expressed as a function of the two endmember porosities

(generally that of clay, φ_C, and sand, φ_S) (Clarke, 1979; Marion et al., 1992). To compare the modeled with the measured porosities, clay volume fraction *c* was converted into clay weight fraction w_C via knowledge of grain densities of clay ρ_C and sand ρ_S (Marion et al., 1992).

For the first geometrical configuration, clay volume fraction *c* is less than the sand porosity φ_S ($c < \varphi_S$) and the porosity of the mixture decreases with increasing clay content:

$$\varphi = \varphi_S - c(1-\varphi_C) \;\; with \;\; w_C = \frac{c(1-\varphi_C)\rho_C}{c(1-\varphi_C)\rho_c + (1-\varphi_S)\rho_S} \tag{3.1}$$

At the transition of both configurations, the clay volume fraction equals the sand pore space ($c = \varphi_S$) and the mixture's porosity reaches its minimum:

$$\varphi = \varphi_S\varphi_C \tag{3.2}$$

In the second geometrical configuration, the clay volume fraction exceeds the sand porosity ($c > \varphi_S$) and the mixture's porosity increases with increasing clay content:

$$\varphi = c\varphi_C \;\; with \;\; w_C = \frac{c(1-\varphi_C)\rho_C}{c(1-\varphi_C)\rho_c + (1-c)\rho_S} \tag{3.3}$$

In our case, the mixtures are binary, but not dimineralic due to the polymineralic RS. However, the measured porosity of 0.41 of pure opal is comparable to that of pure quartz measured at 10 MPa effective normal stress (Marion et al., 1992). Therefore the 23 % quartz (+ 4 % plagioclase) in the RS may be combined with opal as one endmember with φ_S = 0.41. Most of the other minerals of RS are clay minerals (68 %), of which the major portion is made up by illite (87 %) with minor kaolinite/dickite (13 %). We combined these two clay minerals and treated them as one endmember. Since we did not measure illite porosity ourselves and these measurements at comparable effective normal stress have to our knowledge not been reported, we chose a value of φ_C = 0.47, which is kaolinite porosity at 10 MPa effective stress (Marion et al., 1992). This porosity seems reasonable considering a porosity of RS at the same stress reported to be 41 % on average (Ikari and Hüpers, 2021) We used a clay grain density ρ_C of 2.78 g/cm³ reported for illite (Ikari and Hüpers, 2021). Since the proportions among the strong minerals (opal+quartz+plagioclase) varies with clay content (illite+kaolinite/dickite) of our mixtures, we calculated two models using a grain density ρ_S of either quartz (2.65 g/cm³) or opal with (1.99 g/cm³). The latter was determined in this study by means of the dry weight, the bulk volume under ambient pressure and the pore water volume, and fits the reported range of grain densities of biogenic silica (1.7-2.3 g/cm³, Baas Becking and Moore, 1959; Hurd and Theyer, 1977).

Results

Coefficients of both peak and residual sliding friction increase with increasing opal content, with values ranging from μ_P = 0.42 to 0.61 and μ_S = 0.32 to 0.57 for pure RS to pure opal (Fig. 3.3a). The opposite trend is observed for the rate-dependent friction parameter *a-b*. Values of *a-b* generally decrease from 0.007 to -0.007 with increasing opal content, and change from positive to negative at 30 % opal (Fig. 3.3b, 3.4a). Pure RS shows slightly lower *a-b* values than the mixture with 10 % opal, and pure opal reveals slightly higher values than the mixture with 70 % opal. In addition, pure opal exhibits slip instabilities at all velocity steps up to 10 µm/s, with highest stress drops of ~35 kPa and peak slip velocities of ~0.07 µm/s at a loadpoint velocity of 0.01 µm/s (Fig. 3.2b). The trend of parameter *b* over opal content for individual velocities approximately resembles the reciprocal of the trend of *a-b* values (Fig. 3.3c, 3.4c). The same roughly applies to parameter *a*, however only for velocities up to V_U = 0.3 µm/s; at higher velocities the dependence of *a* on opal content seems to vanish (Fig. 3.3f, 3.4b).

Furthermore, there is a distinct pattern in *a-b* values over upstep loadpoint velocity or slip distance for most mixtures, comprising an initial decrease and a subsequent increase with minima at V_U = 0.3 – 3 µm/s (Fig. 3.3e). Similar to the trend over opal content, the trend of *b* values with upstep loadpoint velocity approximately delineates the inverse of the *a-b* trend (Fig. 3.3g). The parameter *a* appears fairly constant over velocity, except for pure opal where *a* decreases strongly with slip velocity (Fig. 3.3f).

Similar to the coefficient of sliding friction, the porosity generally increases with opal content from 0.25 to 0.36 (Fig. 3.3d). However, slope of the opal-porosity relationship increases at around 30 % opal. The measured porosities clearly differ from the ideal packing model. The models predicts a minimum in porosity of 0.19 for a clay content of 34 % when calculated with opal grain density, and of 28 % when calculated with quartz grain density (Fig. 3.3d). Measured porosities however generally decrease with clay content.

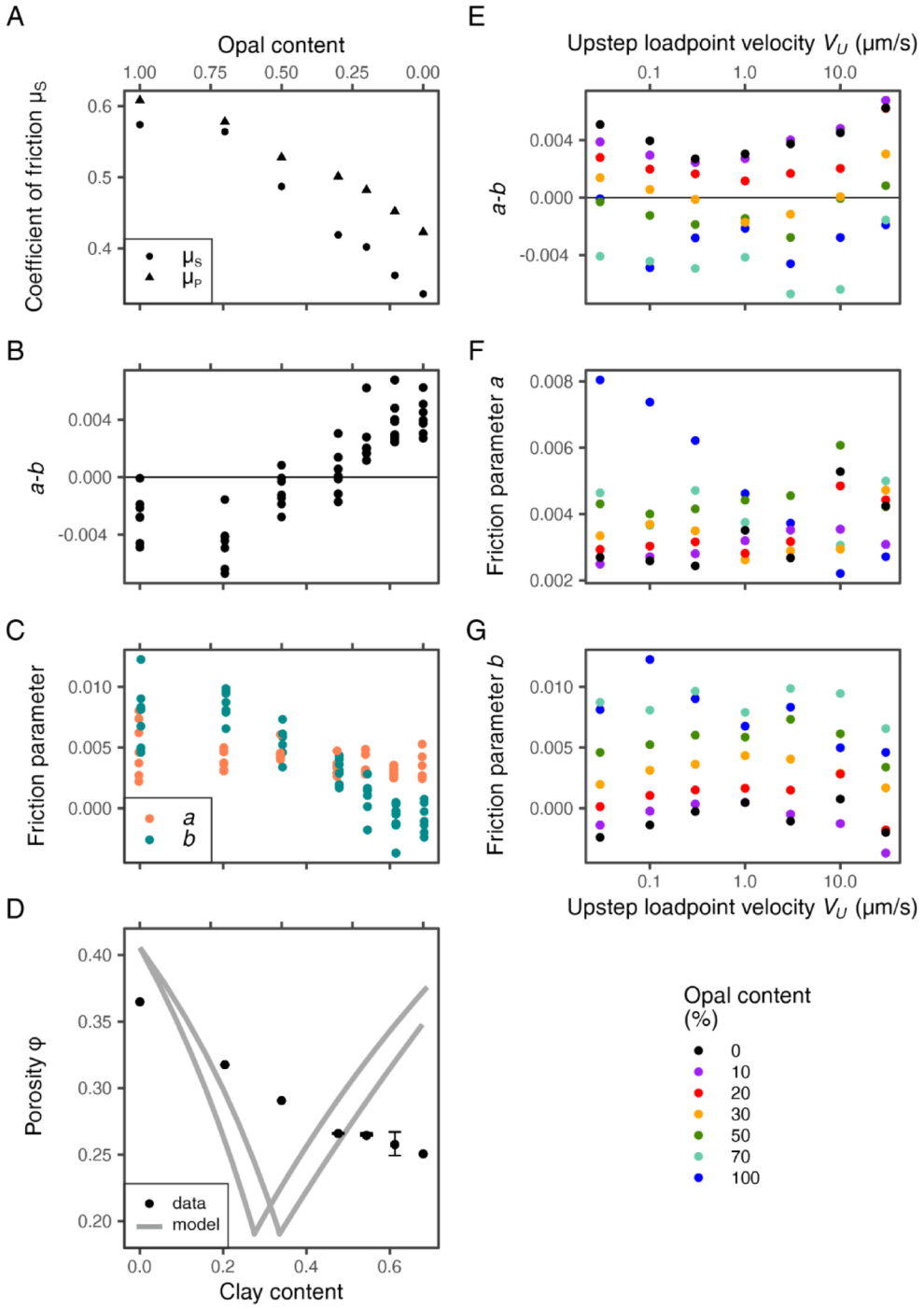

Figure 3.3: On the left, measured parameters over clay and opal content: a) Coefficient of peak and sliding friction, b) the rate-dependent friction parameter *a*-*b*, c) individual friction parameters *a* and *b*, d) measured and modelled porosity, where the left model is based on the grain density of quartz and the right on that of opal; on the right, measured parameters over upstep loadpoint velocity color-coded with opal content: e) *a*-*b*, f) *a*, g) *b*.

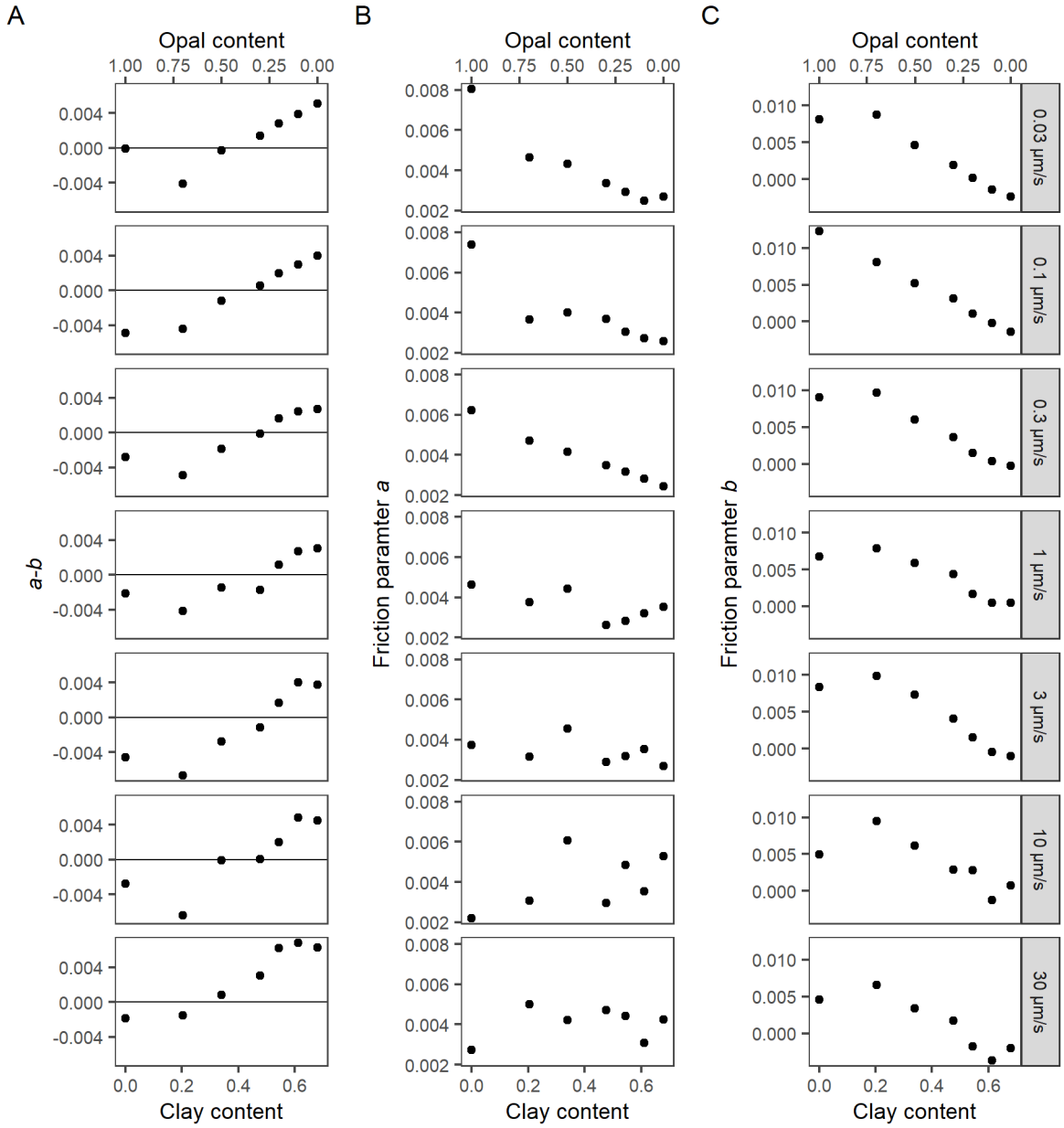

Figure 3.4: The change of rate-dependent friction parameters a) *a-b*, b) *a*, c) *b* over clay and opal content for different upstep loadpoint velocities.

Discussion

Velocity-weakening behavior of weak sediments

This work aims to investigate the effect of hydrous amorphous silica content on the frictional strength and sliding behavior of water saturated clay-rich materials at low temperature, pressure, and slip velocities. According to comprehensive experimental studies of a large variety of natural and synthetic gouges (Ikari et al., 2011a, 2016), weak materials with friction coefficients μ_0 < ~0.5 are suggested to be primarily velocity strengthening (Fig.

3.5a). Furthermore, synthetic gouge mixtures composed of both strong, velocity-weakening and weak, velocity-strengthening minerals, such as quartz and clay have been reported to show almost exclusively velocity-strengthening behavior, even mixtures with only small amounts of clay minerals (Logan and Rauenzahn, 1987; Kopf and Brown, 2003; Ikari et al., 2009b; Tembe et al., 2010). In contrast, Stanislowski et al. (This thesis, Chapter 2.2) found velocity weakening and unstable slip in natural clay-rich and hydrous amorphous silica-bearing samples with friction coefficients as low as μ_0 = 0.18 (Fig. 3.5a, c).

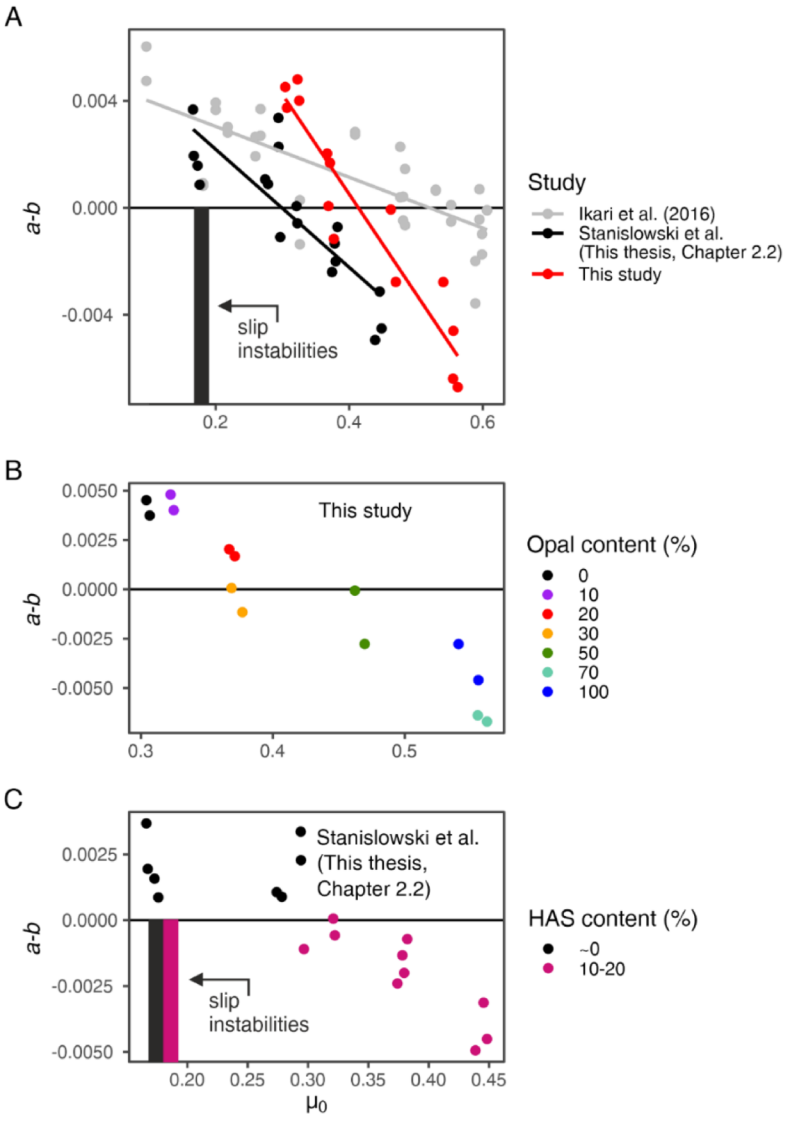

Figure 3.5: The relationship of frictional strength μ_0 and friction velocity dependence, as expressed by the rate-dependent friction parameter *a-b*, at upstep loadpoint velocities of 1-10 µm/s from data of a) Ikari et al. (2016) over a variety of synthetic and natural gouge materials, Stanislowski et al. (This thesis, Chapter 2.2) over inputs sediments to the North Sumatra subduction zone (separately shown in c)), as well as this study (separately shown in b)). HAS = hydrous amorphous silica. Vertical bars that mark occurrences of slip instability were reduced to those samples where negative *a-b* values could not be modelled. Note that the transition from positive to negative *a-b* values of North Sumatra subduction zone inputs as well as of opal-RS mixtures is clearly shifted from the data of Ikari et al. (2016) towards lower friction coefficients.

Here, we find that in gouge mixtures of clay-rich natural shale and opal, velocity weakening occurs in mixtures with clay contents of up to 50 % that are as weak as μ_0 = 0.38 (Fig. 3.5a, b). Both the gouge mixtures tested here and the natural sediments tested by Stanislowski et al. (This thesis, Chapter 2.2) demonstrate a clear trend of decreasing *a-b* values with increasing frictional strength of, which is in agreement with the work of Ikari et al. (2016). However, especially the slope of our data seems to be inclined to that reported by Ikari et al. (2016) (Fig. 3.5a). Although the data of Stanislowski et al. (This thesis, Chapter 2.2) and ours do not follow the same slope, they show a transition of potential instability that is shifted towards lower strengths than in material without

hydrous amorphous silica (Fig. 3.5a). It is evident that these datasets indicate the possibility of threshold amounts of amorphous silica to increase the chance of slip instability in weak materials. In the following discussion, we want to find out how.

Evolution of frictional strength and stability with opal content

Strength

We observe a decreasing coefficient of sliding friction μ_S with an increasing clay content (and decreasing opal content) (Fig. 3.3a), which is consistent with previous work (Skempton, 1964; Lupini et al., 1981; Morrow et al., 2000; Ikari et al., 2007; Moore and Lockner, 2007; Tembe et al., 2010). The measured coefficient of sliding friction μ_S = 0.32 for the endmember RS matches values of 0.29-0.33 from previous studies at the same effective normal stress (Ikari et al., 2009b; den Hartog et al., 2012), with the exception of a value found at < 2 MPa effective normal stress (0.22, Brown et al., 2003). The μ_S value of 0.57 for opal is comparable with previously measured values for pure biogenic silica at effective normal stresses < 14 MPa (0.62, Kopf and Brown, 2003; 0.57, This thesis, Chapter 2.2). Additionally, it is in agreement with μ_S values for pure quartz at effective normal stresses ≤ 50 MPa (0.49-0.62, Logan and Rauenzahn, 1987; 0.56, Mair and Marone, 1999; 0.50-0.61, Brown et al., 2003; 0.61, Carpenter et al., 2016), which we take as an opportunity to compare our data to mixtures of clay with quartz.

The trend of coefficient of sliding friction with clay content for the opal-RS mixtures is similar to those observed for quartz-illite, quartz-kaolinite, and quartz-smectite/montmorillonite mixtures (Fig. 3.6a). Since Rochester shale is predominantly composed of illite and quartz, the trend we observe is most similar to that of quartz-illite mixtures. Absolute values of μ_S for the opal-RS mixtures slightly deviate from those of quartz-illite mixtures, probably partially depending on differences in effective stress and absolute shear strain. With increasing normal stress, grain crushing and comminution of clastic particles becomes more prominent and may lead to pronounced strain hardening in mixtures with low clay content, which in turn strongly affects the measured friction coefficient (Biegel et al., 1989; Tembe et al., 2010). Nevertheless, the evolution of frictional strength with clay content of the opal-RS mixtures generally is consistent with those reported for quartz-illite mixtures.

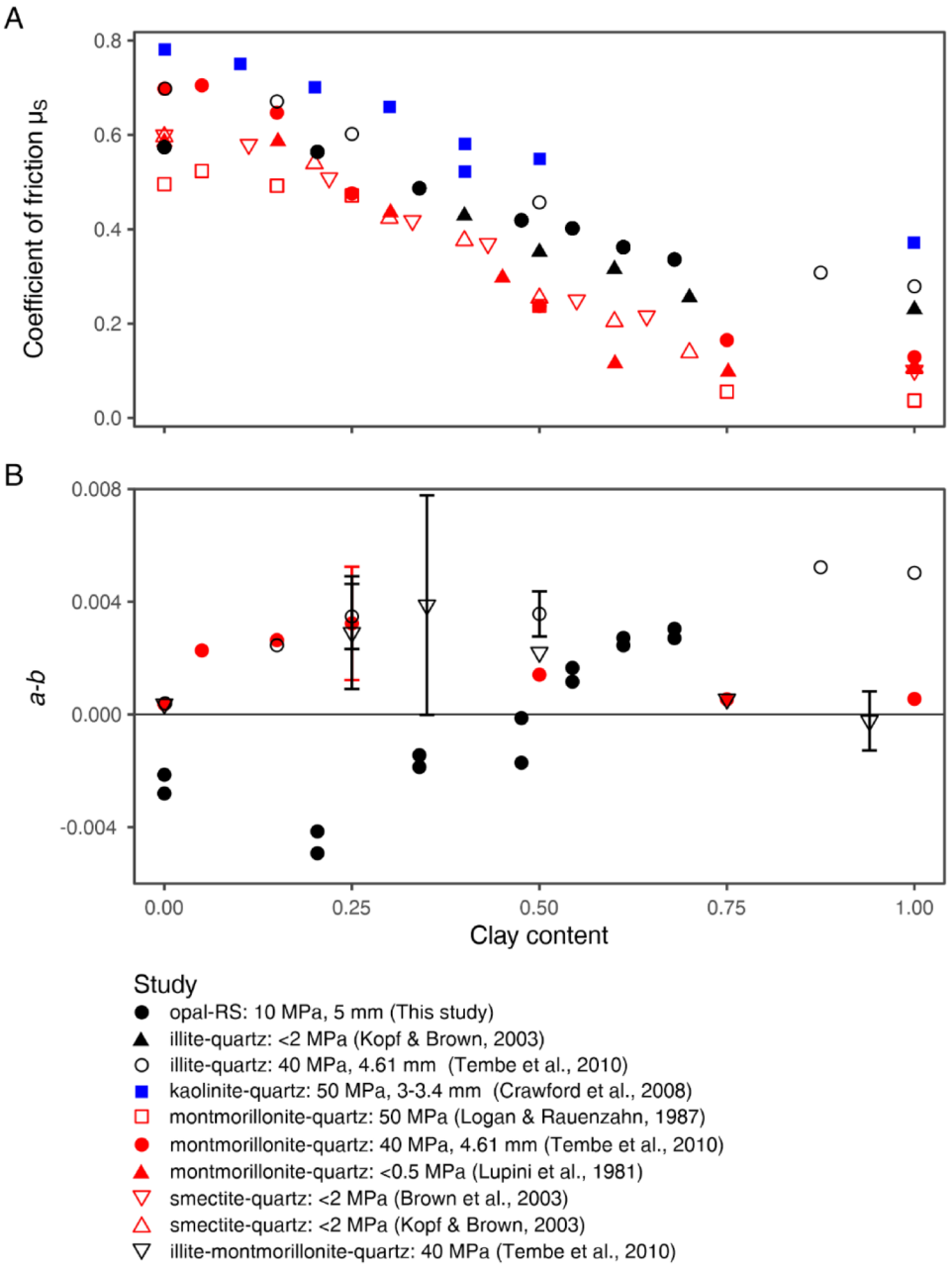

Figure 3.6: a) Coefficients of sliding friction and b) rate-dependent friction parameter *a-b* at upstep loadpoint velocities of 0.3-1 µm/s over clay content for our opal-RS mixtures compared to synthetic gouge mixtures from other studies.

Friction velocity dependence

Our measured *a-b* values for pure RS at upstep loadpoint velocities of V_U = 3, 10, 30 µm/s agree well with previously reported values of 0.004-0.005 at a comparable effective normal stress of 12 MPa (Ikari et al., 2009b) (Fig. 3.3b, f). Values of *a-b* for pure quartz have been reported to range from -0.006 to 0.004 at 20 MPa effective normal stress (Ikari et al., 2011a) and from -0.024 to 0.0032 for velocities of 0.001-10 µm/s at 25 MPa effective normal stress (Mair and Marone, 1999), which includes the range of consistently negative *a-b* values

measured for pure opal (Fig. 3.3b, e). Although values of *a-b* measured for mixtures of illite and quartz at 40 MPa effective stress decrease with increasing quartz content, they are coherently positive (Tembe et al., 2010), and are in clear contrast to those obtained from opal-RS mixtures (Fig. 3.6b). Similarly, mixtures of quartz with montmorillonite or illite+montmorillonite also mostly show velocity strengthening (Fig. 3.6b). Pure biogenic opal has been reported to fail in slip instabilities from 0.0017-30 µm/s at ~14 MPa (Stanislowski et al., This thesis, Chapter 2.2). Measurements on Japan Trench fault wall rock consisting of average 60% of amorphous silica exhibited velocity weakening with average minimum *a-b* values of -0.007 (Ikari et al., 2015b; Kameda et al., 2015). These values match those measured here for gouge mixtures with 70 % opal. Following our data comparison, we propose that biogenic opal is responsible for velocity-weakening frictional behavior when mixed with clay.

However, since the frictional properties of a material are suggested to be determined by grain packing (Lupini et al., 1981; Kohli and Zoback, 2013) and the deformation of frictional contact junctions (Engelder and Scholz, 1976; Logan and Teufel, 1986; Wang and Scholz, 1994), we need to evaluate the evolution of grain packing with opal content, which controls the predominant grain contact populations during frictional sliding at a given mineral composition.

Evolution of grain packing with opal content

To evaluate the evolution of grain packing with opal content of our gouge mixtures, we compare our porosity measurements to those predicted from the ideal packing model, which reveals marked differences (Fig. 3.3d). Measured porosities decrease much more gently with increasing clay content and reach their lowest value of 0.25 at pure RS (68 % clay). Since we did not measure porosity of pure illite, we are unable to say whether porosity would further decrease or increase with increasing clay content. Although the clay content of 28-34 % at the minimum in porosity (0.19) predicted by ideal packing model generally agrees with measurements on quartz-kaolinite mixtures (~20 wt% at 10 MPa, Marion et al., 1992; 20-30 at 0-50 MPa, Crawford et al., 2008), we find a different pattern in the evolution of measured porosity with clay content. The porosity minimum in the ideal packing model is suggested to indicate that the pore space between the coarser particles is entirely filled with the finer platy particles, and this marks the transition from a grain framework to a clay matrix stress support at a specific effective stress loading (Marion et al., 1992; Revil et al., 2002; Crawford et al., 2008; Tembe et al., 2010). It may seem confusing that our porosity measurements do not describe such a transition in grain packing.

The difference between measured and modeled data may result from the influence of the diameter ratio of coarse to fine particles, which primarily determines the packing of binary mixtures (McGeary, 1961). When the particle diameter ratio (coarse/fine) is large, such as in

the studies of Marion et al. (1992) (> 50) and Crawford et al. (2008) (> 30), packing of the mixture is assumed to be close to ideal. However, in this study, both endmember starting materials have been ground to the same maximum grain size of 125 µm, and therefore material mixtures may have quite small particle diameter ratios. In such a case, grain shape can have a large effect on the ideal packing model (Crawford et al., 2008). We assume that discrepancies between measured and modeled porosities that result from uncertainties in clay porosity and from using a binary model for polymineralic mixtures are minor in comparison to the effect of grain size. Consequently, we are unable to infer the initial grain packing of our tested gouge mixtures with the help of the ideal packing model. However, we may be able to approximate it via the evolution of frictional strength with clay content.

Grain packing under uniaxial loading has been shown to dictate strain localization under shear loading, resulting in the three-regime degradation of frictional strength with increasing clay content in a gouge mixture (Lupini et al., 1981). The first transition from high to intermediate strength (regime 1 to 2) is associated with the transition from a stress supporting grain framework to a clay matrix with dispersed strong grains embedded, as evident by the porosity minimum under uniaxial loading (e.g. Marion et al., 1992; Crawford et al., 2008). The second transition from intermediate to low strength (regime 2 to 3) is manifested by a change of strain localization due to clay layer thickness (Tembe et al., 2010). In this work, we focus on the first transition, which has been associated with the transition of unstable to stable sliding before (Kohli and Zoback, 2013).

This transition is manifested by an accelerated decrease of frictional strength with clay content as seen for montmorillonite-quartz and montmorillonite-illite-quartz mixtures at a clay content of approximately 25% (e.g. Tembe et al., 2010). In the tested opal-RS mixtures, we observe a change in the decrease of friction at a similar clay content (~20 %; opal 70 %) (Fig. 3.3a). Since we do not observe a porosity minimum around such clay contents (Fig. 3.3d), it may be assumed that our mixtures do not capture the transition from regime 1 to 2. However, the deflection in porosity trend at a clay content of ~50%, which corresponds to an opal content of ~30%, correlates with a second change in the degradation of frictional strength with clay content (Fig. 3.3a, d). This may serve as evidence for a link between the degradation of strength and porosity evolution over clay content and thus grain packing, however not with respect to the ideal packing model.

Additionally, at the same mineral composition, we record an abrupt transition in the friction parameter *b* from high to low values with decreasing opal content (Fig. 3.3c, 3.4b). The magnitude of the friction parameter *b* is suggested to describe the evolution of friction with contact area (e.g. Dieterich and Kilgore, 1994, 1996). Because contact area growth is related to the size and quality of the initial contact area (e.g. Dieterich and Kilgore, 1994, 1996), the

decrease in the parameter *b* may indicate a transition from sliding at grain contacts of strong minerals to sliding at grain contacts of weak minerals, which implies a change in grain packing. This indication further supports the indication that the mineral mixture with 30 % opal marks the transition between a grain framework stress support and a clay matrix stress support. Based on these considerations, we assume that a grain framework stress support applies to all mixtures with opal contents of 30% or more (up to 50 % clay). We hypothesize that the change in grain configuration is shifted towards higher clay contents due to a low diameter ratio of strong to weak grains, so that grain shape may be an important factor. However, measurements of grain size distributions of the endmember materials are necessary to test this hypothesis.

The influence of individual friction parameters *a* and *b* on friction velocity dependence

A potentially unstable frictional behavior, expressed by negative *a-b* values, in weak mixtures with ≥ 30% opal (≤ 50% clay) may either result from high *b* values or small *a* values that are unexpected at corresponding friction coefficients. Previous work has suggested that the friction response to a velocity perturbation is mostly dependent on the friction parameter *b* (Blanpied et al., 1987; Ikari et al., 2016) and indeed the trends of *a-b* over clay content, as well as over load point velocity, are approximately inverse to those of *b* (Fig. 3.3b, c, f, g, 3.4a, c). The parameter *b* has been suggested to relate to strength loss due to the evolution of contact area via plastic deformation (e.g. Dieterich and Kilgore, 1994, 1996), which is enhanced by dilatancy (Beeler, 2007). Stronger framework minerals can generally have a greater angularity, experience more dilatancy and have low initial contact area, which can strongly evolve over the critical slip distance, whereas in weaker, more platy materials dilatancy is suppressed and the large contact area may quickly be saturated (Géminard et al., 1999; Saffer and Marone, 2003; Ikari et al., 2016). Therefore, the observation of increasing *b* values with an increasing friction coefficient is in agreement with the theoretical framework.

For mixtures with opal contents up to 50 %, the initially increasing and subsequently decreasing *b* values with increasing velocity, with maximum *b* values at velocities of 1 µm/s, may result from time-dependent growth of contact area. Smaller velocities allow a longer duration of a grain contact and thus facilitate contact area growth, while higher velocities reduce the duration of contact area growth and thus the magnitude of *b* (e.g. Dieterich and Kilgore, 1994). However, since in our experiments velocity was increased with increasing slip displacement, it is not possible to separate the effect of both variables. The accumulation of slip displacement has also been suggested to facilitate contact area growth (Dieterich, 1981; Beeler et al., 1996; Scruggs and Tullis, 1998; Mair and Marone, 1999; Ikari et al., 2011a).

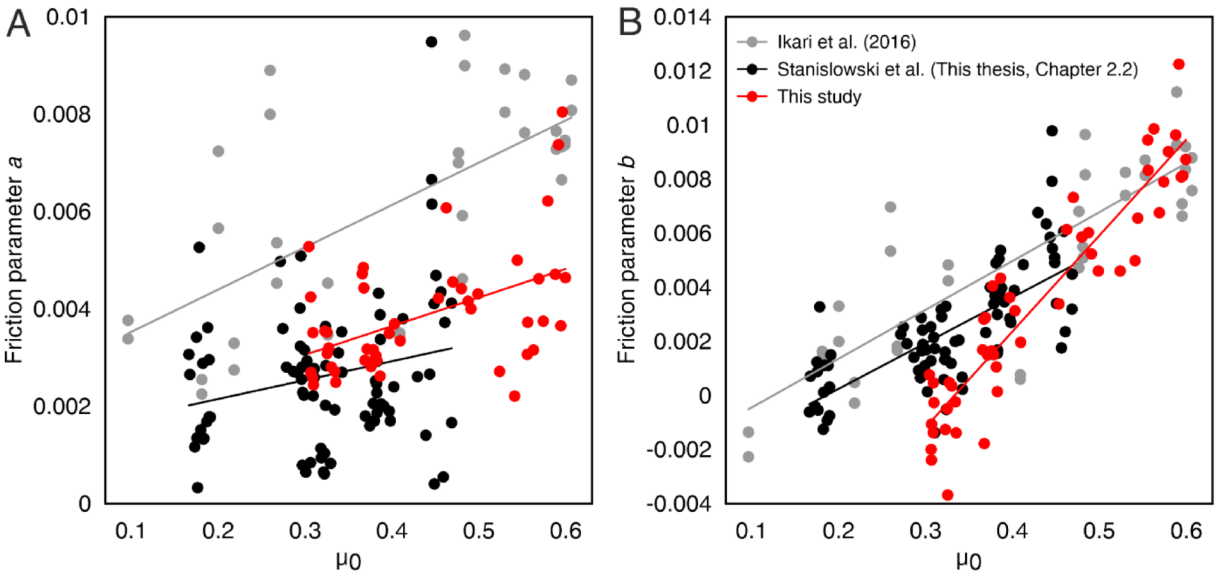

Figure 3.7: Individual friction parameters a) *a* and b) *b* over friction coefficient for velocity upsteps from data of Ikari et al. (2016) over a variety of synthetic and natural gouge materials, of Stanislowski et al. (This thesis, Chapter 2.2) over inputs sediments to the North Sumatra subduction zone, and of this study.

The relationship of *b* values and coefficient of friction for opal-RS mixtures reveals a trend that is very similar to that over a variety of materials excluding hydrous amorphous silica (Ikari et al., 2016) as well as that of natural hydrous amorphous silica-bearing samples (Stanislowski et al., This thesis, Chapter 2.2). A small difference in slope leads to comparable *b* values at higher friction coefficients and slightly lower *b* values towards weaker mixtures (Fig. 3.7b). Therefore, the relation between *b* values and friction coefficient does not explain the observed onset of velocity weakening at unexpectedly low friction coefficients. On the other hand, values of *a* are substantially lower than those measured by Ikari et al. (2016), but fairly similar to those measured by Stanislowski et al. (This thesis, Chapter 2.2) (Fig. 3.7a). These consistently low *a* values allow abruptly increasing *b* values at opal contents of ≥ 30 % with μ_0 = 0.38 to exceed, which results in negative *a*-*b* values (Fig. 3.3b, c, 3.5).

The micromechanical process underlying the parameter *a*, which describes the direct effect of frictional change in response to a velocity perturbation, is still obscure (e.g. Beeler et al., 2007; King and Marone, 2012), but is associated with a thermally activated Arrhenius process and thus hypothesized to represent a viscosity (Blanpied et al., 1998; Baumberger et al., 1999; Rice et al., 2001; Nakatani, 2001). According to Newton's law of viscosity:

$$\eta = \frac{\tau}{\dot{\gamma}} \tag{3.4}$$

at a constant shear stress τ viscosity η is negatively correlated with shear strain rate $\dot{\gamma}$. Since strain rate is inversely related to deformation height, a smaller deformation height leads to a

lower viscosity and thus *a*. While Ikari et al. (2016) used a biaxial device with a double direct shear configuration allowing shear deformation within the entire gouge thickness, in this study as well as in that of Stanislowski et al (This thesis, Chapter 2.2) experiments were performed on a direct shear device with forced localization of shear deformation (Fig. 2.1.2a). Following the line of reasoning, the difference in the magnitude of *a* values among the studies may be partly explainable by the experimental setup, which is generally consistent with explanations given by previous work (Ikari and Hüpers, 2021).

However, as opposed to the study of Ikari et al. (2016), obtained *a* values of this study as well as that of Stanislowski et al. (This thesis, Chapter 2.2), appear to be rather independent of the coefficient of friction (Fig. 3.7a). Therefore, not only the magnitude, but also the trend of the parameter *a* with coefficient of friction μ_0 differs between the studies. When looking at the relation between *a* and μ_0 for different velocities, is becomes clear that the trend of *a* and μ_0 for low velocities is different from that at higher velocities. At low velocities of up to 0.3 µm/s, as opal content and thus μ_0 increases, *a* increases (Fig. 3.4b), which fits the general trend of various materials as well as the theoretical considerations reported by Ikari et al. (2016) (Fig. 3.7a). However, at higher velocities, it seems that the microphysical process scaling the relationship of *a* and opal content (and μ_0) changes or even terminates (Fig. 3.4b), leading to low *a* values at relatively low opal contents and μ_0 values. These observations raise the question of what variables control the velocity-dependent relation between friction parameter *a* and μ_0 seen in our gouge mixtures.

Velocity dependent relation between friction parameter *a* and friction coefficient

When considering *a* to be a viscosity, which in turn depends on strain rate and thus velocity (Eq. 3.4), it follows that *a* also depends on velocity. Aside from the somewhat larger scale of deformation height, the Arrhenius process also acts at grain scale. Specifically, it has been proposed that *a* inversely correlates with the activation volume Ω and activation energy E_0 for plastic deformation at contact junctions and positively correlates with friction coefficient μ_0 (Baumberger et al., 1999; Ikari et al., 2016), expressed as:

$$a = \frac{\kappa T}{H\Omega} = \frac{\mu_0 \kappa T}{E_0} \tag{3.5}$$

where *T* is temperature, κ is the Boltzmann constant, and *H* is material hardness. Since κ and *T* are constants (in this experiment) and *H* is an intrinsic material property, Ω is the only variable that is able to describe *a* in dependence of velocity (middle term, Eq. 3.5). According to Equation 3.5, a velocity-dependent change in Ω also affects μ_0.

At this point, it is useful to clarify the qualitative relationships of the individual parameters. Previous work has shown that the hardness of a monomineralic material is positively correlated with the friction coefficient (e.g. Bowden and Tabor, 1966; Engelder and Scholz, 1976). This relation is also observed in our material mixtures, where opal has a hardness of ~5.95 GPa (Thomas et al., 2008) and the hardness of RS can be approximated by shale hardness of ~0.62 GPa (Bobko and Ulm, 2008). However, in theory, H and μ_0 as well as H and a should be inversely related (Equation 3.5). An explanation for this apparent contradiction is that that the theoretical inverse relationship may be overwhelmed by a strong negative correlation between H and Ω (Ikari et al., 2016). Consequently, Ω is negatively correlated with μ_0 as well as with a. At a given temperature, changes of both Ω with a and Ω with μ_0 are scaled by H.

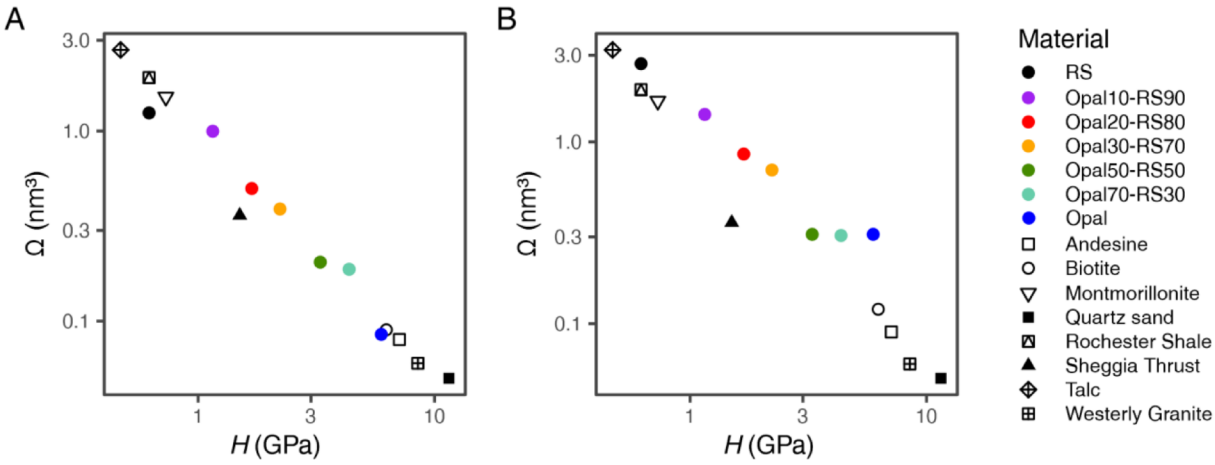

Figure 3.8: a) Minimum values and b) maximum values for volume of plastic deformation Ω over material hardness H. Filled circles illustrate data of this study, all other symbols represent values of Ω from Ikari et al. (2016) and average values of H assigned by Ikari et al. (2016). Data of hardness: talc (Taylor, 1949), the illite-smectite mixed-layer clay rectorite (Zhang et al., 2009), shale (Bobko and Ulm, 2008), mica schist (Beste and Jacobson, 2003; Zhang et al., 2009), granite (Beste and Jacobson, 2003), orthoclase (Taylor, 1949), quartz (Taylor, 1949; Westbrook, 1958; Oliver and Pharr, 1992; Beste and Jacobson, 2003), and calcite (Taylor, 1949; Beste and Jacobson, 2003).

To compare the interrelation of these parameters for our gouge mixtures with that of a variety of materials also tested at room temperature (Ikari et al., 2016), we use minimum and maximum values of a for each gouge mixture to calculate Ω. The relationship of H and Ω of our gouge mixtures reveals the same general trend as that over a variety of materials (Fig. 3.8). However, while using minimum values of Ω yields the same slope as that obtained over materials without hydrous amorphous silica, using maximum values of Ω results in a deviation from that slope (Fig. 3.8). Note that this deviation appears to be relatively small due to the

double logarithmic scale. When considering the velocity dependence of Ω, we see a clear change in the relationship of Ω and *H* at 1 µm/s upstep loadpoint velocity (Fig. 3.9a). At low

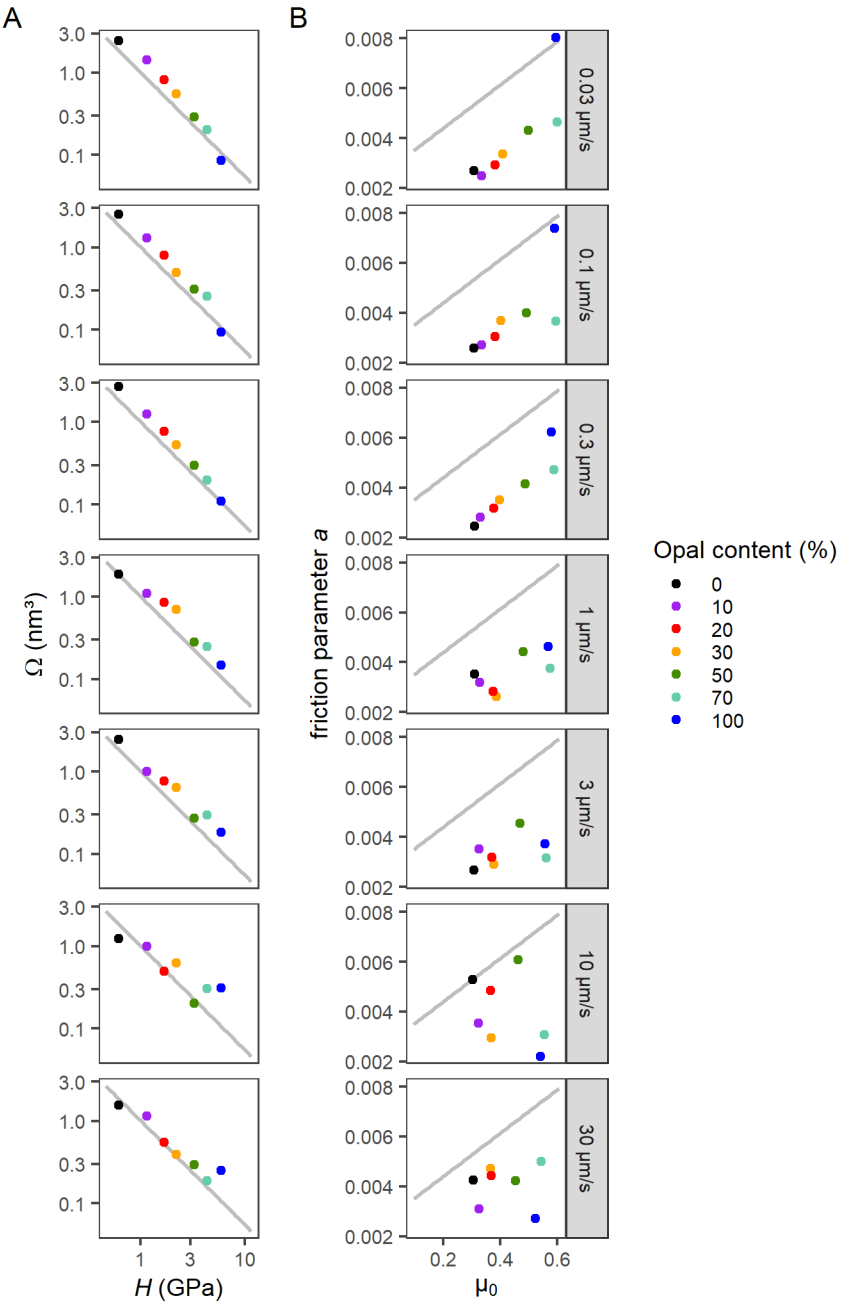

Figure 3.9: The change of a) volume of plastic deformation Ω over material hardness *H*, and b) friction paramteter *a* over friction coefficient μ_0 for different upstep loadpoint velocities. Grey lines represent linear regressions of data from a variety of materials (Ikari et al., 2016).

velocities, the relationship of Ω and *H* of opal-RS mixtures shows the same slope as that over materials without hydrous amorphous silica observed by Ikari et al. (2016). This is in accordance with the similarity in the relationships of *a* and μ_0 at low velocities observed here

and by Ikari et al. (2016) (Fig. 3.9b). At higher velocities, the relationship of Ω and *H* in the samples tested here seems rather weak and differs from that over materials without hydrous amorphous silica (Fig. 3.9a). This is consistent with the difference in the relationships of *a* and μ_0 of opal-RS mixtures and materials without hydrous amorphous silica (Fig. 3.9b). Consequently, the velocity-dependent change in the relation between Ω and *H* can explain the velocity-dependent change in the relation between *a* and μ_0 of our gouge mixtures, and thus the deviation from the relation between *a* and μ_0 over materials without hydrous amorphous silica. However, it is unclear why Ω, the activation volume of plastic deformation, ceases to be related to material hardness *H* at a specific velocity. Based on thoughts of Ikari et al. (2016), we speculate that at the specific velocity of 1 µm/s and corresponding strain rate, interatomic bonds at the frictional contact surfaces of amorphous opal grains start to weaken, which results in the reduction of viscosity (Ojovan, 2008). As a side note, because the change in Ω at 1 µm/s loadpoint velocity correlates with a maximum in *b* values at 1 µm/s, both parameters may have a common microphysical origin. This is plausible since both parameters relate to the process of plastic deformation at frictional contact junctions.

Following our argumentation, we propose that the trend of *a-b* values with coefficient of friction observed for our opal-RS mixtures can be deduced from relatively low *a* values at higher loadpoint velocities. The parameter *a* appears to be affected by a velocity- or strain rate-dependent, and thus viscous process acting at the frictional contacts of the opal grains. While most previous experimental studies have concentrated on the parameter *b*, our data show that the microphysical process behind the parameter *a* should be given more attention. Additionally, for gouge mixtures of strong and weak minerals, the particle diameter ratio needs to be considered due to its influence on grain packing and thus on predominant grain contact populations.

Implications for earthquake hazard assessment

A comparison of our results with those of Stanislowski et al. (This thesis, Chapter 2.2) shows a difference in the amounts of hydrous amorphous silica necessary for (potentially) unstable sliding between the two studies. This difference may reflect the presence or absence of aggregates (Stanislowski et al., This thesis, Chapter 2.2), slight differences in the viscous behavior of frictional contacts of the different hydrous amorphous silica that may arise from different amounts of crystal water for biogenic opal and palagonite, or other compositional controls. Nevertheless, due to similarly low values of the direct effect *a* that lead to velocity weakening, we suspect a common microphysical process, namely the viscous behavior of frictional contacts of hydrous amorphous silica. Therefore, based on our findings, we can support the hypothesis of Stanislowski et al. (This thesis, Chapter 2.2) that threshold amounts

of hydrous amorphous silica can induce frictional instability in weak sediments under low temperature and pressure conditions.

However, the transition to increasing *a-b* values and thus towards velocity strengthening at cut-off velocities of ~ 0.3-1 µm/s for mixtures with opal contents ≤ 50 % implies that rapid slip on shallow faults could be arrested before resulting in full-size slip instability (Kilgore et al., 1993), potentially resulting in a slow slip event (Shibazaki and Iio, 2003; Shibazaki and Shimamoto, 2007). In contrast, the sediments studied by Stanislowski et al. (This thesis, Chapter 2.2) do not show a transition to velocity strengthening at higher velocities, which underlines that palagonite and biogenic opal may have a slightly different viscous behavior. The sediments containing palagonite may thus lead to full slip instabilities.

Our findings not only offer an explanation for shallow seismic slip during 2004 Aceh-Andaman earthquake, but also bear important implications for shallow slow slip events, seismogenesis, and tsunami hazard at other subduction zones, where amorphous silica (preferably palagonite) constitute a part of the mineralogical composition of input sediments. Sources of amorphous silica may be volcanic ash or opaline fossils, which both are abundant in the sedimentary inputs to most subduction zones (Vrolijk, 1990; Rea and Ruff, 1996; Underwood, 2007). The transformation of opal to quartz is suggested to be completed at ~80°C (Keller and Isaacs, 1985), and may thus only be relevant to the trench-most portion of cooler subduction zones. Palagonite reaction kinetics however are still under debate (e.g. Walton and Schiffman, 2003) and therefore this mineral may be maintained in the shallow subduction zone at somewhat greater depths.

Also other materials that show a viscous behavior of their frictional contacts similar as opal and palagonite may cause frictional instability in otherwise weak fault materials and thus the occurrence of shallow slow or large earthquakes. Therefore, further investigations on the viscous behavior of frictional contacts of minerals that are contained in fault materials need to be carried out. A more often expected deviation from the established relation between frictional strength and friction rate dependence may also have implications for earthquake modelling studies that are based on laboratory-derived *a/b* ratios (e.g. Ampuero and Rubin, 2008).

Conclusion

We performed laboratory friction experiments on gouges of pure biogenic opal, pure Rochester Shale, and various mixtures of both components to study the effect on hydrous amorphous silica on the frictional behavior of clay-rich mixtures. With as little as 30 % opal, corresponding to ~50 % clay minerals in our experiment, we observed an onset of velocity-weakening behavior at a friction coefficient of μ_0 = 0.38. Our findings support the hypothesis

that threshold amounts of hydrous amorphous silica are able to induce potentially unstable frictional sliding behavior in weak sediments. These results deviate markedly from the established strength-stability relation, but do not question the microphysical model behind it. However, they underscore the necessity of evaluating the relationship of friction rate dependence and frictional strength in terms of viscous processes at frictional contacts. In particular, the parameter *a*, which has been described as an instantaneous viscosity, is shown to play an important, yet potentially underestimated role for frictional stability.

Acknowledgement

We thank Andre Hüpers for providing the biogenic opal used in this study. Achim Kopf is thanked for laboratory support. Rate- and state friction modeling was performed using the program “RSFit3000”, courtesy of Rob Skarbek and Heather Savage. This work was funded by the European Research Council (ERC) under the European Union’s Horizon 2020 research and innovation programme Grant #714430 to M. Ikari.

4 Conclusions and synthesis

Subduction zones pose a great hazard to coastal populations by producing large earthquakes and tsunamis. Crucial to earthquake and tsunami hazard assessment is the fault slip behavior of the shallow subduction zone, yet little is known about shallow fault slip behavior or the factors controlling it. The overall goal of this thesis was to investigate the intrinsic frictional slip behavior of subduction zone input sediments and its implications for the seismic potential of the shallow portions of the northern Cascadia and the North Sumatra subduction zones. To that end, we performed laboratory friction experiments on subduction zone input sediments, under room temperature, relatively low effective normal stresses, and at a range of driving velocities including plate rates. In addition, the thesis aimed to study the relevance of hydrous amorphous silica to the frictional slip behavior of the North Sumatra, but also of other subduction zones. To systematically assess the effect of opal (hydrous amorphous silica) on the velocity-dependent frictional behavior of clay-rich gouge, we carried out a series of friction experiments on synthetic gouge mixtures. This chapter recaptures the main results of this thesis and puts these in a broader perspective with regard to future earthquake research at subduction zones.

4.1 Shallow seismic potential of the northern Cascadia and the North Sumatra subduction zone

When comparing the results of the friction experiments on input samples of northern Cascadia and North Sumatra presented in this work, it is evident that the potential fault-forming materials have very different intrinsic frictional slip behavior. The northern Cascadia material shows consistently velocity-strengthening behavior and no sign of laboratory slow slip events. Consequently, the material is associated with intrinsically stable behavior (Chapter 2.1). In contrast, the North Sumatra material exhibits velocity-weakening behavior as well as slip instabilities. Therefore, it is considered intrinsically unstable (Chapter 2.2).

However, measurements of frictional strength and slip behavior as well as associated frictional slip stability need to be put into context of extrinsic factors, which affect the intrinsic material properties on the way from the site where the sample was taken to the shallow megathrust. Extrinsic factors that exert a first-order control on both the frictional properties of fault material and the stability conditions are temperature, pressure, and time. Thus, we considered previous work that evaluated these factors at the two subduction zone settings, and work concerned with the effect of the factors on intrinsic frictional behavior of geologic materials. At both subduction zone settings, the temperatures are relatively high compared to other settings (Hyndman and Wang, 1993; Stevens et al., 2021). On the other hand, the

effective pressure on the shallow fault portions may be relatively low due to the possibility of marked overpressure (Davis and Hyndman, 1989; Zhang et al., in prep.; Chapter 2.1). Although the illite-rich hemipelagic mud that potentially forms the megathrust fault at northern Cascadia may velocity-weaken under both high-temperature and high-pressure conditions (Moore et al., 1989; den Hartog et al., 2012), at high temperature and low pressure it may still be velocity strengthening, and thus stably sliding (Chapter 2.1).

We suggested that the presence of aggregates, presumably formed by patchy hydrous amorphous silica cement, may be responsible for the velocity-weakening character of the interpreted fault-forming materials at North Sumatra (Chapter 2.2). Such aggregates have been suggested to remain preserved up to seven times higher effective pressure than tested in our experiments and create high sediment porosity (Hüpers et al., 2015). Uncertainty in reaction kinetics of palagonite (hydrous amorphous silica, found in the samples) as well as indication of high porosity of the predécollement and shallow décollement horizon (Walton and Schiffman, 2003; Dean et al., 2010) lead to the assumption of the presence of aggregates and associated frictional slip behavior at the shallow décollement (Chapter 2.2). Based on these considerations, we suggested that for the two different subduction-zone settings, the intrinsic behavior of the fault-forming input sediments may not be critically altered by extrinsic factors acting toward and within the respective shallow subduction zone (Chapters 2.1 and 2.2).

Transferring these results to the shallow subduction zones, we proposed that, in the absence of a stress shadow, the shallow, trench-most portion of the northern Cascadia subduction zone may not be capable of hosting slow slip events and not necessarily be locked and thus not seismogenic (Chapter 2.1). This inference contrasts with previous work, which made suggestions on shallow locking based on the lack of observed slow slip events (e.g. McGuire et al., 2018). In addition, Coulomb wedge modeling based on our friction measurements indicated marked pore-fluid overpressures on the trench-most shallow décollement. In combination with the measured low sliding friction and low cohesion, we inferred that despite the velocity-strengthening behavior, coseismic slip from a deeper-seated earthquake may easily propagate updip through the shallow portion of the subduction zone (Chapter 2.1). Consequently, although the shallow northern Cascadia subduction zone may be not seismogenic, it may still have seismic and tsunamigenic potential through shallow coseismic slip propagation. These important results can be used as input to numerical elastic models on crustal deformation, which can simulate the slip behavior of a fault and thus represent an important instrument to predict earthquake hazard. With each new data-based input, these models become more realistic. Consequently, our findings based on laboratory data may help improve the prediction of the hazards of a future megathrust earthquake at

Cascadia and thus mitigate the impact of a future large earthquake and potential tsunami on the affected coastline population.

For the North Sumatra subduction zone, we concluded that the shallow portion is seismogenic all the way to the trench (Chapter 2.2). Our results deliver the first evidence of a shallow seismogenic zone at the North Sumatra subduction zone and thus offer an explanation to the shallow coseismic slip and tsunamigenesis during the large, devastating Aceh-Andaman earthquake of 2004. An interesting aspect of the experimental results was the occurrence of laboratory slip instabilities, small-scale seismic cycles, which appeared to be different among the tested lithologies. Since specific characteristics of slip instabilities on faults in nature, such as large or slow earthquakes, obey scaling laws (Chapter 1), our experimental slip instabilities may offer insights in the recurrence and magnitude of earthquakes at the North Sumatra subduction zone. In detail, a comparison of characteristics of instabilities observed in the experiments with those of instabilities observed in the North Sumatra subduction system may help to infer the specific lithology that forms the megathrust fault. Knowledge about the small-scale characteristics of slip instabilities of this lithology could be scaled to the megathrust fault at North Sumatra. This scaling could deliver essential information for expectations of future seismicity at the subduction zone and therefore improve earthquake and tsunami hazard assessment for this region. Such a comparison should be part of future work.

The inferred different shallow fault slip behavior of these two subduction zone settings may be surprising, given that they share a large set of attributes, which can exert control on the frictional behavior. Among these are the relatively high temperatures (Hyndman and Wang, 1993; Stevens et al., 2021), a thick insulating sedimentary section that is divided into a lower hemipelagic lithostratigraphic unit and an upper fan turbiditic unit (Kulm and von Huene, 1973; Davis and Hyndman, 1989; Dugan et al., 2017), a décollement assumed to root in the hemipelagic unit (Davis and Hyndman, 1989; Hyndman et al., 1990; Dean et al., 2010), tsunamigenic potential (Satake et al., 1996; Ammon et al., 2005), and potentially near lithostatic pore pressure on the trench-most décollement (Davis and Hyndman, 1989; Zhang et al., in prep.; Chapter 2.1). A clear difference however, is the vergence of outer prism thrust faults, which is landward for North Sumatra (e.g. McNeill and Henstock, 2014) and seaward for northern Cascadia (e.g. MacKay et al., 1992). In spite of the large number of similarities of the two subduction zones, our investigations demonstrate that their fault slip behavior at shallow depths may be different (Chapter 2.1, 2.2). Consequently, the intrinsic frictional behavior of input sediments that are fault-forming upon subduction is critical to the seismic potential of shallow portions of subduction zones.

4.2 The intrinsic frictional behavior of materials containing hydrous amorphous silica

One of the most important factors determining the intrinsic frictional properties of a geologic material is its mineral composition (e.g. Lupini et al., 1981; Tembe et al., 2010; Ikari et al., 2016). In general, sediments and subduction fault zones dominantly contain a mixture of quartz, clay minerals (typically illite, smectite, chlorite, and kaolinite), and plagioclase (Marone and Saffer, 2007). The effect of these minerals on the velocity-dependent frictional behavior has been extensively studied (Lupini et al., 1981; Logan and Rauenzahn, 1987; Morrow et al., 1992; Saffer and Marone, 2003; Crawford et al., 2008; Ikari et al., 2009a; Tembe et al., 2010). This thesis showed that velocity-weakening behavior of the presumably fault-forming sediments of the North Sumatra subduction zone is likely induced by the presence of another mineral group, namely hydrous amorphous silica (Chapter 2.2). Specifically, threshold amounts of these minerals may lead to mineral aggregation by patchy amorphous silica cementation under relatively low temperatures and pressures. Aggregation, in turn, could create a grain packing of stress-supporting aggregate framework, which allows frictional sliding to be accommodated on hydrous amorphous silica at relatively low frictional strength.

The effect of hydrous amorphous silica on frictional behavior has been the focus of only a few studies. These studies are concerned with extreme dynamic weakening and time-dependent strength recovery of intact quartz rock or amorphous nanopowder at intermediate to seismic slip rates (Goldsby and Tullis, 2002; Di Toro et al., 2004; Hayashi and Tsutsumi, 2010; Nakamura et al., 2012; Rowe et al., 2019). It was proposed that either the formation of silica gel (hydrous amorphous silica) or the presence of amorphous nanopowder at high slip rates is responsible for the observed frictional behavior. However, there is a critical lack of information on how materials containing hydrous amorphous silica grains or aggregates will behave frictionally when sheared at low slip rates.

The study on gouge mixtures of opal and shale presented in Chapter 3 was especially designed to address this knowledge gap. We found that with as little as 30 % opal, the clay-rich gouge is velocity weakening at a relatively low friction coefficient. This result offers an explanation for velocity-weakening behavior of inputs to the North Sumatra subduction zone that contain (~10-30 wt%) hydrous amorphous silica. Knowledge of the intrinsic factors controlling frictional slip behavior improves determining the impact of extrinsic factors on the frictional slip behavior of the input material on the way to the subduction zone, which is vital to the estimation of fault slip behavior and seismicity of the shallow megathrust fault of the North Sumatra subduction zone.

An important finding about hydrous amorphous silica was that since only small amounts are need to induce velocity weakening in a granular material, it is able to induce velocity-weakening behavior in weak sediments (Chapter 2.2, 3). In addition, the large amounts of mineral-bound water (e.g. Stroncik and Schmincke, 2002) that can be released from hydrous amorphous silica during burial represent a potential cause of overpressure and hence an associated reduction in frictional strength (e.g. Hubbert and Rubey, 1959). Faults are likely to form in weak horizons of marine sedimentary columns upon subduction (e.g. Moore, 1989). Our observation that opal-bearing sediments are weak thus bears important implications for the frictional behavior of shallow subduction zones where incoming sediment horizons contain critical amounts of hydrated amorphous silica, either with or without aggregates (Chapter 2.2, 3). Based on the amount and the kind of hydrous amorphous silica, a shallow fault may be able to host large earthquakes or slow slip events (Chapter 3). Hydrous amorphous silica may also influence the depth at which slow and large earthquakes can occur. Specifically, its potential to increase the pore-fluid pressure is important, since pore-fluid pressure modifies the effective stress and thus the depth of nucleation of a large and slow earthquake (e.g. Wang and Hu, 2006; Saffer and Wallace, 2015). Moreover, high pore pressure may also facilitate shallow earthquake propagation (Seno, 2002). In conclusion, hydrous amorphous silica is relevant to fault slip behavior and seismic potential of shallow portions of subduction zones and should thus be considered in future earthquake research.

We concluded that the microphysical process allowing velocity-weakening behavior at a low frictional strength in geologic materials that contain threshold amounts of hydrous amorphous silica results from a viscous process at the frictional contacts of hydrous amorphous silica (Chapter 3). The combination of low frictional strength and velocity-weakening behavior markedly deviates from the established relation that weak materials generally exhibit velocity-strengthening behavior (e.g. Ikari et al., 2016). Since this unexpected combination can have a large impact on fault slip behavior of shallow subduction zones, further studies on the viscous behavior of frictional contacts of other materials are crucial to make progress in earthquake research.

4.3 Implications for other subduction margins

Mineral aggregates in lithologies of the high porosity zone in the input sediments to the Nankai Trough have been proposed to be formed through patchy amorphous silica cementation (Hüpers et al., 2015). At North Sumatra, we found evidence of similar aggregates in lithologies that contain hydrous amorphous silica. Therefore, we inferred that the aggregates we found may have the same origin as those found in the lithologies of the high porosity zone at Nankai, namely hydrous amorphous silica cement (Chapter 2.2). Previous work has shown

that only small amounts of hydrous amorphous silica are necessary to form these aggregates and maintain elevated porosities during ongoing burial (Spinelli et al., 2007; Hüpers et al., 2015). Therefore, it is valuable to consider where hydrous amorphous silica may be present at concentrations high enough to create similar lithologies.

Sources of hydrous amorphous silica may be volcanic ash or opaline fossils. Since subduction margins often host volcanism and opaline plankton, such as radiolaria or diatoms that are abundant in the Pacific and Indian Oceans, hydrous amorphous silica is likely a major constituent of the sedimentary input to various subduction zones. Therefore, the presence of aggregates in subduction zone input sediments may be a more widespread phenomenon that has received little attention. Since hydrous amorphous silica-bearing lithologies hold the potential to form faults upon subduction, which are likely to host shallow earthquakes (Chapters 2.2, 3), it is important to identify subduction zone settings with similar lithologies.

The aggregates found in the lithologies of the high-porosity zone in the input sediments to the Nankai Trough have been proposed to be responsible for the elevated porosities (Hüpers et al., 2015). Since the aggregates that we found are contained in high-porosity lithologies, it may be inferred that the presence of such aggregates generally creates high porosities. At the North Sumatra subduction zone, the high porosity lithologies that contain the aggregates are associated with a high-amplitude negative-polarity seismic reflector in seismic images. This reflector was interpreted as a weak, porous, and overpressured horizon in the input sediments as well as within the outer prism of the subduction zone, suggested to form the décollement upon subduction (Dean et al., 2010).

High-amplitude negative-polarity seismic reflectors have also been identified at several other subduction margins, where they mark the décollement. Among these are the Nankai Trough (Bangs et al., 2004; Moore & Shipley, 1993; Mikada et al., 2002; Moore et al., 2005), and central Cascadia (MacKay et al., 1992; Cochrane et al., 1994; Moore et al., 1995a). However, at northern Barbados, for instance, the seismic reflector has been correlated through drill cores with both the décollement and predécollement, which form in a porous, overpressured radiolaria-rich claystone (Shipley et al., 1994; Moore et al., 1995b, 1998; Bangs et al., 1999). Because radiolaria have opal skeletons, the findings at northern Barbados are markedly similar to that at North Sumatra. Although it has been suggest in previous work that elevated smectite contents influence the lithostratigraphic position of the décollement at northern Barbados (Deng and Underwood, 2001), the fault slip behavior of the décollement may equally well be controlled by the frictional properties of hydrous amorphous silica. Hence, a shallow seismogenic zone or shallow rupture propagation at the northern Barbados subduction zone could be possible, which would pose a great risk for the population along the Lesser Antilles. This subduction zone should therefore be strong focus of future work. Other

subduction zones that are less well-studied using seismic imaging or sampling may have similar weak, overpressured and hydrous amorphous silica-bearing lithostratigraphic horizons.

This thesis raises the possibility that subduction zones with a shallow seismogenic zone may be more common than predicted by the seismogenic zone model. This implies that earthquake and tsunami hazards could be highly underestimated at some subduction zone settings. An important lesson learned is that hydrous amorphous silica is relevant to the slip behavior of shallow megathrust faults. As such, it should be a focus of future laboratory studies. Furthermore, as seen for hydrous amorphous silica, the viscous behavior of frictional contacts of a material can determine the relation between frictional strength and frictional slip behavior of a material, a concept vital to seismic faulting.

Appendices

Besides the investigations the northern Cascadia and North Sumatra subduction zones, in which I was leading author, I contributed as a co-author to two studies on the fault slip behavior of the Nankai Trough subduction zone at southwest Japan. This site has faced major earthquakes in the 1940's and poses a constant threat to the Japanese population. It is the best-studied subduction zone in the world, largely owed to the work of many outstanding scientists done during the ten year long multi-stage NanTroSEIZE project. Participating in IODP Expedition 358 in the context of NanTroSEIZE on board D/V Chikyu as a physical properties specialist has strengthened my interest to study the seismicity of this and other subduction zones. Below, I listed the abstracts of the two friction studies, as well as that of the Preliminary Report of IODP Expedition 358.

Friction experiments under in-situ stress reveal unexpected velocity-weakening in Nankai accretionary prism samples

Alexander Roesner[1,*], Matt J. Ikari[1], Demian M. Saffer[2], **Katja Stanislowski[1]**, Agathe M. Eijsink[1], Achim J. Kopf[1]

[1] MARUM—Center for Marine Environmental Sciences and Faculty of Geosciences, University of Bremen, Bremen, Germany

[2] Department of Geosciences, Pennsylvania State University, University Park, PA 16802, USA

Abstract

The Nankai Trough hosts diverse fault slip modes, ranging from slow slip events to megathrust earthquake ruptures. We performed laboratory friction experiments on samples collected by the Integrated Ocean Drilling Program offshore Kii Peninsula, Japan. This study systematically investigates the effect of effective normal stress on frictional strength and the velocity-dependence of friction for natural fault zone and wall rock samples collected from depths of 270 to ~450 meters below seafloor (mbsf), and over a range of shearing velocity spanning from 0.01–30 μm/s. In addition, cohesive strength was determined before and after each velocity step experiment while the sample was unloaded. We tested both powdered and intact specimens at estimated in-situ effective stresses, as well as at higher stresses representing deeper portions of the megasplay fault (Sites C0004, C0010) and the frontal thrust zone (Sites C0007, C0006). The apparent coefficient of sliding friction μ_S varies between 0.22–0.53 and correlates inversely with clay content. Direct measurements of cohesive

strength show that on average 11% of the residual shear strength, and up to ~30% for some specimens, can be attributed to cohesion. Friction coefficient slightly decreases as a function of increasing effective normal stress, attributed to a decreasing proportion of cohesive strength. The lowest μs values are observed for samples from the frontal thrust zone Site C0007 and the megasplay fault Site C0010. All samples show a combination of velocity-strengthening and velocity-weakening behavior, but intact samples tested under in-situ effective normal stress and low shearing velocities (<~1 μm/s) exhibit consistently large velocity-weakening frictional behavior. The observed velocity-weakening behavior is related to the induration state of the material, which affects the real area of contact along shear surfaces. This is supported by direct measurements of cohesive strength, showing that higher cohesion values in intact samples correspond with a more pronounced evolutionary effect in velocity step tests that, in turn, map to lower values of the rate-dependent friction parameter *a-b*. We propose that fault zones in the Nankai subduction zone are likely to be velocity-weakening, and thus potentially able to host the nucleation of unstable slip, from seismogenic depths to the seafloor. We also find that testing disaggregated fault zone samples and employing effective stresses exceeding those in-situ lead to overestimation of *a-b*, emphasizing the importance of testing intact samples under in-situ conditions in laboratory friction studies.

Spatial patterns in frictional behavior of sediments along the Kumano transect in the Nankai Trough

Hanaya Okuda[1,2], Matt J. Ikari[3], Alexander Roesner[3], **Katja Stanislowski[3]**, Andre Hüpers[3], Achim J. Kopf[3], Asuka Yamaguchi[1,2]

[1] Department of Ocean Floor Geoscience, Atmosphere and Ocean Research Institute, University of Tokyo, Chiba, Japan 8

[2] Department of Earth and Planetary Science, University of Tokyo, Tokyo, Japan

[3] MARUM – Center for Marine Environmental Sciences, University of Bremen, Bremen, Germany

Abstract

Seismic activities at subduction zones are governed by the sediments' frictional properties, which in turn are affected by diagenetic processes. To see the spatial patterns in frictional properties across the Nankai Trough, SW Japan, and their relations to seismic activities, we used sediment samples (10 to 59% clay content) along the Kumano transect covering a large spatial range from the inputs via the outer prism to the inner prism, including

the deepest sample ever recovered. We performed laboratory friction experiments under in-situ effective normal stresses and seawater-saturated conditions. Our results generally demonstrate that the friction coefficient inversely correlates with the clay mineral content. However, the outer prism sediments show higher friction coefficients than sediments from the other locations for a comparable clay mineral content. All samples show velocity-weakening behavior at low velocities, but the outer prism and the deep inner prism sediments show velocity strengthening at higher velocities. Based on the experimental results combined with a Coulomb wedge model, we find that the overpressured prism toe region has a décollement friction coefficient of 0.57, which is higher than the outer and inner prism regions where décollement friction likely ranges from 0.24 to 0.41. The calculated critical nucleation length for slip instability suggests that the décollement beneath the outer prism area is more frictionally unstable than that beneath the inner prism. This inference is consistent with the spatial distribution of very-low-frequency earthquakes and slow slip events at the shallow Nankai Trough.

International Ocean Discovery Program Expedition 358 Preliminary Report – NanTroSEIZE Plate Boundary Deep Riser 4: Nankai Seismogenic/Slow Slip Megathrust

Harold Tobin, Takehiro Hirose, Matt Ikari, Kyuichi Kanagawa, Gaku Kimura, Masataka Kinoshita, Hiroko Kitajima, Demian Saffer, Asuka Yamaguchi, Nobuhisa Eguchi, Lena Maeda, Sean Toczko, and **the Expedition 358 Scientists**

Abstract

International Ocean Discovery Program (IODP) Expedition 358 was carried out from October 2018 through March 2019 on the D/V Chikyu in an attempt to reach a plate boundary fault zone at seismogenic depths for the first time in scientific ocean drilling. The goal was to extend Hole C0002P from ~2900 to ~5200 meters below seafloor (mbsf) and cross the seismically interpreted main décollement fault zone with logging while drilling (LWD), downhole stress measurements, cuttings sampling, mud gas sampling, and partial coring by drilling a sidetrack to create a new hole (C0002Q). Although drilling reached 3262.5 mbsf, the deepest to date in all of scientific ocean drilling, the effort to drill to and sample the target—the megathrust fault zone—was not successful. Operational challenges in establishing sidetrack holes and advancing them at reasonable rates of penetration limited the new cased hole interval to less than 60 m total at a depth shallower than the previously established casing depth of 2922 mbsf. Combined, the cuttings, logs, and ~60 cm of recovered core from sidetrack

Holes C0002Q–C0002T revealed hemipelagic sediments and fine silty turbidites consistent in lithology and physical properties with those recovered in the same depth interval at the same site during Integrated Ocean Drilling Program Expedition 348. Cuttings revealed evidence of only weakly deformed rock, with relatively common calcite veins but few other structural indicators. Because no downhole leak-off tests were made and very little borehole imaging was performed, no further insight into the tectonic context was acquired.

After riser drilling at Site C0002 was terminated, drilling at alternate contingency Sites C0024 and C0025 was carried out. Site C0024 targeted the frontal thrust region to sample and log hanging wall rocks and the shallow portion of the décollement zone, and Site C0025 accessed sediments in the Kumano fore-arc basin. At Site C0024, a dedicated logging hole was drilled and a very complete suite of logs were acquired from 0 to 869 mbsf. Preliminary interpretation of log response and images suggests the frontal thrust zone was encountered from about 813 mbsf to the base of the hole, with a zone of notably low resistivity and steep bedding from 850 mbsf to the bottom of the hole. Core samples revealed lithologic units interpreted to be hemipelagic and turbiditic basin fill, trench fill, and Shikoku Basin sediments and encountered deformation potentially associated with a back thrust imaged in seismic reflection data. However, coring had to be terminated at about 620 mbsf, well short of the frontal thrust zone. Site C0025 recovered fore-arc basin sediments underlain by those interpreted to have been deposited in a trench-slope basin setting; no clear transition into older, inner accretionary wedge material was identified during preliminary analysis. Coring from 400 to 571 mbsf yielded datable material and possible evidence for diapiric intrusion of sediments.

References

Ammon, C.J. et al., 2005, Rupture process of the 2004 Sumatra-Andaman earthquake: Science, v. 308, p. 1133–1139, doi:10.1126/SCIENCE.1112260.

Ampuero, J.-P., and Rubin, A.M., 2008, Earthquake nucleation on rate and state faults – Aging and slip laws: Journal of Geophysical Research: Solid Earth, v. 113, doi:https://doi.org/10.1029/2007JB005082.

Araki, E., Saffer, D.M., Kopf, A.J., Wallace, L.M., Kimura, T., Machida, Y., Ide, S., and Davis, E., 2017, Recurring and triggered slow-slip events near the trench at the Nankai Trough subduction megathrust: Science, v. 356, p. 1157–1160, doi:10.1126/science.aan3120.

Baas Becking, L.G.M., and Moore, D., 1959, Density Distribution in Sediments: Journal of Sedimentary Research, v. Vol. 29, p. 47–55, doi:10.1306/74D7087B-2B21-11D7-8648000102C1865D.

Banerjee, P., Pollitz, F., Nagarajan, B., and Bürgmann, R., 2007, Coseismic Slip Distributions of the 26 December 2004 Sumatra–Andaman and 28 March 2005 Nias Earthquakes from gps Static Offsets: Bulletin of the Seismological Society of America, v. 97, p. S86–S102, doi:10.1785/0120050609.

Bangs, N.L.B., Shipley, T.H., Moore, J.C., and Moore, G.F., 1999, Fluid accumulation and channeling along the northern Barbados Ridge decollement thrust: Journal of Geophysical Research: Solid Earth, v. 104, p. 20399–20414, doi:10.1029/1999jb900133.

Baumberger, T., Berthoud, P., and Caroli, C., 1999, Physical analysis of the state- and rate-dependent friction law. II. Dynamic friction: Physical Review B, v. 60, p. 3928–3939, doi:10.1103/PhysRevB.60.3928.

Beeler, N.M., 2007, 13. Laboratory-Observed Faulting in Intrinsically and Apparently Weak Materials: The Seismogenic Zone of Subduction Thrust Faults, p. 370–449, doi:10.7312/DIXO13866-013.

Beeler, N.M., 2009, Constructing constitutive relationships for seismic and aseismic fault slip: Pure and Applied Geophysics, v. 166, p. 1775–1798, doi:10.1007/S00024-009-0523-0.

Beeler, N.M., Tullis, T.E., Blanpied, M.L., and Weeks, J.D., 1996, Frictional behavior of large displacement experimental faults: Journal of Geophysical Research B: Solid Earth, v. 101, p. 8697–8715, doi:10.1029/96JB00411.

Beeler, N.M., Tullis, T.E., Kronenberg, A.K., and Reinen, L.A., 2007, The instantaneous rate

dependence in low temperature laboratory rock friction and rock deformation experiments: Journal of Geophysical Research: Solid Earth, v. 112, p. 7310, doi:10.1029/2005JB003772.

Beeler, N.M., Tullis, T.E., and Weeks, J.D., 1994, The roles of time and displacement in the evolution effect in rock friction: Geophysical Research Letters, v. 21, p. 1987–1990, doi:10.1029/94GL01599.

Berger, G., Schott, J., and Loubet, M., 1987, Fundamental processes controlling the first stage of alteration of a basalt glass by seawater: an experimental study between 200° and 320°C: Earth and Planetary Science Letters, v. 84, p. 431–445.

Bernabé, Y., Fryer, D.T., and Hayes, J.A., 1992, The effect of cement on the strength of granular rocks: Geophysical Research Letters, v. 19, p. 1511–1514, doi:10.1029/92GL01288.

Beroza, G.C., and Ide, S., 2011, Slow earthquakes and nonvolcanic tremor: Annual Review of Earth and Planetary Sciences, v. 39, p. 271–296, doi:10.1146/ANNUREV-EARTH-040809-152531.

Beste, U., and Jacobson, S., 2003, Micro scale hardness distribution of rock types related to rock drill wear: Wear, v. 254, p. 1147–1154, doi:https://doi.org/10.1016/S0043-1648(03)00327-2.

Bhattacharya, P., Rubin, A.M., Bayart, E., Savage, H.M., and Marone, C., 2015, Critical evaluation of state evolution laws in rate and state friction: Fitting large velocity steps in simulated fault gouge with time-, slip-, and stress-dependent constitutive laws: Journal of Geophysical Research: Solid Earth, v. 120, p. 6365–6385, doi:10.1002/2015JB012437.

Biegel, R.L., Sammis, C.G., and Dieterich, J.H., 1989, The frictional properties of a simulated gouge having a fractal particle distribution: Journal of Structural Geology, v. 11, p. 827–846, doi:10.1016/0191-8141(89)90101-6.

Bilek, S.L., and Lay, T., 2018, Subduction zone megathrust earthquakes: Geosphere, v. 14, doi:10.1130/GES01608.1.

Blanpied, M.L., Marone, C.J., Lockner, D.A., Byerlee, J.D., and King, D.P., 1998, Quantitative measure of the variation in fault rheology due to fluid-rock interactions: Journal of Geophysical Research: Solid Earth, v. 103, p. 9691–9712, doi:10.1029/98JB00162.

Blanpied, M.L., Tullis, T.E., and Weeks, J.D., 1987, Frictional behavior of granite at low and

high sliding velocities: Geophysical Research Letters, v. 14, p. 554–557, doi:10.1029/GL014I005P00554.

Bletery, Q., Sladen, A., Jiang, J., and Simons, M., 2016, A Bayesian source model for the 2004 great Sumatra-Andaman earthquake: Journal of Geophysical Research Solid Earth, v. 121, p. 5116–5135, doi:10.1002/2016JB012911.

Bobko, C., and Ulm, F.-J., 2008, The nano-mechanical morphology of shale: Mechanics of Materials, v. 40, p. 318–337, doi:https://doi.org/10.1016/j.mechmat.2007.09.006.

Bowden, F.P., and Tabor, D., 1966, Friction, lubrication and wear: a survey of work during the last decade: British Journal of Applied Physics, v. 17, p. 1521, doi:10.1088/0508-3443/17/12/301.

Bowden, F.P., and Tabor, D., 1964, The Friction and Lubrication of Solids: Oxford, England, University Press.

Brace, W.F., and Byerlee, J.D., 1966, Stick-slip as a mechanism for earthquakes: Science, v. 153, p. 990–992, doi:10.1126/SCIENCE.153.3739.990.

Brown, K.M., Kopf, A., Underwood, M.B., and Weinberger, J.L., 2003, Compositional and fluid pressure controls on the state of stress on the Nankai subduction thrust: A weak plate boundary: Earth and Planetary Science Letters, v. 214, p. 589–603, doi:10.1016/S0012-821X(03)00388-1.

Brudzinski, M.R., and Allen, R.M., 2007, Segmentation in episodic tremor and slip all along Cascadia: Geology, v. 35, p. 907–910, doi:10.1130/G23740A.1.

Bürgmann, R., 2018, The geophysics, geology and mechanics of slow fault slip: Earth and Planetary Science Letters, v. 495, p. 112–134, doi:10.1016/J.EPSL.2018.04.062.

Byerlee, J., 1990, Friction, overpressure and fault normal compression: Geophysical Research Letters, v. 17, p. 2109–2112, doi:10.1029/GL017I012P02109.

Byrne, D.E., Davis, D.M., and Sykes, L.R., 1988, Loci and maximum size of thrust earthquakes and the mechanics of the shallow region of subduction zones: Tectonics, v. 7, p. 833–857, doi:10.1029/TC007I004P00833.

Carpenter, B.M., Ikari, M.J., and Marone, C., 2016, Laboratory observations of time-dependent frictional strengthening and stress relaxation in natural and synthetic fault gouges: Journal of Geophysical Research: Solid Earth, v. 121, p. 1183–1201, doi:10.1002/2015JB012136.

Chester, F.M., and Logan, J.M., 1987, Composite planar fabric of gouge from the Punchbowl

Fault, California: Journal of Structural Geology, v. 9, p. 621-IN6, doi:10.1016/0191-8141(87)90147-7.

Chlieh, M. et al., 2007, Coseismic slip and afterslip of the great Mw 9.15 Sumatra-Andaman earthquake of 2004: Bulletin of the Seismological Society of America, v. 97, doi:10.1785/0120050631.

Clarke, R.H., 1979, Reservoir Properties of Conglomerates and Conglomeratic Sandstones: GEOLOGIC NOTES: AAPG Bulletin, v. 63, p. 799–803, doi:10.1306/2F9182D9-16CE-11D7-8645000102C1865D.

Cochrane, G.R., Moore, J.C., Mackay, M.E., and Moore, G.F., 1994, Velocity and inferred porosity model of the Oregon accretionary prism for multichannel seismic reflection data: implications on sediment dewatering and overpressure: Journal of Geophysical Research, v. 99, p. 7033–7043, doi:10.1029/93JB03206.

Collettini, C., Niemeijer, A., Viti, C., and Marone, C., 2009, Fault zone fabric and fault weakness: Nature, v. 462, p. 907–910, doi:10.1038/NATURE08585.

Cook, N.G.W., 1981, Stiff Testing Machines, Stick Slip Sliding, and the Stability of Rock Deformation, *in* Mechanical Behavior of Crustal Rocks: The Handin Volume, Geophysical Monograph 24, American Geophysical Union, p. 93–102, doi:10.1029/gm024p0093.

Crawford, B.R., Faulkner, D.R., and Rutter, E.H., 2008, Strength, porosity, and permeability development during hydrostatic and shear loading of synthetic quartz-clay fault gouge: Journal of Geophysical Research: Solid Earth, v. 113, doi:10.1029/2006JB004634.

Dahlen, F.A., 1990, Critical Taper Model of Fold-and-Thrust Belts and Accretionary Wedges: Annual Review of Earth and Planetary Sciences, v. 18, p. 55–99, doi:10.1146/annurev.ea.18.050190.000415.

Davis, E.E., and Hyndman, R.D., 1989, Accretion and recent deformation of sediments along the northern Cascadia subduction zone: Geological Society of America Bulletin, v. 101, p. 1465–1480, doi:10.1130/0016-7606(1989)101<1465:AARDOS>2.3.CO;2.

Dean, S.M., McNeill, L.C., Henstock, T.J., Bull, J.M., Gulick, S.P.S., Austin, J.A., Bangs, N.L.B., Djajadihardja, Y.S., and Permana, H., 2010, Contrasting Decollement and Prism Properties over the Sumatra 2004-2005 Earthquake Rupture Boundary: Science, v. 329, p. 207–210, doi:10.1126/science.1189373.

Deng, X., and Underwood, M.B., 2001, Abundance of smectite and the location of a plate-boundary fault, Barbados accretionary prism: GSA Bulletin, v. 113, p. 495–507,

doi:10.1130/0016-7606(2001)113<0495:AOSATL>2.0.CO;2.

Dieterich, J.H., 1986, A model for the nucleation of earthquake slip, *in* Earthquake source mechanics, American Geophysical Union, p. 37–47.

Dieterich, J.H., 1981, Constitutive Properties of Faults With Simulated Gouge, *in* Mechanical Behavior of Crustal Rocks: The Handin Volume, Geophysical Monograph 24, American Geophysical Union, p. 103–120, doi:10.1029/GM024p0103.

Dieterich, J.H., 1992, Earthquake nucleation on faults with rate-and state-dependent strength: Tectonophysics, v. 211, p. 115–134, doi:10.1016/0040-1951(92)90055-B.

Dieterich, J.H., 1979, Modeling of rock friction: 1. Experimental results and constituve equations: Journal of geophysical research, v. 84, p. 2161–2168, doi:10.1007/BF00876539.

Dieterich, J.H., 1978, Time-Dependent Friction and the Mechanics of Stick-Slip, *in* Byerlee J.D., Wyss M. (eds) Rock Friction and Earthquake Prediction. Contributions to Current Research in Geophysics (CCRG), Birkhäuser, Basel.

Dieterich, J.H., 1972, Time-dependent friction in rocks: Journal of Geophysical Research, v. 77, p. 3690–3697, doi:10.1029/JB077i020p03690.

Dieterich, J.H., and Kilgore, B.D., 1994, Direct observation of frictional contacts: New insights for state-dependent properties: Pure and Applied Geophysics PAGEOPH, v. 143, p. 283–302, doi:10.1007/BF00874332.

Dieterich, J.H., and Kilgore, B., 1996, Implications of fault constitutive properties for earthquake prediction.: Proceedings of the National Academy of Sciences, v. 93, p. 3787–3794, doi:10.1073/pnas.93.9.3787.

Domenico, P.A., and Mifflin, M.D., 1965, Water from low-permeability sediments and land subsidence: Water Resources Research, v. 1, p. 563–576, doi:10.1029/WR001I004P00563.

Dugan, B., McNeill, L.C., Petronotis, K.E., and Expedition 362 Scientists, 2017, The role of input materials in shallow seismogenic slip and forearc plateau development, *in* Expedition 362 Preliminary Report: Sumatra subduction zone. International Ocean Discovery Program, College Station, TX, doi:10.14379/iodp.pr.362.2017.

Dutilleul, J., Bourlange, S., Conin, M., and Géraud, Y., 2020, Quantification of bound water content, interstitial porosity and fracture porosity in the sediments entering the North Sumatra subduction zone from Cation Exchange Capacity and IODP Expedition 362 resistivity data: Marine and Petroleum Geology, v. 111, p. 156–165.

Engelder, J.T., and Scholz, C.H., 1976, The role of asperity indentation and ploughing in rock friction—II: Influence of relative hardness and normal load: International Journal of Rock Mechanics and Mining Sciences & Geomechanics Abstracts, v. 13, p. 155–163, doi:10.1016/0148-9062(76)90820-2.

Expedition 301 Scientists, 2005, Site U1301, *in* Fisher, A.T., Urabe, T.,Klaus, A., and the Expedition 301 Scientists, Proc. IODP, 301: College Station TX (Integrated Ocena Drilling Program Management International, Inc.), doi:10.2204/iodp.proc.301.106.2005.

Expedition 316 Scientists, 2009a, Expedition 316 Site C0004, *in* Kinoshita, M., Tobin, H., Ashi, J., Kimura, G., Lallemant, S., Screaton, E.J., Curewitz, D., Masago, H., Moe, K.T., and the Expedition 314/315/316 Scientists. Proc. IODP, v. 314/315/31, doi:10.2204/iodp.proc.314315316.133.2009.

Expedition 316 Scientists, 2009b, Expedition 316 Site C0007, *in* Kinoshita, M., Tobin, H., Ashi, J., Kimura, G., Lallemant, S., Screaton, E.J., Curewitz, D., Masago, H., Moe, K.T., and the Expedition 314/315/316 Scientists. Proc. IODP, v. 314/315/31, doi:10.2204/iodp.proc.314315316.135.2009.

Fagereng, Å., and Ikari, M.J., 2020, Low-Temperature Frictional Characteristics of Chlorite-Epidote-Amphibole Assemblages: Implications for Strength and Seismic Style of Retrograde Fault Zones: Journal of Geophysical Research: Solid Earth, v. 125, doi:10.1029/2020JB019487.

Faulkner, D.R., Mitchell, T.M., Behnsen, J., Hirose, T., and Shimamoto, T., 2011, Stuck in the mud? Earthquake nucleation and propagation through accretionary forearcs: Geophysical Research Letters, v. 38, p. 1–5, doi:10.1029/2011GL048552.

Faulkner, D.R., and Rutter, E.H., 2001, Can the maintenance of overpressured fluids in large strike-slip fault zones explain their apparent weakness? Geology, v. 29, p. 503–506, doi:10.1130/0091-7613(2001)029<0503:CTMOOF>2.0.CO;2.

Fine, R.A., and Millero, F.J., 1973, Compressibility of water as a function of temperature and pressure: The Journal of Chemical Physics, v. 59, p. 5529–5536, doi:10.1063/1.1679903.

Fisher, A.T., Alt, J., and Bach, W., 2014, Hydrogeologic Properties, Processes, and Alteration in the Igneous Ocean Crust: Elsevier, v. 7, 507–551 p., doi:10.1016/B978-0-444-62617-2.00018-9.

Fujiwara, T., Kodaira, S., No, T., Kaiho, Y., Takahashi, N., and Kaneda, Y., 2011, The 2011 Tohoku-Oki earthquake: Displacement reaching the trench axis: Science, v. 334, p.

1240, doi:10.1126/SCIENCE.1211554.

Gao, H., Schmidt, D.A., and Weldon, R.J., 2012, Scaling relationships of source parameters for slow slip events: Bulletin of the Seismological Society of America, v. 102, p. 352–360, doi:10.1785/0120110096.

Gao, X., and Wang, K., 2014, Strength of stick-slip and creeping subduction megathrusts from heat flow observations: Science, v. 345, p. 1038–1041, doi:10.1126/science.1255487.

Geersen, J., McNeill, L., Henstock, T.J., and Gaedicke, C., 2013, The 2004 Aceh-Andaman Earthquake: Early clay dehydration controls shallow seismic rupture: Geochemistry, Geophysics, Geosystems, v. 14, p. 3315–3323, doi:10.1002/GGGE.20193.

Géminard, J.-C., Losert, W., and Gollub, J.P., 1999, Frictional mechanics of wet granular material: Physical Review E, v. 59, p. 5881–5890, doi:10.1103/PhysRevE.59.5881.

Goldfinger, C. et al., 2012, Turbidite Event History—Methods and Implications for Holocene Paleoseismicity of the Cascadia Subduction Zone: v. No 1661-F.

Goldsby, D.L., and Tullis, T.E., 2002, Low frictional strength of quartz rocks at subseismic slip rates: Geophysical Research Letters, v. 29, doi:10.1029/2002GL015240.

Gu, J.C., Rice, J.R., Ruina, A.L., and Tse, S.T., 1984, Slip motion and stability of a single degree of freedom elastic system with rate and state dependent friction: Journal of the Mechanics and Physics of Solids, v. 32, p. 167–196, doi:10.1016/0022-5096(84)90007-3.

Gulick, S.P.S., Austin, J.A., McNeill, L.C., Bangs, N.L.B., Martin, K.M., Henstock, T.J., Bull, J.M., Dean, S., Djajadihardja, Y.S., and Permana, H., 2011, Updip rupture of the 2004 Sumatra earthquake extended by thick indurated sediments: Nature Geoscience 2011 4:7, v. 4, p. 453–456, doi:10.1038/ngeo1176.

Gutenberg, B., and Richter, C.F., 1942, Earthquake magnitude, intensity, energy, and acceleration*: Bulletin of the Seismological Society of America, v. 32, p. 163–191, doi:10.1785/BSSA0320030163.

Han, S., Bangs, N.L., Carbotte, S.M., Saffer, D.M., and Gibson, J.C., 2017, Links between sediment consolidation and Cascadia megathrust slip behaviour: Nature Geoscience, v. 10, p. 954–959, doi:10.1038/s41561-017-0007-2.

Handin, J., 1969, On the Coulomb-Mohr failure criterion: Journal of Geophysical Research, v. 74, p. 5343–5348, doi:10.1029/JB074I022P05343.

den Hartog, S.A.M., Peach, C.J., de Winter, D.A.M., Spiers, C.J., and Shimamoto, T., 2012, Frictional properties of megathrust fault gouges at low sliding velocities: New data on effects of normal stress and temperature: Journal of Structural Geology, v. 38, p. 156–171, doi:10.1016/j.jsg.2011.12.001.

Hayashi, N., and Tsutsumi, A., 2010, Deformation textures and mechanical behavior of a hydrated amorphous silica formed along an experimentally produced fault in chert: Geophysical Research Letters, v. 37, doi:10.1029/2010GL042943.

Henstock, T.J., McNeill, L.C., and Tappin, D.R., 2006, Seafloor morphology of the Sumatran subduction zone: Surface rupture during megathrust earthquakes? Geology, v. 34, p. 485–488, doi:10.1130/22426.1.

Hetland, E.A., and Simons, M., 2010, Post-seismic and interseismic fault creep II: Transient creep and interseismic stress shadows on megathrusts: Geophysical Journal International, v. 181, p. 99–112, doi:10.1111/j.1365-246X.2009.04482.x.

Hirose, H., Hirahara, K., Kimata, F., Fujii, N., and Miyazaki, S., 1999, A slow thrust slip event following the two 1996 Hyuganada earthquakes beneath the Bungo Channel, southwest Japan: Geophysical Research Letters, v. 26, p. 3237–3240, doi:10.1029/1999GL010999.

Hirose, H., and Obara, K., 2005, Repeating short- and long-term slow slip events with deep tremor activity around the Bungo channel region, southwest Japan: Earth, Planets and Space, v. 57, p. 961–972, doi:10.1186/BF03351875.

Hodder, A.P.W., Naish, T.R., and Nelson, C.S., 1993, A two-stage model for the formation of smectite from detrital volcanic glass under shallow-marine conditions: Marine Geology, v. 109, p. 279–285, doi:10.1016/0025-3227(93)90066-5.

Hubbert, M.K., and Rubey, W.W., 1959, Role of Fluid Pressure in Mechanics of Overthrust Faulting: v. 70, 115–166 p., doi:10.1130/0016-7606(1959)70.

Hüpers, A. et al., 2017, Release of mineral-bound water prior to subduction tied to shallow seismogenic slip off Sumatra: Science, v. 356, p. 841–844, doi:10.1126/science.aal3429.

Hüpers, A., Ikari, M.J., Dugan, B., Underwood, M.B., and Kopf, A.J., 2015, Origin of a zone of anomalously high porosity in the subduction inputs to Nankai Trough: Marine Geology, v. 361, p. 147–162, doi:10.1016/J.MARGEO.2015.01.004.

Hurd, D.C., and Theyer, F., 1977, Changes in the physical and chemical properties of biogenic silica from the central equatorial Pacific; Part II, Refractive index, density, and

water content of acid-cleaned samples: American Journal of Science, v. 277, p. 1168–1202, doi:10.2475/AJS.277.9.1168.

Husker, A., Ferrari, L., Arango-Galván, C., Corbo-Camargo, F., and Arzate-Flores, J.A., 2018, A geologic recipe for transient slip within the seismogenic zone: Insight from the Guerrero seismic gap, Mexico: Geology, v. 46, p. 35–38, doi:10.1130/G39202.1.

Hyndman, R.D., and Wang, K., 1995, The rupture zone of Cascadia great earthquakes from current deformation and the thermal regime: Journal of Geophysical Research, v. 100, p. 22,133-22,154.

Hyndman, R.D., and Wang, K., 1993, Thermal constraints on the zone of major thrust earthquake failure: the Cascadia Subduction Zone: Journal of Geophysical Research, v. 98, p. 2039–2060, http://dx.doi.org/10.1029/92JB02279.

Hyndman, R.D., Yamano, M., and Oleskevich, D.A., 1997, The seismogenic zone of subduction thrust faults: Island Arc, v. 6, p. 244–260, doi:10.1111/j.1440-1738.1997.tb00175.x.

Hyndman, R.D., Yorath, C.J., Clowes, R.M., Davis, E.E., and E, D.E., 1990, The northern Cascadia subduction zone at Vancouver Island: seismic structure and tectonic history: Canadian Journal of Earth Sciences, v. 27, p. 313–329, doi:10.1139/e90-030.

Ide, S., Beroza, G.C., Shelly, D.R., and Uchide, T., 2007, A scaling law for slow earthquakes: Nature, v. 447, p. 76–79, doi:10.1038/NATURE05780.

Ikari, M.J., 2019, Laboratory slow slip events in natural geological materials: Geophysical Journal International, v. 218, p. 354–387, doi:10.1093/gji/ggz143.

Ikari, M.J., Carpenter, B.M., and Marone, C., 2016, A microphysical interpretation of rate- and state-dependent friction for fault gouge: Geochemistry, Geophysics, Geosystems, v. 17, p. 1660–1677, doi:10.1002/2016GC006286.

Ikari, M.J., and Hüpers, A., 2021, Velocity-weakening friction induced by laboratory-controlled lithification: Earth and Planetary Science Letters, v. 554, p. 116682, doi:10.1016/J.EPSL.2020.116682.

Ikari, M.J., Hüpers, A., and Kopf, A.J., 2013, Shear strength of sediments approaching subduction in the Nankai Trough, Japan as constraints on forearc mechanics: Geochemistry, Geophysics, Geosystems, v. 14, p. 2716–2730, doi:10.1002/ggge.20156.

Ikari, M.J., Ito, Y., Ujiie, K., and Kopf, A.J., 2015a, Spectrum of slip behaviour in Tohoku fault zone samples at plate tectonic slip rates: Nature Geoscience, v. 8, p. 870–874,

doi:10.1038/NGEO2547.

Ikari, M.J., Kameda, J., Saffer, D.M., and Kopf, A.J., 2015b, Strength characteristics of Japan Trench borehole samples in the high-slip region of the 2011 Tohoku-Oki earthquake: Earth and Planetary Science Letters, v. 412, p. 35–41, doi:10.1016/j.epsl.2014.12.014.

Ikari, M.J., and Kopf, A.J., 2011, Cohesive strength of clay-rich sediment: Geophysical Research Letters, v. 38, p. 1–5, doi:10.1029/2011GL047918.

Ikari, M.J., and Kopf, A.J., 2017, Seismic potential of weak, near-surface faults revealed at plate tectonic slip rates: Science Advances, v. 3, p. 1–7, doi:10.1126/sciadv.1701269.

Ikari, M.J., Kopf, A.J., Hüpers, A., and Vogt, C., 2018, Lithologic control of frictional strength variations in subduction zone sediment inputs: Geosphere, v. 14, p. 604–625, doi:10.1130/GES01546.1.

Ikari, M.J., Marone, C., and Saffer, D.M., 2011a, On the relation between fault strength and frictional stability: Geology, v. 39, p. 83–86, doi:10.1130/G31416.1.

Ikari, M.J., Niemeijer, A.R., and Marone, C., 2011b, The role of fault zone fabric and lithification state on frictional strength, constitutive behavior, and deformation microstructure: Journal of Geophysical Research: Solid Earth, v. 116, p. 1–25, doi:10.1029/2011JB008264.

Ikari, M.J., and Saffer, D.M., 2011, Comparison of frictional strength and velocity dependence between fault zones in the Nankai accretionary complex: Geochemistry, Geophysics, Geosystems, v. 12, doi:10.1029/2010GC003442.

Ikari, M.J., and Saffer, D.M., 2012, Permeability contrasts between sheared and normally consolidated sediments in the Nankai accretionary prism: Marine Geology, v. 295–298, p. 1–13, doi:10.1016/j.margeo.2011.11.006.

Ikari, M.J., Saffer, D.M., and Marone, C., 2007, Effect of hydration state on the frictional properties of montmorillonite-based fault gouge: Journal of Geophysical Research: Solid Earth, v. 112, p. 1–12, doi:10.1029/2006JB004748.

Ikari, M.J., Saffer, D.M., and Marone, C., 2009a, Frictional and hydrologic properties of a major splay fault system, Nankai subduction zone: Geophysical Research Letters, v. 36, doi:10.1029/2009GL040009.

Ikari, M.J., Saffer, D.M., and Marone, C., 2009b, Frictional and hydrologic properties of clay-rich fault gouge: Journal of Geophysical Research: Solid Earth, v. 114, p. 1–18, doi:10.1029/2008JB006089.

Ishii, M., Shearer, P.M., Houston, H., and Vidale, J.E., 2005, Extent, duration and speed of the 2004 Sumatra-Andaman earthquake imaged by the Hi-Net array: Nature, v. 435, p. 933–936, doi:10.1038/NATURE03675.

Ito, Y., and Obara, K., 2006, Very low frequency earthquakes within accretionary prisms are very low stress-drop earthquakes: Geophysical Research Letters, v. 33, doi:10.1029/2006GL025883.

Kameda, J., Shimizu, M., Ujiie, K., Hirose, T., Ikari, M., Mori, J., Oohashi, K., and Kimura, G., 2015, Pelagic smectite as an important factor in tsunamigenic slip along the Japan Trench: Geology, v. 43, p. 155–158, doi:10.1130/G35948.1.

Kanamori, H., 1978, Quantification of Earthquakes: Nature, v. 271, p. 411–414, doi:10.1038/271411a0.

Kanamori, H., and Brodsky, E.E., 2004, The physics of earthquakes: Reports on Progress in Physics, v. 67, p. 1429, doi:10.1088/0034-4885/67/8/R03.

Kanamori, H., and Brodsky, E.E., 2001, The Physics of earthquakes (L. Bergstrom, K. Johansson, & C. Nilsson, Eds.): Physics today, v. 36, p. 34–40, doi:10.1063/1.1387590.

Kanu, C., and Johnson, K., 2011, Arrest and recovery of frictional creep on the southern Hayward fault triggered by the 1989 Loma Prieta, California, earthquake and implications for future earthquakes: Journal of Geophysical Research, v. 116, doi:10.1029/2010JB007927.

Katsumata, A., and Kamaya, N., 2003, Low-frequency continuous tremor around the Moho discontinuity away from volcanoes in the southwest Japan: Geophysical Research Letters, v. 30, p. 20–24, doi:https://doi.org/10.1029/2002GL015981.

Keller, M.A., and Isaacs, C.M., 1985, An evaluation of temperature scales for silica diagenesis in diatomaceous sequences including a new approach based on the Miocene Monterey Formation, California: Geo-Marine Letters 1985 5:1, v. 5, p. 31–35, doi:10.1007/BF02629794.

Kilgore, B.D., Blanpied, M.L., and Dieterich, J.H., 1993, Velocity dependent friction of granite over a wide range of conditions: Geophysical Research Letters, v. 20, p. 903–906, doi:10.1029/93GL00368.

King, D.S.H., and Marone, C., 2012, Frictional properties of olivine at high temperature with applications to the strength and dynamics of the oceanic lithosphere: Journal of Geophysical Research: Solid Earth, v. 117, p. 12203, doi:10.1029/2012JB009511.

Kitajima, H., and Saffer, D.M., 2012, Elevated pore pressure and anomalously low stress in

regions of low frequency earthquakes along the Nankai Trough subduction megathrust: Geophysical Research Letters, v. 39, doi:10.1029/2012GL053793.

Kodaira, S., Iidaka, T., Kato, A., Park, J.O., Iwasaki, T., and Kaneda, Y., 2004, High pore fluid pressure may cause silent slip in the Nankai Trough: Science, v. 304, p. 1295–1298, doi:10.1126/SCIENCE.1096535.

Kohli, A.H., and Zoback, M.D., 2013, Frictional properties of shale reservoir rocks: Journal of Geophysical Research: Solid Earth, v. 118, p. 5109–5125, doi:10.1002/JGRB.50346.

Kopf, A., 2013, Effective strength of incoming sediments and its implications for plate boundary propagation: Nankai and Costa Rica as type examples of accreting vs. erosive convergent margins: Tectonophysics, v. 608, p. 958–969, doi:10.1016/j.tecto.2013.07.023.

Kopf, A., and Brown, K.M., 2003, Friction experiments on saturated sediments and their implications for the stress state of the Nankai and Barbados subduction thrusts: Marine Geology, v. 202, p. 193–210.

Koulali, A., McClusky, S., Wallace, L., Allgeyer, S., Tregoning, P., D'Anastasio, E., and Benavente, R., 2017, Slow slip events and the 2016 Te Araroa Mw 7.1 earthquake interaction: Northern Hikurangi subduction, New Zealand: Geophysical Research Letters, v. 44, p. 8336–8344, doi:10.1002/2017GL074776.

Kulm, L.D., and von Huene, R., 1973, Initial Reports of the Deep Sea Drilling Project 18.:

Lay, T. et al., 2005, The great Sumatra-Andaman earthquake of 26 December 2004: Science, v. 308, p. 1127–1133, doi:10.1126/science.1112250.

Lay, T., and Bilek, S., 2007, 15. Anomalous Earthquake Ruptures at Shallow Depths on Subduction Zone Megathrusts: The Seismogenic Zone of Subduction Thrust Faults, p. 476–511, doi:10.7312/DIXO13866-015.

Leeman, J.R., Saffer, D.M., Scuderi, M.M., and Marone, C., 2016, Laboratory observations of slow earthquakes and the spectrum of tectonic fault slip modes: Nature Communications, v. 7, doi:10.1038/ncomms11104.

Liu, Y., and Rice, J.R., 2005, Aseismic slip transients emerge spontaneously in three-dimensional rate and state modeling of subduction earthquake sequences: Journal of Geophysical Research: Solid Earth, v. 110, p. 1–14, doi:10.1029/2004JB003424.

Lockner, D.A., and Byerlee, J.D., 1986, Laboratory measurements of velocity-dependent frictional strength: U.S Geological Survey Open-File Report, v. 86–417.

Logan, J.M., Dengo, C.A., Higgs, N.G., and Wang, Z.Z., 1992, Fabrics of Experimental Fault Zones: Their Development and Relationship to Mechanical Behavior: v. 51, 33–67 p., doi:10.1016/S0074-6142(08)62814-4.

Logan, J.M., and Rauenzahn, K.A., 1987, Frictional dependence of gouge mixtures of quartz and montmorillonite on velocity, composition and fabric: Tectonophysics, v. 144, p. 87–108, doi:10.1016/0040-1951(87)90010-2.

Logan, J.M., and Teufel, L.W., 1986, The effect of normal stress on the real area of contact during frictional sliding in rocks: pure and applied geophysics 1986 124:3, v. 124, p. 471–485, doi:10.1007/BF00877212.

Loveless, J.P., and Meade, B.J., 2011, Spatial correlation of interseismic coupling and coseismic rupture extent of the 2011 MW = 9.0 Tohoku-oki earthquake: Geophysical Research Letters, v. 38, doi:https://doi.org/10.1029/2011GL048561.

Lowry, A.R., 2006, Resonant slow fault slip in subduction zones forced by climatic load stress: Nature, v. 442, p. 802–805, doi:10.1038/nature05055.

Lu, X., Rosakis, A.J., and Lapusta, N., 2010, Rupture modes in laboratory earthquakes: Effect of fault prestress and nucleation conditions: Journal of Geophysical Research: Solid Earth, v. 115, p. 1–25, doi:10.1029/2009JB006833.

Lupini, J.F., Skinner, A.E., and Vaughan, P.R., 1981, The drained residual strength of cohesive soils: Geotechnique, v. 31, p. 181–213, doi:10.1680/GEOT.1981.31.2.181.

Lyle, O.A., and Lyle, M.W., 2002, Determination of biogenic opal in pelagic marine sediments: a simple method revisited, *in* Lyle, M., Wilson, P.A., Janecek, T.R., et al., Proc. ODP, Init. Repts., 199: College Station, TX (Ocean Drilling Program), doi:10.2973/odp.proc.ir.199.106.2002.

MacKay, M.E., Moore, G.F., Cochrane, G.R., Casey Moore, J., and Kulm, L.V.D., 1992, Landward vergence and oblique structural trends in the Oregon margin accretionary prism: Implications and effect on fluid flow: Earth and Planetary Science Letters, v. 109, p. 477–491, doi:10.1016/0012-821X(92)90108-8.

Mair, K., and Marone, C., 1999, Friction of simulated fault gouge for a wide range of velocities and normal stresses: Journal of Geophysical Research: Solid Earth, v. 104, p. 28899–28914, doi:10.1029/1999JB900279.

Marion, D., Nur, A., Yin, H., and Han, D., 1992, Compressional velocity and porosity in sand-clay mixtures: GEOPHYSICS, v. 57, p. 554–563, doi:10.1190/1.1443269.

Marone, C., 1998, Laboratory-Derived Friction Laws and Their Application To Seismic

Faulting: Annual Review of Earth and Planetary Sciences, v. 26, p. 643–696, doi:10.1146/annurev.earth.26.1.643.

Marone, C., Raleigh, C.B., and Scholz, C.H., 1990, Frictional behavior and constitutive modeling of simulated fault gouge: Journal of Geophysical Research, v. 95, p. 7007–7025, doi:10.1029/JB095IB05P07007.

Marone, C., and Saffer, D.M., 2007, 12. Fault Friction and the Upper Transition from Seismic to Aseismic Faulting: The Seismogenic Zone of Subduction Thrust Faults, p. 346–369, doi:10.7312/DIXO13866-012.

Marone, C., and Scholz, C.H., 1988, The depth of seismic faulting and the upper transition from stable to unstable slip regimes: Geophysical Research Letters, v. 15, p. 621–624, doi:10.1029/GL015I006P00621.

McGeary, R.K., 1961, Mechanical Packing of Spherical Particles: Journal of the American Ceramic Society, v. 44, p. 513–522, doi:10.1111/J.1151-2916.1961.TB13716.X.

McGuire, J.J., Collins, J.A., Davis, E., Becker, K., and Heesemann, M., 2018, A Lack of Dynamic Triggering of Slow Slip and Tremor Indicates That the Shallow Cascadia Megathrust Offshore Vancouver Island Is Likely Locked: Geophysical Research Letters, v. 45, p. 11,095-11,103, doi:10.1029/2018GL079519.

McNeill, L.C. et al., 2017, Site U1480: Proceedings of the International Ocean Discovery Program, v. 362, doi:10.14379/iodp.proc.362.103.2017.

McNeill, L.C., and Henstock, T.J., 2014, Forearc structure and morphology along the Sumatra-Andaman subduction zone: Tectonics, v. 33, p. 112–134, doi:10.1002/2012TC003264.

Moore, J.C. et al., 1998, Consolidation patterns during initiation and evolution of a plate-boundary decollement zone: northern Barbados accretionary prism: Geology, v. 26, p. 811–814, doi:10.1130/0091-7613(1998)026<0811:CPDIAE>2.3.CO;2.

Moore, J.C., 1989, Tectonics and hydrogeology of accretionary prisms: role of the décollement zone: Journal of Structural Geology, v. 11, p. 95–106, doi:10.1016/0191-8141(89)90037-0.

Moore, D.E., and Lockner, D.A., 2007, Friction of the Smectite Clay, *in* The seismogenic zone of subduction zone thrust faults, p. 317–345.

Moore, J.C., Moore, G.F., Cochrane, G.R., and Tobin, H.J., 1995a, Negative-polarity seismic reflections along faults of the Oregon accretionary prism: indicators of overpressuring: Journal of Geophysical Research, v. 100, doi:10.1029/94JB02049.

Moore, J.C., and Saffer, D., 2001, Updip limit of the seismogenic zone beneath the accretionary prism of Southwest Japan: An effect of diagenetic to low-grade metamorphic processes and increasing effective stress: Geology, v. 29, p. 183–186, doi:10.1130/0091-7613(2001)029<0183:ULOTSZ>2.0.CO;2.

Moore, D.E., Summers, R., and Byerlee, J.D., 1989, Sliding behavior and deformation textures of heated illite gouge: Journal of Structural Geology, v. 11, p. 329–342, doi:10.1016/0191-8141(89)90072-2.

Moore, G.F., Zhao, X., Shipley, T.H., Bangs, N., and Moore, J.C., 1995b, Structural Setting of the Leg 156 Area, Northern Barbados Ridge Accretionary Prism, *in* Shipley, T.H., Ogawa, Y., Blum, P., et al. Proceedings of the Ocean Drilling Program, 156 Initial Reports, v. 156, doi:10.2973/odp.proc.ir.156.102.1995.

Morrow, C.A., Moore, D.E., and Lockner, D.A., 2000, The effect of mineral bond strength and adsorbed water on fault gouge frictional strength: Geophysical Research Letters, v. 27, p. 815–818, doi:10.1029/1999GL008401.

Morrow, C., Radney, B., and Byerlee, J., 1992, Frictional Strength and the Effective Pressure Law of Montmorillonite and Illite Clays: International Geophysics, v. 51, p. 69–88, doi:10.1016/S0074-6142(08)62815-6.

Nakamura, Y., Muto, J., Nagahama, H., Shimizu, I., Miura, T., and Arakawa, I., 2012, Amorphization of quartz by friction: Implication to silica-gel lubrication of fault surfaces: Geophysical Research Letters, v. 39, doi:https://doi.org/10.1029/2012GL053228.

Nakatani, M., 2001, Conceptual and physical clarification of rate and state friction: Frictional sliding as a thermally activated rheology: Journal of Geophysical Research: Solid Earth, v. 106, p. 13347–13380, doi:10.1029/2000JB900453.

Obana, K., Scherwath, M., Yamamoto, Y., Kodaira, S., Wang, K., Spence, G., Riedel, M., and Kao, H., 2015, Earthquake Activity in Northern Cascadia Subduction Zone Off Vancouver Island Revealed by Ocean-Bottom Seismograph Observations: Bulletin of the Seismological Society of America, v. 105, p. 489–495, doi:10.1785/0120140095.

Obara, K., 2002, Nonvolcanic deep tremor associated with subduction in southwest Japan: Science, v. 296, p. 1679–1681, doi:10.1126/SCIENCE.1070378.

Obara, K., and Kato, A., 2016, Connecting slow earthquakes to huge earthquakes: Science, v. 353, p. 253–257, doi:10.1126/science.aaf1512.

Ohnaka, M., Kuwahara, Y., and Yamamoto, K., 1987, Constitutive relations between dynamic physical parameters near a tip of the propagating slip zone during stick-slip

shear failure: Tectonophysics, v. 144, p. 109–125, doi:10.1016/0040-1951(87)90011-4.

Ohnaka, M., Kuwahara, Y., Yamamoto, K., and Hirasawa, T., 1986, Dynamic breakdown processes and the generating mechanism for high-frequency elastic radiation during stick-slip instabilities: Earthquake Source Mechanics, v. 37, p. 13–24.

Ojovan, M.I., 2008, Viscosity and Glass Transition in Amorphous Oxides (M. Bowick, Ed.): Advances in Condensed Matter Physics, v. 2008, doi:10.1155/2008/817829.

Oleskevich, D.A., Hyndman, R.D., and Wang, K., 1999, The updip and downdip limits to great subduction earthquakes: Thermal and structural models of Cascadia, south Alaska, SW Japan, and Chile: Journal of Geophysical Research: Solid Earth, v. 104, p. 14965–14991, doi:10.1029/1999JB900060.

Oliver, W.C., and Pharr, G.M., 1992, An improved technique for determining hardness and elastic modulus using load and displacement sensing indentation experiments: Journal of Materials Research, v. 7, p. 1564–1583, doi:DOI: 10.1557/JMR.1992.1564.

Osborne, M.J., and Swarbrick, R.E., 1997, How Overpressure and Diagenesis Interact in Sedimentary Basins – Consequences for Porosity Preservation in HPHT Reservoir Sandstones: Proceedings of an International Conference on Petroleum Systems of SE Asia and Australasia, p. 947–954, http://archives.datapages.com/data/ipa/data/044/044001/947_ipa0440947.htm (accessed August 2021).

Pacheco, J.F., and Sykes, L.R., 1992, Seismic moment catalog of large shallow earthquakes, 1900 to 1989: Bulletin of the Seismological Society of America, v. 82, p. 1306–1349.

Pacheco, J.F., Sykes, L.R., and Scholz, C.H., 1993, Nature of seismic coupling along simple plate boundaries of the subduction type: Journal of Geophysical Research, v. 98, doi:10.1029/93JB00349.

Peng, Z., and Gomberg, J., 2010, An integrated perspective of the continuum between earthquakes and slow-slip phenomena: Nature Geoscience, v. 3, p. 599–607, doi:10.1038/NGEO940.

Perfettini, H., and Ampuero, J.P., 2008, Dynamics of a velocity strengthening fault region: Implications for slow earthquakes and postseismic slip: Journal of Geophysical Research, v. 113, doi:10.1029/2007JB005398.

Pollitz, F.F., and Evans, E.L., 2017, Implications of the earthquake cycle for inferring fault locking on the Cascadia megathrust: Geophysical Journal International, v. 209, p. 167–

185, doi:10.1093/gji/ggx009.

Pytte, A.M., and Reynolds, R.C., 1989, The thermal transformation of Smectite to Illite, *in* Naeser, N. D., McCulloh, T. H.: Thermal history of sedimentary basins, Springer, doi:10.1007/978-1-4612-3492-0_8.

Rabinowicz, E., 1951, The nature of the static and kinetic coefficients of friction: Journal of Applied Physics, v. 22, p. 1373–1379, doi:10.1063/1.1699869.

Rabinowitz, H.S., Savage, H.M., Skarbek, R.M., Ikari, M.J., Carpenter, B.M., and Collettini, C., 2018, Frictional Behavior of Input Sediments to the Hikurangi Trench, New Zealand: Geochemistry, Geophysics, Geosystems, v. 19, doi:10.1029/2018GC007633.

Radiguet, M., Cotton, F., Vergnolle, M., Campillo, M., Walpersdorf, A., Cotte, N., and Kostoglodov, V., 2012, Slow slip events and strain accumulation in the Guerrero gap, Mexico: Journal of Geophysical Research: Solid Earth, v. 117, doi:10.1029/2011JB008801.

Rathbun, A.P., and Marone, C., 2010, Effect of strain localization on frictional behavior of sheared granular materials: Journal of Geophysical Research: Solid Earth, v. 115, p. 1204, doi:10.1029/2009JB006466.

Rea, D.K., and Ruff, L.J., 1996, Composition and mass flux of sediment entering the world's subduction zones: Implications for global sediment budgets, great earthquakes, and volcanism: Earth and Planetary Science Letters, v. 140, p. 1–12, doi:10.1016/0012-821X(96)00036-2.

Reinen, L.A., and Weeks, J.D., 1993, Determination of rock friction constitutive parameters using an iterative least squares inversion method: Journal of Geophysical Research Solid Earth, v. 98, p. 15937–15950, doi:10.1029/93JB00780.

Revil, A., Grauls, D., and Brévart, O., 2002, Mechanical compaction of sand/clay mixtures: Journal of Geophysical Research: Solid Earth, v. 107, p. ECV 11-1-ECV 11-15, doi:10.1029/2001JB000318.

Rice, J.R., Lapusta, N., and Ranjith, K., 2001, Rate and state dependent friction and the stability of sliding between elastically deformable solids: Journal of the Mechanics and Physics of Solids, v. 49, p. 1865–1898, doi:https://doi.org/10.1016/S0022-5096(01)00042-4.

Rice, J.R., and Ruina, A.L., 1983, Stability of steady frictional slipping: Journal of Applied Mechanics, Transactions ASME, v. 50, p. 343–349, doi:10.1115/1.3167042.

Riddihough, R., 1984, Recent Movements of the Juan De Fuca Plate System.: Journal of

Geophysical Research, v. 89, p. 6980–6994, doi:10.1029/JB089iB08p06980.

Roesner, A., Ikari, M.J., Saffer, D.M., Stanislowski, K., Eijsink, A.M., and Kopf, A.J., 2020, Friction experiments under in-situ stress reveal unexpected velocity-weakening in Nankai accretionary prism samples: Earth and Planetary Science Letters, v. 538, p. 116180, doi:10.1016/j.epsl.2020.116180.

Rogers, G., and Dragert, H., 2003, Episodic tremor and slip on the Cascadia subduction zone: The chatter of silent slip: Science, v. 300, p. 1942–1943, doi:10.1126/science.1084783.

Rosenberger, K., Underwood, M.B., Vrolijk, P., and Haines, S., 2020, Data report: clay mineral assemblages in hemipelagic sediments entering the Sumatra subduction zone, IODP Sites U1480 and U1481, Expedition 362:, doi:10.14379/IODP.PROC.362.204.2020.

Rowe, C.D., Lamothe, K., Rempe, M., Andrews, M., Mitchell, T.M., Di Toro, G., White, J.C., and Aretusini, S., 2019, Earthquake lubrication and healing explained by amorphous nanosilica: Nature Communications, v. 10, p. 320, doi:10.1038/s41467-018-08238-y.

Rowe, K.T., Screaton, E.J., and Ge, S., 2012, Coupled fluid flow and deformation modeling of the frontal thrust region of the Kumano Basin transect, Japan: Implications for fluid pressures and decollement downstepping: Geochemistry, Geophysics, Geosystems, v. 13, doi:10.1029/2011GC003861.

Ruff, L., and Kanamori, H., 1980, Seismicity and the subduction process: Physics of the Earth and Planetary Interiors, v. 23, p. 240–252, doi:10.1016/0031-9201(80)90117-X.

Ruina, A., 1983, Slip instability and state variable friction laws.: Journal of Geophysical Research, v. 88, p. 10359–10370, doi:10.1029/JB088iB12p10359.

Ruiz, S., Metois, M., Fuenzalida, A., Ruiz, J., Leyton, F., Grandin, R., Vigny, C., Madariaga, R., and Campos, J., 2014, Intense foreshocks and a slow slip event preceded the 2014 Iquique M_w 8.1 earthquake: Science, v. 345, p. 1165 LP – 1169, doi:10.1126/science.1256074.

Sacks, I.S., Linde, A.T., Suyehiro, S., and Snoke, J.A., 1978, Slow earthquakes and stress redistribution: Nature, v. 275, p. 599–602, doi:10.1038/275599a0.

Saffer, D.M., Frye, K.M., Marone, C., and Mair, K., 2001, Laboratory results indicating complex and potentially unstable frictional behavior of smectite clay: Geophysical Research Letters, v. 28, p. 2297–2300, doi:10.1029/2001GL012869.

Saffer, D.M., and Marone, C., 2003, Comparison of smectite- and illite-rich gouge frictional

properties: Application to the updip limit of the seismogenic zone along subduction megathrusts: Earth and Planetary Science Letters, v. 215, p. 219–235, doi:10.1016/S0012-821X(03)00424-2.

Saffer, D.M., and Tobin, H.J., 2011, Hydrogeology and Mechanics of Subduction Zone Forearcs: Fluid Flow and Pore Pressure: Annual Review of Earth and Planetary Sciences, v. 39, p. 157–186, doi:10.1146/annurev-earth-040610-133408.

Saffer, D.M., and Wallace, L.M., 2015, The frictional, hydrologic, metamorphic and thermal habitat of shallow slow earthquakes: Nature Geoscience, v. 8, p. 594–600, doi:10.1038/NGEO2490.

Satake, K., Shimazaki, K., Tsuji, Y., and Ueda, K., 1996, Time and size of a giant earthquake in Cascadia inferred from Japanese tsunami records of January 1700: Nature, v. 379, p. 246–249, doi:10.1038/379246a0.

Schleicher, A.M., van der Pluijm, B.A., and Warr, L.N., 2010, Nanocoatings of clay and creep of the San Andreas fault at Parkfield, California: Geology, v. 38, p. 667–670, doi:10.1130/G31091.1.

Schmalzle, G.M., McCaffrey, R., and Creager, K.C., 2014, Central Cascadia subduction zone creep: Geochemistry, Geophysics, Geosystems, v. 15, p. 1515–1532, doi:10.1002/2013GC005172.

Scholz, C.H., 1998, Earthquakes and friction laws: Nature, v. 391, p. 37–42, doi:10.1038/34097.

Scholz, C.H., 1972, Static fatigue of quartz: Journal of Geophysical Research, v. 77, p. 2104–2114, doi:10.1029/JB077I011P02104.

Scholz, C.H., and Engelder, J.T., 1976, The role of asperity indentation and ploughing in rock friction - I. Asperity creep and stick-slip: International Journal of Rock Mechanics and Mining Sciences and, v. 13, p. 149–154, doi:10.1016/0148-9062(76)90819-6.

Schumann, K., Behrmann, J.H., Stipp, M., Yamamoto, Y., Kitamura, Y., and Lempp, C., 2014, Geotechnical behavior of mudstones from the shimanto and boso accretionary complexes, and implications for the nankai accretionary prism: Earth, Planets and Space, v. 66, doi:10.1186/1880-5981-66-129.

Schwartz, S.Y., and Rokosky, J.M., 2007, Slow slip events and seismic tremor at circum-pacific subduction zones: Reviews of Geophysics, v. 45, doi:10.1029/2006RG000208.

Scruggs, V.J., and Tullis, T.E., 1998, Correlation between velocity dependence of friction and strain localization in large displacement experiments on feldspar, muscovite and biotite

gouge: Tectonophysics, v. 295, p. 15–40, doi:10.1016/S0040-1951(98)00113-9.

Seno, T., 2002, Tsunami earthquakes as transient phenomena: Geophysical Research Letters, v. 29, p. 54–58, doi:https://doi.org/10.1029/2002GL014868.

Seyler, C.E., Kirkpatrick, J.D., Savage, H.M., Hirose, T., and Faulkner, D.R., 2020, Rupture to the trench? Frictional properties and fracture energy of incoming sediments at the Cascadia subduction zone: Earth and Planetary Science Letters, v. 546, p. 116413, doi:10.1016/j.epsl.2020.116413.

Shibazaki, B., and Iio, Y., 2003, On the physical mechanism of silent slip events along the deeper part of the seismogenic zone: Geophysical Research Letters, v. 30, doi:10.1029/2003GL017047.

Shibazaki, B., and Shimamoto, T., 2007, Modelling of short-interval silent slip events in deeper subduction interfaces considering the frictional properties at the unstable-stable transition regime: Geophysical Journal International, v. 171, p. 191–205, doi:10.1111/J.1365-246X.2007.03434.X.

Shimamoto, T., 1986, Transition between frictional slip and ductile flow for halite shear zones at room temperature: Science, v. 231, p. 711–714, doi:10.1126/SCIENCE.231.4739.711.

Shimamoto, T., and Logan, J.M., 1981, Effects of simulated clay gouges on the sliding behavior of Tennessee sandston: Tectonophysics, v. 75, p. 243–255, doi:10.1016/0040-1951(81)90276-6.

Shipboard Scientific Party, 2001, Site 1174, *in* Proc. ODP Initial Reports 190, doi:10.2973/odp.proc.ir.190.105.2001.

Shipley, T.H., Moore, G.F., Bangs, N.L., Moore, J.C., and Stoffa, P.L., 1994, Seismically inferred dilatancy distribution, northern Barbados Ridge decollement: Implications for fluid migration and fault strength: Geology, v. 22, p. 411–414, doi:10.1130/0091-7613(1994)022<0411:SIDDNB>2.3.CO;2.

Singh, S.C., Hananto, N.D., and Chauhan, A.P., 2011, Enhanced reflectivity of backthrusts in the recent great Sumatran earthquake rupture zones: Geophys. Res. Lett., v. 38, p. L04302, doi:10.1029/2010gl046227.

Skarbek, R.M., and Savage, H.M., 2019, RSFit3000: A MATLAB GUI-based program for determining rate and state frictional parameters from experimental data: Geosphere, v. 15, p. 1665–1676, doi:10.1130/ges02122.1.

Skempton, A.W., 1964, Long-term stability of clay slopes: Geotechnique, v. 14, p. 77–102.

Solum, J.G., Hickman, S.H., Lockner, D.A., Moore, D.E., Van Der Pluijm, B.A., Schleicher, A.M., and Evans, J.P., 2006, Mineralogical characterization of protolith and fault rocks from the SAFOD Main Hole: Geophysical Research Letters, v. 33, doi:10.1029/2006GL027285.

Spinelli, G.A., Mozley, P.S., Tobin, H.J., Underwood, M.B., Hoffman, N.W., and Bellew, G.M., 2007, Diagenesis, sediment strength, and pore collapse in sediment approaching the Nankai Trough subduction zone: GSA Bulletin, v. 119, p. 377–390, doi:10.1130/B25920.1.

Stevens, D.E., Henstock, T.J., and McNeill, L.C., 2021, Evolution of the Thermal and Dehydration State of Sediments Entering the North Sumatra Subduction Zone: Geochemistry, Geophysics, Geosystems, v. 22, p. e2020GC009306, doi:10.1029/2020GC009306.

Stroncik, N.A., and Schmincke, H.-U., 2002, Palagonite – a review: International Journal of Earth Sciences , v. 91, p. 680–697, doi:10.1007/s00531-001-0238-7.

Subarya, C., Chlieh, M., Prawirodirdjo, L., Avouac, J.P., Bock, Y., Sieh, K., Meltzner, A.J., Natawidjaja, D.H., and McCaffrey, R., 2006, Plate-boundary deformation associated with the great Sumatra-Andaman earthquake: Nature, v. 440, p. 46–51, doi:10.1038/NATURE04522.

Sun, T., Wang, K., Fujiwara, T., Kodaira, S., and He, J., 2017, Large fault slip peaking at trench in the 2011 Tohoku-oki earthquake: Nature Communications, v. 8, doi:10.1038/NCOMMS14044.

Taylor, E.W., 1949, Correlation of the Mohs's scale of hardness with the Vickers's hardness numbers: Mineralogical Magazine and Journal of the Mineralogical Society, v. 28, p. 718–721, doi:DOI: 10.1180/minmag.1949.28.206.08.

Tembe, S., Lockner, D.A., and Wong, T.F., 2010, Effect of clay content and mineralogy on frictional sliding behavior of simulated gouges: Binary and ternary mixtures of quartz, illite, and montmorillonite: Journal of Geophysical Research: Solid Earth, v. 115, p. 1–22, doi:10.1029/2009JB006383.

Thomas, P.S., Smallwood, A.S., Ray, A.S., Briscoe, B.J., and Parsonage, D., 2008, Nanoindentation hardness of banded Australian sedimentary opal: Journal of Physics D: Applied Physics, v. 41, doi:10.1088/0022-3727/41/7/074028.

Tichelaar, B.W., and Ruff, L.J., 1993, Depth of seismic coupling along subduction zones: Journal of Geophysical Research, v. 98, p. 2017–2037, doi:10.1029/92JB02045.

Tobin, H.J., and Saffer, D.M., 2009, Elevated fluid pressure and extreme mechanical weakness of a plate boundary thrust, Nankai Trough subduction zone: Geology, v. 37, p. 679–682, doi:10.1130/G25752A.1.

Di Toro, G., Goldsby, D.L., and Tullis, T.E., 2004, Friction falls towards zero in quartz rock as slip velocity approaches seismic rates: Nature, v. 427, p. 436–439, doi:10.1038/NATURE02249.

Trütner, S., Hüpers, A., Ikari, M.J., Yamaguchi, A., and Kopf, A.J., 2015, Lithification facilitates frictional instability in argillaceous subduction zone sediments: Tectonophysics, v. 665, p. 177–185, doi:10.1016/j.tecto.2015.10.004.

Tse, S.T., and Rice, J.R., 1986, Crustal earthquake instability in relation to the depth variation of frictional slip properties: Journal of Geophysical Research, v. 91, p. 9452, doi:10.1029/JB091IB09P09452.

Tsutsumi, A., Fabbri, O., Karpoff, A.M., Ujiie, K., and Tsujimoto, A., 2011, Friction velocity dependence of clay-rich fault material along a megasplay fault in the Nankai subduction zone at intermediate to high velocities: Geophysical Research Letters, v. 38, doi:10.1029/2011GL049314.

Tsutsumi, A., and Shimamoto, T., 1997, High-velocity frictional properties of gabbro: Geophysical Research Letters, v. 24, p. 699–702, doi:10.1029/97GL00503.

Tullis, T.E., 1988, Rock friction constitutive behavior from laboratory experiments and its implications for an earthquake prediction field monitoring program: Pure and Applied Geophysics PAGEOPH, v. 126, p. 555–588, doi:10.1007/BF00879010.

Tullis, T.E., and Weeks, J.D., 1986, Constitutive behavior and stability of frictional sliding of granite: Pure and Applied Geophysics, v. 124, p. 383–414, doi:10.1007/BF00877209.

Ujiie, K., and Tsutsumi, A., 2010, High-velocity frictional properties of clay-rich fault gouge in a megasplay fault zone, Nankai subduction zone: Geophysical Research Letters, v. 37, p. 24310, doi:10.1029/2010GL046002.

Underwood, M.B., 2007, Sediment Inputs to Subduction Zones: Why Lithostratigraphy and Clay Mineralogy Matter, *in* The seismogenic zone of subduction thrust faults, p. 42–85.

Underwood, M.B., 2002, Strike-parallel variations in clay minerals and fault vergence in the Cascadia subduction zone: Geology, v. 30, p. 155–158, doi:10.1130/0091-7613(2002)030<0155:SPVICM>2.0.CO;2.

Underwood, M.B., and Moore, G.F., 1995, Trenches and trench-slope basins, *in* Busby, C.J. and Ingersoll, R. V. eds., Tectonics of Sedimentary Basins, Blackwell, p. 179–219.

Vidale, J.E., Elisworth, W.L., Cole, A., and Marone, C., 1994, Variations in rupture process with recurrence interval in a repeated small earthquake: Nature, v. 368, p. 624–626, doi:10.1038/368624A0.

Vogt, C., Lauterjung, J., and Fischer, R.X., 2002, INVESTIGATION OF THE CLAY FRACTION (<2 μm) OF THE CLAY MINERALS SOCIETY REFERENCE CLAYS: Clays and Clay Minerals, v. 50, p. 388–400.

Voss, N., Dixon, T.H., Liu, Z., Malservisi, R., Protti, M., and Schwartz, S., 2018, Do slow slip events trigger large and great megathrust earthquakes? Science Advances, v. 4, doi:10.1126/sciadv.aat8472.

Vrolijk, P., 1990, On the mechanical role of smectite in subduction zones: Geology, v. 18, p. 703–707, doi:10.1130/0091-7613(1990)018<0703:OTMROS>2.3.CO;2.

Walton, A.W., and Schiffman, P., 2003, Alteration of hyaloclastites in the HSDP 2 Phase 1 Drill Core 1. Description and paragenesis: Geochemistry, Geophysics, Geosystems, v. 4, doi:10.1029/2002GC000368.

Wang, K., and He, J., 1999, Mechanics of low-stress forearcs: Nankai and Cascadia: Journal of Geophysical Research: Solid Earth, v. 104, p. 15191–15205, doi:10.1029/1999jb900103.

Wang, K., and Hu, Y., 2006, Accretionary prisms in subduction earthquake cycles: The theory of dynamic Coulomb wedge: Journal of Geophysical Research: Solid Earth, v. 111, p. 1–16, doi:10.1029/2005JB004094.

Wang, W., and Scholz, C.H., 1994, Micromechanics of the velocity and normal stress dependence of rock friction: pure and applied geophysics 1994 143:1, v. 143, p. 303–315, doi:10.1007/BF00874333.

Wang, K., and Tréhu, A.M., 2016, Invited review paper: Some outstanding issues in the study of great megathrust earthquakes—The Cascadia example: Journal of Geodynamics, v. 98, p. 1–18, doi:10.1016/j.jog.2016.03.010.

Wech, A.G., and Creager, K.C., 2011, A continuum of stress, strength and slip in the Cascadia subduction zone: Nature Geoscience, v. 4, p. 624–628, doi:10.1038/ngeo1215.

Wells, D.L., and Coppersmith, K.J., 1994, New empirical relationships among magnitude, rupture length, rupture width, rupture area, and surface displacement: Bulletin of the Seismological Society of America, v. 84, p. 974–1002.

Westbrook, J.H., 1958, Temperature Dependence of Strength and Brittleness of Some

Quartz Structures: Journal of the American Ceramic Society, v. 41, p. 433–440, doi:10.1111/J.1151-2916.1958.TB12891.X.

White, R.J., Spinelli, G.A., Mozley, P.S., and Dunbar, N.W., 2011, Importance of volcanic glass alteration to sediment stabilization: offshore Japan: Sedimentology, v. 58, p. 1138–1154, doi:10.1111/J.1365-3091.2010.01198.X.

Yuan, T., Spence, G.D., and Hyndman, R.D., 1994, Seismic velocities and inferred porosities in the accretionary wedge sediments at the Cascadia margin: Journal of Geophysical Research, v. 99, p. 4413–4427, doi:10.1029/93JB03203.

Zhang, Z., and Schwartz, S.Y., 1992, Depth distribution of moment release in underthrusting earthquakes at subduction zones: J. Geophys. Res., v. 97, p. 537–544, doi:10.1029/91JB02345.

Zhang, G., Wei, Z., and Ferrell, R.E., 2009, Elastic modulus and hardness of muscovite and rectorite determined by nanoindentation: Applied Clay Science, v. 43, p. 271–281, doi:10.1016/J.CLAY.2008.08.010.

Acknowledgements

When I started this project, I was fascinated. But I started from scratch. Matt introduced me to the world of earthquakes and friction, and his enthusiasm and dedication were contagious. He was patient when I needed it, and pushed me to do better when I thought I didn't need it but probably did. He also introduced me to many outstanding scientists and made it possible for me to participate in a truly incredible expedition. So thank you, Matt, for this crazy, amazing adventure!

I first met Achim during my Bachelors when he was one of my lecturers. With every further encounter, he more and more became "Mr. I can make it possible" to me. Achim, thanks for making things possible.

Working on my project has been really exciting. And it has also been hard at times. My colleagues and also friends, Alex, Philipp, and Aagje, were always there to share experiences and solve problems, as well as to celebrate even the smallest successes. We had great team work going on! Thanks you guys, you have made these years as great as they were.

And also the "Kopfies" and the "Mörzies", you guys have created such a nice working environment, on land and at sea.

Åke, I really appreciate it that you agreed to be reviewer for this thesis.

I thank my family for letting me play with mud and collect rocks since I was able to crawl, and for supporting me in playing with mud and rocks throughout my ridiculously long academic career.

And of course, I am so thankful for my friends who cheer me up when I need it without me asking for it, and who distract me when I need to clear my head.

Finally, Lukas, thank you so much for your incredible support. And for making me happy.

…Now, after four years at MARUM, several months at sea, hundreds of hours in the lab, thousands of hours in front of my computer, and one thesis, I am even more fascinated with earthquake research. And I still think I know very little of what there is to learn and to study.

Versicherung an Eides Statt / *Affirmation in lieu of an oath*

gem. § 5 Abs. 5 der Promotionsordnung vom 18.06.2018 /
according to § 5 (5) of the Doctoral Degree Rules and Regulations of 18 June, 2018

Ich / I, Katja Stanislowski
(Vorname / First *Name*, Name / *Name*, Anschrift / *Address*, ggf. Matr.-Nr. / *student ID no., if applicable)*

versichere an Eides Statt durch meine Unterschrift, dass ich die vorliegende Dissertation selbständig und ohne fremde Hilfe angefertigt und alle Stellen, die ich wörtlich dem Sinne nach aus Veröffentlichungen entnommen habe, als solche kenntlich gemacht habe, mich auch keiner anderen als der angegebenen Literatur oder sonstiger Hilfsmittel bedient habe und die zu Prüfungszwecken beigelegte elektronische Version (PDF) der Dissertation mit der abgegebenen gedruckten Version identisch ist. / *With my signature I affirm in lieu of an oath that I prepared the submitted dissertation independently and without illicit assistance from third parties, that I appropriately referenced any text or content from other sources, that I used only literature and resources listed in the dissertation, and that the electronic (PDF) and printed versions of the dissertation are identical.*

Ich versichere an Eides Statt, dass ich die vorgenannten Angaben nach bestem Wissen und Gewissen gemacht habe und dass die Angaben der Wahrheit entsprechen und ich nichts verschwiegen habe*. / I affirm in lieu of an oath that the information provided herein to the best of my knowledge is true and complete.*

Die Strafbarkeit einer falschen eidesstattlichen Versicherung ist mir bekannt, namentlich die Strafandrohung gemäß § 156 StGB bis zu drei Jahren Freiheitsstrafe oder Geldstrafe bei vorsätzlicher Begehung der Tat bzw. gemäß § 161 Abs. 1 StGB bis zu einem Jahr Freiheitsstrafe oder Geldstrafe bei fahrlässiger Begehung. / *I am aware that a false affidavit is a criminal offence which is punishable by law in accordance with § 156 of the German Criminal Code (StGB) with up to three years imprisonment or a fine in case of intention, or in accordance with § 161 (1) of the German Criminal Code with up to one year imprisonment or a fine in case of negligence.*

Ort / *Place*, Datum / *Date*

Unterschrift / *Signature*